

Development and characterization  
of curcuminoid-loaded lipid nanoparticles

D i s s e r t a t i o n

zur Erlangung des akademischen Grades

Doctor rerum naturalium (Dr. rer. nat.)

vorgelegt der

Naturwissenschaftlichen Fakultät I

Biowissenschaften

der Martin-Luther-Universität Halle-Wittenberg

von

Herrn Andreas Noack

Geboren am 05.01.1985 in Dresden

Gutachter/in

1. Prof. Dr. rer. nat. habil. Karsten Mäder
2. Prof. Dr.-Ing. habil. Dr. h. c. Joachim Ulrich
3. Prof. Dr. rer. nat. habil. Dagmar Fischer

Halle (Saale), 05.12.2012

“There is no sadder sight in the world  
than to see a beautiful theory  
killed by a brutal fact.”

-

*Thomas Henry Huxley*

# Table of contents

<b>1. Introduction</b>	<b>1</b>
1.1 The potential of phytochemicals for cancer chemoprevention	1
1.2 Curcumin - the magic bullet?	4
1.3 Lipid nanoparticles as drug delivery systems	8
1.4 Objective of the thesis	12
<b>2. Materials</b>	<b>14</b>
<b>3. Experimental section</b>	<b>16</b>
3.1 Fabrication of the nanoparticles	16
3.2 Particle characterization	19
3.2.1 Laser diffraction	19
3.2.2 Photon correlation spectroscopy	19
3.2.3 Transmission electron microscopy	19
3.2.4 Asymmetric flow field-flow fractionation	20
3.3 Physicochemical characterization	23
3.3.1 Zeta potential measurements	23
3.3.2 Differential scanning calorimetry	23
3.3.3 X-ray diffraction	24
3.3.4 Nuclear magnetic resonance spectroscopy	24
3.3.5 Raman spectroscopy	24
3.3.6 Fluorescence spectroscopy	24
3.4 Curcuminoid stability	26
3.4.1 Loading efficiency & storage stability	26
3.4.2 Curcuminoid stability in physiological media	26
3.5 Biological <i>in vitro</i> characterization	26
3.5.1 <i>In vitro</i> release	26
3.5.2 <i>In vitro</i> digestion	28
3.5.3 Cell culture experiments	30
<b>4. Results and Discussion</b>	<b>33</b>
4.1 Critical parameters of the particle production	33
4.2 Particle characteristics	38
4.2.1 Particle size distribution	38
4.2.2 Particle long-term stability	40

4.2.3	Transmission electron microscopy	42
4.2.4	Asymmetric flow field-flow fractionation	44
4.2.5	Conclusion	52
4.3	Physicochemical characteristics	54
4.3.1	Zeta potential	54
4.3.2	Differential scanning calorimetry	57
4.3.3	X-ray diffraction	61
4.3.4	Nuclear magnetic resonance spectroscopy	62
4.3.5	Raman spectroscopy	66
4.3.6	Fluorescence spectroscopy	69
4.3.7	Conclusion	73
4.4	Curcuminoid stability	76
4.4.1	Loading efficiency & storage stability	76
4.4.2	Curcuminoid stability in physiological media	77
4.5	Biological <i>in vitro</i> characteristics	78
4.5.1	<i>In vitro</i> release	78
4.5.2	<i>In vitro</i> digestion	81
4.5.3	Cytotoxicity assessment	92
4.5.4	Conclusion	96
5.	Summary and Outlook	100
6.	Zusammenfassung und Ausblick	103
7.	References	IV
8.	Appendix	XXI

## List of abbreviations

MCT	Medium chain triglycerides
RCO	Refined castor oil
SBO	Soy bean oil
e.g. MCT-NE	Oil-based nanoemulsions
TM	Trimyristin
TM-NE	Trimyristin supercooled nanoemulsions
TM-NS	Trimyristin crystalline nanoparticles
TS	Tristearin
TS-NS	Tristearin crystalline nanoparticles
e.g. MCTCurc-NE	Curcuminoid loaded lipid nanoparticles
SLN	Solid lipid nanoparticles
PCS	Photon correlation spectroscopy
LD	Laser diffraction
TEM	Transmission electron microscopy
AF4	Asymmetric flow field-flow fractionation
MALLS	Multi-angle laser light scattering
DSC	Differential scanning calorimetry
XRD	X-ray diffraction
<sup>1</sup> H NMR	<sup>1</sup> H Nuclear magnetic resonance
SGF	Simulated Gastric Fluid
FaSSIF	Fasted state simulated intestinal fluid
FeSSIF	Fed state simulated intestinal fluid
HPTLC	High performance thin layer chromatography
MTT	3-(4,5-dimethylthiazol-2-yl)-2,5-diphenyl tetrazolium bromide

All other abbreviations are explained in the particular text passages.

# 1. Introduction

## 1.1 *The potential of phytochemicals for cancer chemoprevention*

Cancerous diseases are one of the most common causes of death in the world. The prevalence of cancer is still increasing, because of the steady rise in life expectancy, the drastic change of environmental conditions and the promotion of an unhealthy personal lifestyle. The diagnosis and treatment of cancer causes immense costs within the national health systems and although no efforts are spared in the therapy, cancer still poses a “death penalty” for many patients. In the end, the current therapeutic approaches have brought no resounding success and the quest for an effective anticancer therapy is still ongoing.

A major prerequisite for a successful cancer therapy is the full elucidation of the complex process of carcinogenesis. In the last decades medical science has made great efforts to achieve this aim and the understanding of this process deepens and more and more therapeutic targets are identified. Generally, carcinogenesis can be divided into three stages (1). In the initiation stage a normal cell comes into contact with a carcinogen and turns into an initiated cell. Some factors have been postulated to have an enhanced carcinogenic potential, amongst others xenobiotic substances (smoking, alcohol), hormones and persistent inflammatory processes. The following promotion stage is a lengthy process of several years, where the initiated cells turn into preneoplastic cells. In the final progression stage the preneoplastic cells turn into neoplastic cells, which results in the occurrence of typical cancer symptoms, like tumor growth and metastasis. The conventional therapeutic approach focuses on the treatment of the disease in the progression stage, by applying surgery, chemotherapy and radiation to remove the tumor. However, this way poses an extensive and troublesome intervention in the patient’s life and the prospects of a full regeneration is not guaranteed. An alternative way would be the earlier intervention in the initiation or promotion stage of carcinogenesis. The scientific approach of inhibiting cancer in its early stages is summarized under the term chemoprevention, originally introduced by Sporn et al. (2). The basic idea of chemoprevention is not the invention of a “magic-bullet” against cancer, but the identification of substances which lower the risk of developing a cancerous disease. These substances are thought to be applied as a supplement of the daily diet and their beneficial effects shall develop through long-time application. Wattenberg originally classified chemopreventive agents into blocking agents and suppressing agents (3). Blocking agents

impede the interaction of carcinogens with crucial cellular molecules, like DNA, RNA and proteins. Suppressing agents inhibit the already initiated cell to reach the promotion or progression stage, respectively (1). Substances, reversing the initiated state or inducing apoptosis in initiated cells, can be added as third group to this classification.

Plant-derived drugs are in the focus of cancer research since many years (4,5). Some phytochemicals, e.g. vinca alkaloids, taxanes and camptothecin, have already entered clinical use and were shown to be potent drugs for the chemotherapy of cancerous diseases (6,7). The ingredients of common dietary plants and of traditionally applied herbs are therefore intensively studied to find potential new drugs. Besides the quest for new chemotherapeutic drugs, phytochemicals are also investigated for their potential to prevent the initial development of cancer (1). Up to now several phytochemicals were described to interfere with cell signaling pathways connected to carcinogenesis and these substances were suggested to be potential chemopreventive drugs (8-10). A summary of some prominent and closely investigated compounds is given in Figure 1.1-1.

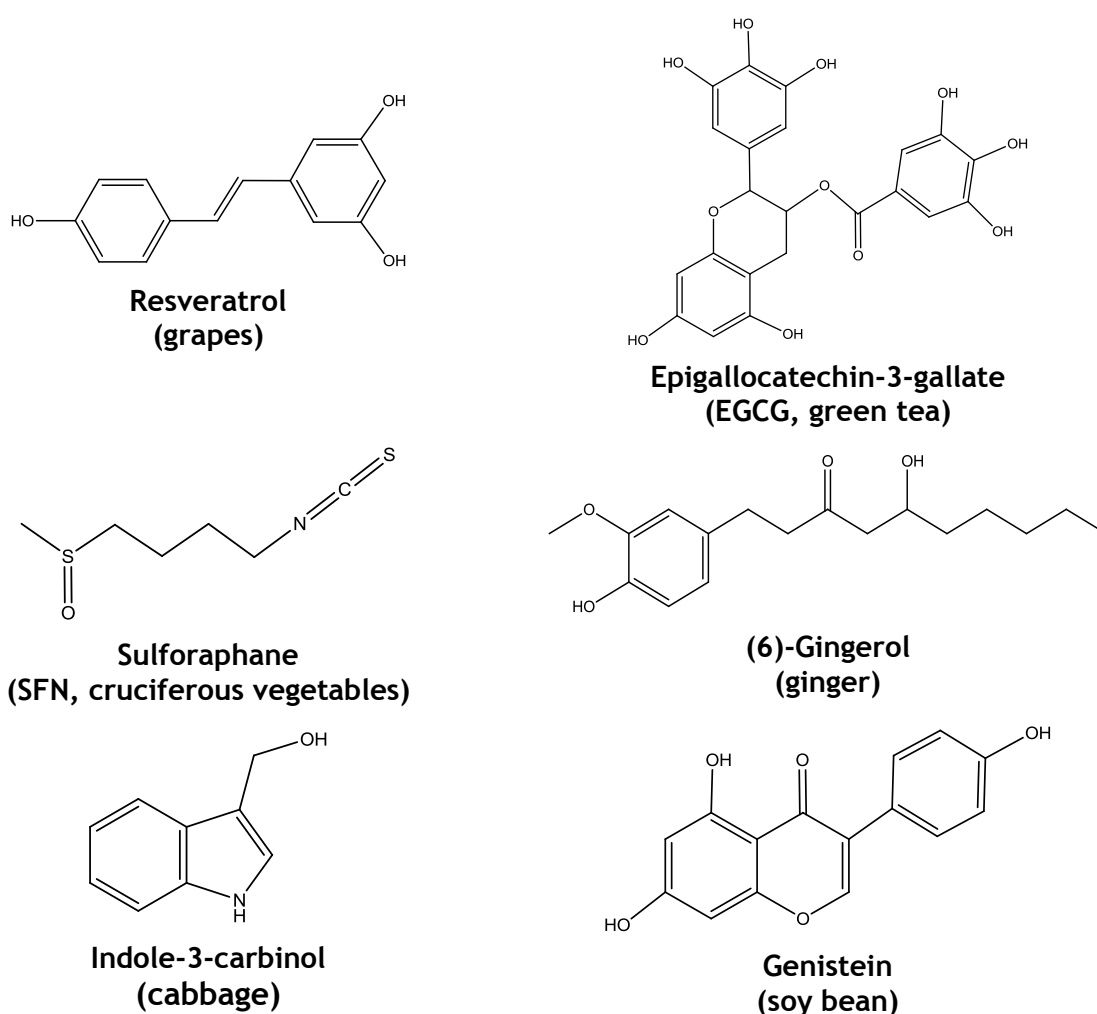


Figure 1.1-1 representative summary of phytochemicals with chemopreventive potential and their dietary sources.

Most frequently an anti-oxidative and anti-inflammatory activity of plant-derived drugs has been demonstrated by *in vitro* studies (1,5). On the one hand, the anti-oxidative ability of phytochemicals was thought to be caused by the direct reaction with an oxidative xenobiotic, resulting in its detoxification. On the other hand, phytochemicals, like sulforaphane and other isothiocyanates have also shown the potential to increase the level of detoxifying enzymes in different cell lines (11-13). The increased level of metabolizing enzymes decreases the oxidative stress within the cell. High oxidative stress, in turn, is proposed to be an initial factor for the development of cancer. The anti-inflammatory potential of phytochemicals, e.g. soy bean isoflavones and evodiamine was reported to be caused by a suppression of NF- $\kappa$ B and COX-2, which are key mediators of the inflammatory signaling cascade (14-16). Persistent inflammation is thought to be another promoting factor for the development of cancer (17). Moreover, within tumors an inflammatory environment was also verified, promoting proliferation of malignant cells and vascularization of the tumor tissue (18,19). Thus, an application of anti-inflammatory phytochemicals might also have a preventive potential against cancerous diseases (14,15). The anti-oxidative activity is for some phytochemicals accompanied by an anti-inflammatory effect. Prominent examples for this combined activity are green tea polyphenols, resveratrol and curcumin. Besides the aforementioned anti-oxidant and anti-inflammatory activities, some plant-derived drugs exhibit further effects, which might be of importance for their chemopreventive potential. Resveratrol, for instance, was reported to induce pro-apoptotic mechanisms *in vitro* and an anti-metastatic effect was also shown *in vivo* (20-23). In addition, Curcumin was also shown to be active against cancer in various ways (24,25). These two examples illustrate that herbal substances do probably not act in a singular way but influence a variety of transcription factors and enzymes, which finally results in the traceable effects. Thus, a singular mechanism of action might be hard to define for most of the investigated phytochemicals.

This résumé also effects the evaluation of the chemopreventive potential of these substances. Many of them show intriguing effects in preclinical *in vitro* studies, but these effects have not been validated thoroughly by animal experiments or regular clinical trials. The problem of transferring the postulated *in vitro* effects to verifiable effects *in vivo* was reviewed in detail by Howells et al. (26). As a consequence, a comprehensive *in vivo* examination of phytochemicals is urgently needed to assess the actual value of these compounds.

It remains further unclear whether chemopreventive phytochemicals are administered as purified drug formulation (table, capsule etc.) or if the daily diet of the patient should be adjusted by the increased consume of vegetables containing chemopreventive substances. In addition, the potential adverse reactions to a therapy with these phytochemicals have to be examined critically. Plant-derived drugs have been propagated as being highly



compliant, exhibiting only few adverse effects. However, the severe impact of phytochemicals on important cellular mechanisms puts this statement into question. Therefore, *in vivo* experiments should be also carried out to provide more information about the occurrence of unwanted effects of phytochemicals.

## 1.2 Curcumin - the magic bullet?

The polyphenol curcumin (diferuloylmethane) is a compound of the dietary plant turmeric (*Curcuma longa L.*). Turmeric is a commonly cultivated plant in south and south-east asia. The vibrant yellow color of its rhizome is caused by polyphenols, amongst which curcumin is the main compound (Fig. 1.2.-1).

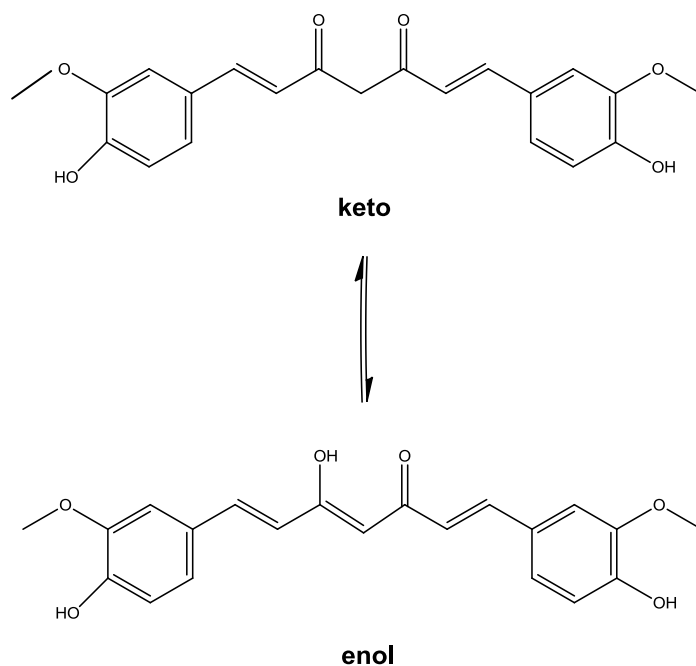


Figure 1.2.-1 Chemical structure of curcumin

The powdered rhizome of turmeric finds wide-spread use in asian cookery, e.g. as chromophoric compound of curry, and it is also used as coloring pigment. In Germany, curcumin is also permitted as a food pigment (E100). Turmeric powder has been further used as therapeutic agent in traditional Indian and Chinese medicine since a long time (27). Today, turmeric is still applied in Indian medicine for the treatment of wounds, insect bites and different skin diseases (28,29).

Curcumin was isolated by Vogel in 1842 and its chemical structure was confirmed in the early 20<sup>th</sup> century. It is composed of two phenolic rings, which are connected by an

unsaturated carbon chain. The main characteristic of the molecule is its di-keto group at position 3 and 5 of the carbon chain, which underlies a keto-enol tautomerism. The enol-form was found to be the predominant structure when curcumin was dissolved in organic solvents, e.g. chloroform and DMSO (30). Besides curcumin, extracts of turmeric contain demethoxycurcumin and bis-demethoxycurcumin, too. Therefore, in the following sections the term curcuminoids will be used to include all compounds with comparable structure and properties. Curcuminoids are almost insoluble in water, but they dissolve well in polar organic solvents, like ethanol or acetone. The polyphenolic structure of the curcuminoids decomposes rapidly under the influence of light (31). Furthermore, curcuminoids are degraded quickly in alkaline aqueous environment (pH 9-10) to ferulic acid and feruloylmethane (32).

Curcuminoids have been in the focus of biomedical research for many years and numerous articles about the activities of curcuminoids were published. An anti-inflammatory effect of curcuminoids was already proposed in advance, due to the traditional application of turmeric as ingredient of wound-healing pharmaceuticals. The underlying molecular mechanisms were investigated by various research groups and accordant reports postulated the inhibition of transcription factors and enzymes related to inflammation (Tab. 1.2-1). In connection with the anti-inflammatory properties, curcuminoids are also capable antioxidants, by inducing the transcription of metabolic phase-II enzymes and by acting anti-oxidative themselves (Tab. 1.2-1). As inflammation and oxidative stress are thought to be linked to carcinogenesis, the aforementioned results were also seen as an indication for the chemopreventive activity of curcuminoids. Therefore, curcuminoids were intensively tested for their potential against cancer and they were demonstrated to act inhibitory at different stages of carcinogenesis (28,33). Curcuminoids were shown to interact with different signaling pathways of the cell cycle regulation, resulting in growth inhibition or apoptosis in various cancer cell lines (Tab. 1.2-1). Apoptosis, the programmed cell-death, is the desired elimination pathway of malignant cells. So, the ability of the curcuminoids to induce apoptosis in cancer cells is a key property for their application in chemopreventive and chemotherapeutic therapy. The different anti-cancer activities of curcuminoids were mainly demonstrated by *in vitro* experiments at cancer cell lines. Interestingly, the drug was tested at various different cell lines and exhibited in most of them a detectable anti-proliferative effect.

Besides their activity against cancer, curcuminoids were also reported to have potential in the treatment of neurodegenerative diseases, cardiovascular diseases, diabetes and rheumatoid arthritis (24,34-36). Although many of these reported effects were demonstrated by *in vitro* experiments with a limited transferability towards the *in vivo* situation it is still an impressive band-width of potential therapeutic applications.

The data on *in vivo* experiments with curcuminoids are not as comprehensive as the *in vitro* data. However, the anti-inflammatory and the chemopreventive potential of the curcuminoids were demonstrated by several animal studies (Tab. 1.2-1).

**Table 1.2-1 Overview of a selection of reports about curcuminoid activities *in vitro* and *in vivo***

Disease	Dose	Effect	Reference
<b>Cancer</b>			
<i>in vitro</i>	10 $\mu\text{mol/l}$	Growth inhibition, apoptosis of MCF-7 cells	(37,38)
<i>in vitro</i>	12.5 $\mu\text{mol/l}$	Induction of apoptosis in HL-60 cells through caspase-3 activation	(39)
<i>in vitro</i>	10 $\mu\text{mol/l}$	Growth inhibition, apoptosis of B-cell lymphoma	(40)
<i>in vitro</i>	50 $\mu\text{mol/l}$	Induction of apoptosis through p53 activation in human basal carcinoma cells	(41)
<i>in vitro</i>	5-10 $\mu\text{mol/l}$	Growth inhibition of Jurkat cells	(42)
Mice	50-200 mg/kg	Inhibition of development of lymphoma cells	(43)
Mice	500 mg/kg	Growth reduction of implanted tumors	(25)
Mice	100 - 200 mg/kg	Growth inhibition of implanted tumors in combination with cis-platin	(44)
<b>Chemoprevention</b>			
Mice	2 % of daily diet	Prevention of BP-induced tumor formation in forestomach	(45)
Mice	2 % of daily diet	Prevention of DMBA-induced tumor formation on skin	(45)
Rats	0.2 % of daily diet	Prevention of MNNG tumor formation in stomach	(46)
Rats	1 % of daily diet	Prevention of mammary tumor after radiation	(47)
<b>Inflammation</b>			
<i>in vitro</i>	100 $\mu\text{mol/l}$	Inhibition of NF-B activation in IEC cells	(48)
<i>in vitro</i>	2-60 $\mu\text{mol/l}$	Inhibition of NF-B activation in ML-1a cells	(49)
<i>in vitro</i>	5-75 $\mu\text{mol/l}$	Inhibition of COX-2 expression in HT-29 cells	(50)
<i>in vitro</i>	3-100 $\mu\text{mol/l}$	Inhibition of LOX and COX expression in mouse epidermis	(51)
Mice	0.25 % of daily diet	Attenuation of DNB-induced colitis	(52)
Rats	2 % of daily diet	Prevents TNBS-induced colitis	(53)
<b>Anti-oxidative properties</b>			
<i>in vitro</i>	5-50 $\mu\text{mol/l}$	Activation of Nrf-2 and detoxifying enzymes	(54)
<i>in vitro</i>	1-10 $\mu\text{mol/l}$	Anti-oxidative activity in human brain tissues	(55)
Mice	250 mg/kg	Induction of glutathion-S-transferase	(56)

Abbreviations: BP: benzo[a]pyrene; DMBA: 7,12-Dimethylbenz[a]anthracene; MNNG: Methylnitronitrosoguanidine; PMA: phorbol 12-myristate 13-acetate; DNB: Dinitrobenzene, TNBS: trinitrobenzene sulfonic acid; MMP: Matrix metalloproteinase

Besides the verification of pharmacological effects, animal experiments were also used to investigate the pharmacokinetic properties of the curcuminoids (57,58). The absorption after oral application was of special interest, because this is seen as the most convenient way for a long-term therapy with curcuminoids. The results of the various pharmacological studies were summarized by Anand et al. and Howells et al. (26,59). Both reviews highlighted the overall low bioavailability of curcuminoids after oral ingestion. The level of absorbed drug in the intestine was reported to be low, because of the poor water solubility. Moreover, the absorbed part of the drug was rapidly metabolized within the intestinal tissue. The main metabolites were glucuronides, sulfates, tetrahydrocurcumin and hexahydrocurcumin (60). Thus, the fraction of non-metabolized curcuminoids in the blood was negligibly small.

Curcuminoids have also been studied in several phase I clinical trials to examine the pharmacokinetic properties of curcuminoids within the human body (28,59,61-63). Although huge doses of up to 12 g/day were administered in the particular studies, only very low blood levels were achieved (61-63). Thus, the bioavailability of curcuminoids in humans was concluded to be similar to that in animals. One encouraging finding was the good compliance of the curcuminoids, also at very high doses. Though, the incidence of adverse reactions might have been prevented by the overall low absorbed amount of drug in the intestine. Therefore, a concluding verification of the risks of a regular application of curcuminoids has not yet been possible. In addition to the pharmacokinetic studies, further clinical trials have been launched, which investigated the impact of curcuminoids on certain cancers (28,64). Especially cancers of the gastro-intestinal tract have been in the focus of the ongoing trials, because it is believed that the curcuminoids are absorbed locally and act directly at the desired area.

However, the low bioavailability of curcuminoids poses a main hurdle for the regular application and further examination of this promising substance class. Hence, there is a clear need for the development of a suitable pharmaceutical formulation to improve the oral bioavailability of the curcuminoids. Up to now, a broad spectrum of curcuminoid formulations has been published. Amongst others, curcuminoids were incorporated into different colloidal carriers, e.g. liposomes, polymeric nanoparticles, mixed micelles, polymeric micelles, self-microemulsifying systems, solid lipid nanoparticles (65-72). The improvement of the oral bioavailability of curcuminoids by nano-scaled formulations was demonstrated by several research groups (71,73-76). Thus, the incorporation of curcuminoids into submicron-particles might be an answer to the lack of intestinal absorption. One advantage of curcuminoid-loaded nanoparticles is the administration of an already finely dispersed drug, so that solubilization within the intestine should be easier compared to the application of the pure curcuminoid powder.

The present reports about the beneficial effects of curcuminoids clearly show the high potential of this substance as chemopreventive but also as chemotherapeutic drug. However, big expectations have been raised, but few hypotheses about curcuminoids have been verified clinically so far. The incorporation of curcuminoids within nanoparticles for oral delivery presents an interesting alternative to improve the bioavailability. The aforementioned studies are only seen as a beginning of this research topic and still a lot more knowledge has to be gained. First, the stability of the curcuminoids in gastrointestinal fluids after loading into nanoparticles has to be assessed in more detail. In addition, the fate of nanoparticles within the gastrointestinal tract has not been elucidated thoroughly so far. It has not been reported conveniently, whether drug-loaded nanoparticles are absorbed within the intestine or if the particles are digested and drug is released into the intestinal fluid. Another interesting point is the role of the lymphatic system during intestinal absorption of the curcuminoids. The formulation of curcuminoid-loaded nanoparticles might enhance the lymphatic uptake of the drug, which probably results in a decrease of first-pass metabolism.

### ***1.3 Lipid nanoparticles as drug delivery systems***

The oral delivery of poorly water-soluble drugs is a major challenge of pharmaceutical formulation development. On the basis of the Biopharmaceutics Classification System (BCS), many of the current drug candidates can be assigned to Class II (low solubility, high permeability) or Class IV (low solubility, low permeability). The low solubility of certain drugs in water entails in most cases a low oral bioavailability, because the fraction of undissolved drug cannot be absorbed by the intestinal tissue. Pharmaceutical development faces the challenge to find formulations, which improve the bioavailability of these problematic drug candidates.

Lipid-based formulations present a viable option for enhancing the bioavailability of poorly water-soluble, lipophilic drugs. The presence of lipids within the gastro-intestinal tract (GIT) results in massive changes of the intestinal milieu to enable the digestion and absorption of the lipid structures. The motility of the stomach and the small intestine are increased to disperse the ingested lipid into small droplets. The lipid is first partly digested by the gastric lipase. Subsequently, the pancreatic lipase degrades the incoming lipid quantitatively in the small intestine. At the same time, the secretion of bile is stimulated. Bile contains phospholipids and bile salts, which form mixed micelles to solubilize the lipid degradation products. Thereafter, the degradation products are transported by the mixed micelles to the intestinal wall, where the lipid is absorbed by

the enterocytes or the lymphatic system. In general, lipid digestion provides also some opportunities to improve the absorption of lipophilic drugs. First, by dissolving the drug in the lipid phase, prior to ingestion, the drug enters the GIT already in a solubilized state and the dissolution in the small intestine is circumvented. So the first step for drug absorption, the dissolution of the drug, is already done outside the GIT. Second, the increased amount of phospholipids and bile salts during lipid digestion provides an enhanced incorporation of the drug into mixed micelles and consequently the drug may not precipitate within the intestine again. Third, the incorporation into the mixed micelles supplies the transport of the drug to the intestinal wall and the uptake by the enterocytes. In addition, lymphatic drug absorption is also increased, when the substance is administered together with a lipid (77,78). Hence, lipid-based formulations are improving the bioavailability of poorly water soluble drugs by “simply” utilizing the biological mechanisms of lipid digestion.

Colloidal lipid carriers, such as liposomes, microemulsions, mixed micelles and lipid nanoparticles, have attracted growing interest in pharmaceutical research, particularly for the delivery of lipophilic and poorly water soluble drugs (79,80). Although these carriers are mainly created for intravenous application, the oral intake of drug loaded lipid nanoparticles was also researched recently and some interesting features with regard to the fate of drug and lipid matrix in the GIT were found (81-83). However, the term “Colloidal lipid carriers” implies various different formulations, but the focus of the present section will be mainly on lipid nanoparticles, which are composed of a lipid matrix and a surrounding surfactant layer. The lipid matrix can be composed of:

- isotropic liquids (nanoemulsion)
- liquid crystalline lipids (e.g. thermotropic smectic or lyotropic cubic)
- solid, crystalline lipids (solid lipid nanoparticles, SLN).

The utilization of biocompatible and fully biodegradable lipids as particle matrix is a major advantage of lipid nanoparticles compared to polymeric ones. In the case of nanoemulsions, dietary oils, such as soy bean oil or olive oil can be used. In addition, many solid lipids, which can be used for the production of SLN, have the GRAS-state (Generally regarded as safe) of the FDA.

Nanoemulsions have been used in the clinic for parenteral nutrition (e.g. Lipofundin<sup>®</sup> N, Lipidem) and as drug carrier (e.g. Diazepam-Lipuro<sup>®</sup>, Propofol-MCT<sup>®</sup> Fresenius) since many years. The lipid matrix of the marketed products consists mostly of medium chain triglycerides, soy bean oil or olive oil. The production of nanoemulsions is regularly done with high-pressure homogenization. Drug-loaded nanoemulsions are generally designed for a single or short-term application to the patients. A regular long-term therapy with

nanoemulsions has not been developed yet, because of the comparably high production costs and potential stability problems, e.g. drug leakage and particle agglomeration.

The use of nanoparticles with a liquid crystalline lipid core as potential new drug-delivery system has been reported recently (81,84-86). The liquid crystalline lipid within the nanoparticles is still fluid, but highly viscous. Certain lipids, e.g. glycerolmonooleate, glyceroldioleate and cholesterylmyristate, are capable of building such liquid crystalline structures. The specific inner structure of the liquid crystalline lipid is proposed to be capable of loading high amounts of drug compared to fluid or solid lipids (87).

Solid lipid nanoparticles have been researched and reviewed intensively as drug delivery system since almost two decades (80,87-90). SLN are composed of a solid lipid core and surrounding surfactant layer and they have been developed as an alternative drug delivery system to polymeric nanoparticles (80,88,89). Various kinds of lipids, such as triglycerides, partial glycerides, fatty acids, cholesterol and waxes, and mixtures of the aforementioned substances have been used for the preparation of SLN (91-95). The postulated advantages of SLN compared to other nanoparticle formulations, like polymer nanoparticles or nanoemulsions, were the high biocompatibility and the effective entrapment of drugs within the solid lipid matrix (96-98). However, certain lipid matrices were shown to tend to a high crystalline order which forced the drug to be localized on the surface of the particle (93,99). In addition, the crystallization of colloidal lipids was shown to be a complex process, entailing potential problems, e.g. drug expulsion and particle destabilization (99,100).

For the fabrication of SLN the following methods have been reported:

- high pressure homogenization (80,84,91,100-103)
- precipitation from a warm microemulsion (104)
- solvent evaporation and solvent diffusion methods (95,105-107)

The most frequently used technique is high-pressure homogenization, because of the absence of organic solvents, the easy processing of large product amounts and the capability of processing high lipid contents (up to 40 % (w/w) lipid). The other methods were also shown to produce reliable and stable formulations, but their application demands, e.g. high amounts of surfactant or organic solvents, and they are actually more adequate for a small lab-scale production.

Besides the intravenous administration, SLN have been also applied for the oral delivery of different drugs in animal experiments (82,92,108-111). Muchow et al. suggested that the platelet-like shape of crystalline lipid nanoparticles and their mucoadhesive behavior is beneficial for oral and dermal application (112). The authors claimed that the particles can attach well to the surface of the gut wall and the incorporated drug is released close

to the enterocytes. In addition, the digestion of the lipid particle matrix might have also a supporting effect on the solubilization of the drug within the intestine, in the way it was described at the beginning of this chapter. The incorporation in SLN increased the oral bioavailability of the chemotherapeutic drugs camptothecin and vinpocetin administered to mice or rats, respectively (108,109). Zhang et al. showed the potential of SLN for the oral delivery of peptides, like insulin (110). Though, their experiments did not show satisfyingly, why the peptide is not digested within the intestine. Another study was conducted by Müller et al. as they developed a cyclosporine-A loaded SLN formulation and showed this preparation to give comparable blood levels than the commercial product Sandimmun® Optoral (82). The ascribed potential of SLN should be used in this study to improve the oral bioavailability of curcuminoids. One reason for the application of lipid nanoparticles is their degradability within the gastrointestinal lipases. It was suggested that the curcuminoid-loaded particles arrive within the small intestine followed by a rapid degradation of the lipid matrix and an instant release of the curcuminoids into the intestinal medium. Due to the small particle size, the curcuminoids are already finely dispersed by entering the body and an effective solubilization of the drug within the mixed micelles of the small intestine is therefore favorable.



## **1.4 Objective of the thesis**

The various beneficial effects of curcumin have been illustrated in detail in chapter 1.2. It was concluded that the postulated properties of curcumin were not verified satisfyingly by *in vivo* experiments and curcumin has not found its way into a wide-spread medicinal use, yet. The main hindrance for the application and comprehensive *in vivo* evaluation was discussed to be the low oral bioavailability of the drug. Therefore, an applicable delivery system has to be found to provide a sufficient absorption of curcumin after oral ingestion. In this study, lipid nanoparticles were investigated as a potential drug delivery system for curcumin, because they were reported to be capable for the oral delivery of several other drugs before (82,92,108,112).

Therefore, the major objective of this study was the development of a suitable colloidal lipid formulation for the curcuminoids and its substantial physicochemical and *in vitro* characterization. In order to achieve this aim, the following scopes were addressed:

### **1. Development of different formulations:**

Different lipids and emulsifiers were processed by high pressure homogenization to create a nanoparticle formulation. The achievable particle size for lipid formulations, produced by homogenization, was expected to be around 150 - 200 nm (100,113,114). Based on the available literature data, a loading amount of 3 - 5 % (w/w) curcuminoids into the lipid phase was seen as realistic aim (73,93).

### **2. Characterization of the particle size and particle geometry:**

Different analytical techniques were applied to characterize the produced preparations with regard to particle size and particle form. The evaluation of the particle geometry of the solid lipid nanoparticles by means of AF4/MALLS and TEM was of special interest, because of the irregular shape of these particles.

### **3. Physicochemical characterization of the nanoparticles:**

The determination of the lipid modification within the particles was in the focus of this work, because it was reported earlier that lipids show special characteristics in the colloidal state (115-117). The localization and physical state of the curcuminoids within the nanoparticles was investigated by different physicochemical methods, because this issue was not examined in detail so far (118).

### **4. Evaluation of the drug stability:**

The drug stability during long-time storage of the curcuminoid-loaded nanoparticles was assessed. Additionally, the formulations were incubated in physiological media and the stability of the drug was determined.

### **5. *In vitro* testing of the developed formulations:**

The drug release from the colloidal carrier was investigated by a newly developed method, based on fluorescence imaging. The digestion of the lipid nanoparticles was simulated under gastric and intestinal conditions, to verify the digestability of the preparations. The cytotoxicity of the drug-free and curcuminoid-loaded formulations was evaluated by cell culture experiments with Caco-2 cells.

## 2. Materials

<b>Particle production</b>			
<b>Name</b>	<b>Trade name</b>	<b>Batch No.</b>	<b>Company</b>
Curcuminoids <sup>a</sup>	Curcumin	08974233	Carl Roth GmbH & Co. KG
Medium chain triglycerides <sup>a</sup>	Miglyol <sup>®</sup> 812	81028198	Caesar & Loretz GmbH
Soy bean oil	-	73322068	Caesar & Loretz GmbH
Refined castor oil	-	3612201	Henry Lamotte GmbH
Trimyristin <sup>a</sup>	Dynasan 114	905167	Sasol Germany GmbH
Tristearin <sup>a</sup>	Dynasan 118	902838	Sasol Germany GmbH
Poloxamer 188	Lutrol <sup>®</sup> F68	WPND546E	BASF
Poloxamer 407	Lutrol <sup>®</sup> F127	WPHB615B	BASF
Cremophor <sup>®</sup> RH 40	-	36462924U0	BASF
Solutol <sup>®</sup> HS 15	-	70291616K0	BASF
Lecithin	Lipoid S45	47020	Lipoid GmbH
<b>Zeta potential</b>			
TRIS (2-amino-2-hydroxymethyl-propane-1,3-diol)	-	16816MA-063	Sigma-Aldrich
<b><sup>1</sup>H-NMR</b>			
D <sub>2</sub> O (contains 0.75 % (w/v) sodium 3-(trimethylsilyl)-2,2,3,3-d <sub>4</sub> propionate)	-	MKBB2073	Sigma-Aldrich
<b>In vitro digestion</b>			
Pepsin (from porcine gastric mucosa)	-	BCBC0336	Sigma-Aldrich
Lecithin	Phospholipon <sup>®</sup> 90 G	80830	Lipoid GmbH
Bile extract (porcine)	-	013K0129	Sigma-Aldrich
Pancreatin (from porcine pancreas)	-	064K1451	Sigma-Aldrich
<b>Cell culture experiments</b>			
Minimum essential medium	-	0875W	Biochrom AG
Fetal bovine serum	-	0608T	Biochrom AG
Non-essential amino acids	-	1269W	Biochrom AG
L-glutamine (200 mM)	-	1035L	Biochrom AG
Gentamicin (lyophilized, 10 mg/ml)	-	0073W	Biochrom AG
Trypsin 0.25 % /EDTA 0.02 % in PBS	-	0963W	Biochrom AG

<sup>a</sup> See appendix for certificate of analysis

## Frequently used solutions

### Simulated Gastric Fluid (pH 1.2, USP 31)

- 0.1 mol/l hydrochloric acid
- 0.03 mol/l sodium chloride
- 0.02 % (w/v) sodium azide

### Sørensen phosphate buffer (pH 6.8)

- 53.4 % (v/v) potassiumdihydrogenphosphate 0.067 mol/l
- 46.6 % (v/v) di-sodiumhydrogenphosphate-dihydrate 0.067 mol/l
- 0.02 % (w/v) sodium azide

### 3. Experimental section

#### 3.1 Fabrication of the nanoparticles

The lipid nanoparticles were produced by high pressure homogenization. The lipid phase, consisting of medium chain triglycerides (MCT), refined castor oil (RCO), soy bean oil (SBO), trimyristin (TM) or tristearin (TS), was coarsely emulsified in the water phase by a high speed dispersion device (Ultra-Turrax®, IKA, Germany) This pre-emulsion was further processed with a high pressure homogenizer [Stansted Fluid Power Ltd., UK, (113)]. The lipid concentration in the formulations was 10 % (w/w) and the formulations were either prepared drug-free or loaded with 0.1 % (w/w) curcuminoids if not stated otherwise (Fig. 3.1-1).

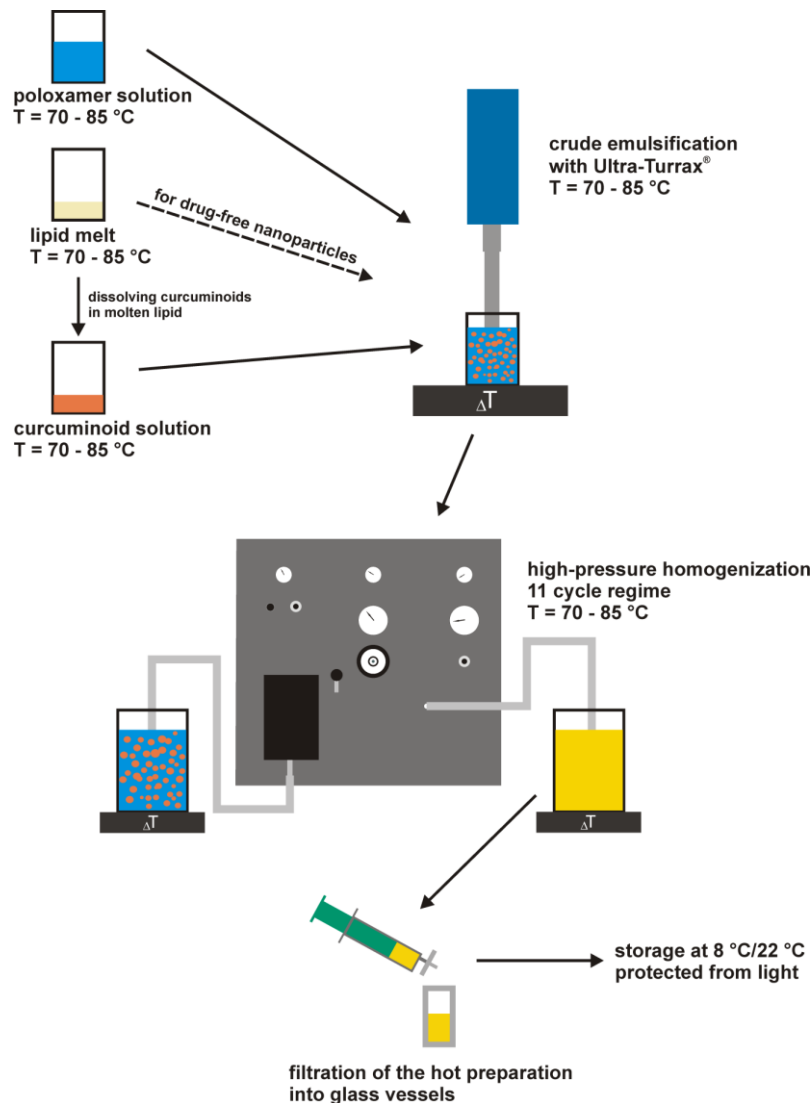


Figure 3.1-1 Schematic overview of the lipid nanoparticle production

Generally, the lipid phase was heated to 70 - 85 °C. The curcuminoids were dissolved in the hot and molten lipid phase. Thereafter, a pre-heated solution of 2.5 % (w/v) Poloxamer 188 and 0.05 % (w/v) sodium azide was added to the lipid phase. Aqueous solutions of 2.5 % (w/v) Poloxamer 407, 2.5 % (w/v) Cremophor® RH 40 and 2 % (w/v) Solutol® HS 15/0.5 % (w/v) lecithin (Lipoid S 45) were alternatively applied as emulsifying agents. The lipid and the emulsifier solution were heated to a temperature of 70-85 °C. A pre-emulsion was formed by using an Ultra-Turrax® at 14.000 rpm for 5 minutes. The resulting dispersion was further homogenized in an eleven cycle homogenizing regime. The homogenizer pump was heated up with a metal jacket to 75-80 °C to avoid recrystallization of the high-melting lipids and to decrease the viscosity of the lipids. Additionally the homogenizing valve was heated with a water bath to the same temperature. The first cycle was run at a main pressure of 50 MPa. For the following three cycles the main pressure was kept at 50 MPa and the second stage pressure was increased to 10 MPa. Subsequently, the pressure was increased every three cycles to 70 MPa and 100 MPa, respectively, and the second stage pressure was constantly kept at 10 MPa during the whole procedure. For the last cycle, the main pressure was decreased to 50 MPa and the second pressure was shut down. After homogenizing, the hot dispersion was given through a 0.8 µm polyethersulfone filter. The first 3 - 4 ml of the filtrate was always discarded, because of the potential filter adsorption of the curcuminoids. The formulation was cooled down slowly to room temperature and stored in glass vessels at 8 °C. The prepared batches, containing TM, were split and the portions were either stored at 8 °C or at 22 °C, respectively. The storage of the TM nanoparticles at 8 °C resulted in a crystallization of the lipid matrix, whereas the lipid core of the nanoparticles kept fluid when the preparation was stored at 22 °C. An overview of the produced formulations is given in Table 3.1-1. To avoid photolytical decomposition of the curcuminoids the samples were kept protected from light.

Table 3.1-1 Overview of the different lipid nanoparticle formulations. The leading formulations were comprehensively investigated. The supplementary formulations, presented below, were only used for selected experiments.

*Leading formulations of the present work*

<i>Name</i>	<i>Composition</i>
<b>MCT-NE</b>	10 % MCT, 2.5 % poloxamer 188
<b>MCTCurc-NE</b>	10 % MCT, 2.5 % poloxamer 188, 0.1 % curcuminoid
<b>TM-NE</b>	10 % trimyristin, 2.5 % poloxamer 188, fluid lipid matrix (nanoemulsion)
<b>TMCurc-NE</b>	10 % trimyristin, 2.5 % poloxamer 188, 0.1% curcuminoid, fluid lipid matrix (nanoemulsion)
<b>TM-NS</b>	10 % trimyristin, 2.5 % poloxamer 188, solid lipid matrix (SLN)
<b>TMCurc-NS</b>	10 % trimyristin, 2.5 % poloxamer 188, 0.1% curcuminoid, solid lipid matrix (SLN)
<b>TS-NS</b>	10 % tristearin, 2.5 % poloxamer 188, lipid matrix solid (SLN)
<b>TSCurc-NS</b>	10 % tristearin, 2.5 % poloxamer 188, 0.1 % curcuminoid, solid lipid matrix (SLN)

*Supplementary formulations for special purposes*

<i>Name</i>	<i>Composition</i>	<i>Experimental application</i>
<b>MCT-NE SL</b>	10 % MCT, 2 % Solutol <sup>®</sup> HS 15/0.5 % lecithin	Particle size, Zeta potential
<b>MCT-NE P407</b>	10 % MCT, 2.5 % poloxamer 407	Particle size
<b>MCT-NE C40</b>	10 % MCT, 2.5 % Cremophor <sup>®</sup> RH 40	Particle size
<b>RCO-NE</b>	10 % refined castor oil, 2.5 % poloxamer 188	Particle size
<b>RCO-NE SL</b>	10 % refined castor oil, 2 % Solutol <sup>®</sup> HS 15/0.5 % lecithin	Particle size
<b>SBO-NE</b>	10 % soy bean oil, 2.5 % poloxamer 188	Particle size

## **3.2 Particle characterization**

### **3.2.1 Laser diffraction**

The particle size distribution of the lipid nanoparticles was routinely determined by laser diffraction (Mastersizer, Malvern, UK) a few hours after preparation. The particle size distributions of all formulations were also determined after six and twelve months of storage at 8 °C and protected from light. Every sample was analyzed in quintuplicate. Measurements were conducted with a laser obscuration of 2-3 % to avoid oversaturation of the blue light laser. The obtained data were evaluated with the Mastersizer 2000 software (v5.22, Malvern, UK). The volume weighted size distribution of the nanoparticles was calculated by applying the Mie theory. The results were calculated under the assumption of a spherical particle shape, a refractive index of the dispersant of 1.45 and an absorption of 0.001. The  $d_{10}$ ,  $d_{50}$  (median), the volume weighted mean and the  $d_{90}$  were used for the evaluation of the particle size distribution and for the comparison with other particle sizing methods.

### **3.2.2 Photon correlation spectroscopy**

The lipid nanoparticles were further examined by photon correlation spectroscopy (HPPS, Malvern, UK). The measurements were carried out at 25 °C. The scattered light was detected in the backscattering mode at 173°. The preparations were adequately diluted with bidistilled and filtered (pore size 0.2  $\mu\text{m}$ ) water. The diluted samples were measured in triplicate and the measurement position was fixed in the middle of the cuvette. Every measurement had at least 10 runs and every run lasted 10 s. The z-average diameters and polydispersity indices were calculated using the instrument's software (Dispersion technology software, v4.20, Malvern, UK). The refractive index of the medium (water) and the dispersant was assumed to be 1.33 and 1.45, respectively. The sample viscosity was assumed to be equal to water (0.89 mPa\*s), if not stated otherwise.

### **3.2.3 Transmission electron microscopy**

The shape and the size of MCTCurc-NE, TMCurc-NE, TMCurc-NS and TSCurc-NS were investigated by transmission electron microscopy (TEM). Negatively stained samples were prepared by spreading 3  $\mu\text{l}$  of the formulation onto a Cu grid coated with a formvar film. After 1 min of adsorption, excess liquid was blotted off with filter paper. After washing with water (3 times for 1 min), the grids were placed on a droplet of 1 % (w/v) aqueous



uranyl acetate and drained off after 1 min. The dried specimens were examined with a EM 900 transmission electron microscope (Zeiss, Germany) at an acceleration voltage of 80 kV. Electron micrographs were taken with a Variospeed SSCCD camera SM-1k-120 (TRS, Germany).

For freeze fracture, the lipid nanoparticles were freeze fixed using a propane jet-freeze device JFD 030 (BAL-TEC, Balzers, Liechtenstein). Thereafter the samples were freeze-fractured at -150 °C without etching with a freeze fracture/ freeze etching system BAF 060 (BAL-TEC, Balzers, Liechtenstein). The surfaces were shadowed with platinum to achieve a good topographic contrast (2 nm layer, shadowing angle 45°) and subsequently with carbon to stabilize the ultra-thin metal film (20 nm layer, shadowing angle 90°). The replicas were floated in sodium chloride (4 % (w/v) NaCl; Roth, Karlsruhe, Germany) for 30 minutes, rinsed in distilled water (10 minutes), washed in 30 % (v/v) acetone (Roth, Karlsruhe, Germany) for 30 minutes and rinsed again in distilled water (10 min). Thereafter, the replicas were mounted on copper grids coated with formvar film and investigated with a transmission electron microscope.

### **3.2.4 Asymmetric flow field-flow fractionation**

A summary of the theory of field-flow fractionation is given in the Appendix.

#### **3.2.4.1 Particle size analysis**

The lipid nanoparticles were separated by an asymmetrical flow field-flow fractionation system (AF4, Eclipse F, Wyatt Technology Europe, Germany) connected to an isocratic pump and a micro vacuum degasser (Agilent 1100 Series, Agilent Technologies, Germany). The channel was equipped with a trapezoidal spacer (length 265 mm, largest width 21 mm, thickness 350  $\mu\text{m}$  or 490  $\mu\text{m}$ ). A membrane consisting of regenerated cellulose ( $M_w$  cutoff: 10 kDa, Microdyn Nadir GmbH, Germany) was used as accumulation wall. The channel was connected to a multi-angle laser light scattering detector (MALLS, DAWN EOS Wyatt Technology Europe, Germany), measuring the intensity of the scattered light at 15 different angles. The eluent was bidistilled water, which was filtered (0.1  $\mu\text{m}$ , PVDF, Millipore, USA) before use and preserved with 0.02 % (w/v) sodium azide. The lipid nanoparticles were diluted with the respective eluent 1:1000 before the measurement. The parameters of the applied Separation Method 1 are shown in Table 3.2-1. The evaluation of the raw data was done with Astra software 4.90 (Wyatt) using the particle mode. The MALLS raw data were fitted by a function, which was based on the RGD approximation. If the samples contained non-spherical particles (e.g. crystalline TM and TS nanoparticles), the obtained data were fitted to  $(K^*c^*R(\theta))^{1/2}$  vs.  $\sin^2(\theta/2)$  (Berry

formalism). For samples with spherical form (e.g. MCT and TM nanoemulsions), the data were fitted to  $R(\theta)$  vs.  $\sin^2(\theta/2)$ . The  $r_{RMSz}$  (z-average) and the  $r_{RMSw}$  (mass weighted mean radius) were obtained as characteristic size results over the whole peak area of the sample. For the comparison with other methods, the  $d_{RMSz}$  and  $d_{RMSw}$  were calculated from the respective radii. The geometric radius  $r_{GEOM}$  of spherical particles is directly proportional to the  $r_{RMS}$  and can be calculated by the following equation (119):

$$r_{GEOM} = r_{RMS} \sqrt{\frac{5}{3}} \quad \text{or} \quad d_{GEOM} = 2r_{RMS} \sqrt{\frac{5}{3}} \quad (1)$$

The mass weighted size distributions of the nanoparticles were calculated by the binning method. A spherical shape was assumed for the droplets of the nanoemulsions (120). SLN are known to be of anisometric, platelet-like shape (121). Therefore, a rod-like geometry was assumed for fitting data of the SLN samples, presenting the best available approximation of the program. A sigma spread factor of 20 was used and the  $d_{10}$ ,  $d_{50}$  and the  $d_{90}$  were obtained as characteristic particle sizes from the cumulative distribution curve.

The investigated formulations were: MCTCurc-NE, TMCurc-NE, TMCurc-NS, TSCurc-NS. All samples were stored at 8 °C, except TMCurc-NE, before the AF4 measurements. The time span between production of the nanoparticles and its analysis did not exceed two months for all formulations. The stability of the preparations during this time span was confirmed by LD measurements (chapter 4.2.2, Tab. 4.2-2). Every preparation was measured in triplicate and all examined samples were taken from the same batch. The relative errors of the calculated  $r_{RMSz}$  and  $r_{RMSw}$  were between 1 % and 3 % for all measurements, except for MCTCurc-NE, where the relative error of  $r_{RMSz}$  was between 5 % and 8 %.

**Table 3.2-1 AF4 separation method 1.**

<b>Eluent:</b>		<i>bidistilled water preserved with 0.02 % (m/v) sodium azide</i>			
<b>Detector Flow:</b>		<i>1 ml/min</i>	<b>Inject Flow:</b> <i>0.20 ml/min</i>		
<b>Spacer height:</b>		<i>350 μm</i>			
Step	Δ t [min]	Mode	X start [ml/min]	X end [ml/min]	Focus Flow [ml/min]
1	1	Elution	2	2	-
2	1	Focus	-	-	2
3	2	Focus + Injection	-	-	2
4	1	Focus	-	-	2
5	2	Focus + Injection	-	-	2
6	3	Focus	-	-	2
7	5	Elution	2	0.5	-
8	35	Elution	0.5	0	-
9	10	Elution	0	0	-
10	10	Elution + Injection <sup>a</sup>	0	0	-

<sup>a</sup> Injection mode was additionally initialized to remove sample residues out of the injection loop

### 3.2.4.2 Particle shape analysis

Samples of TMCurc-NE and TMCurc-NS were diluted 1:100 with bidistilled water and the aforementioned AF4 system was used for the experiments. The samples were fractionated with Separation Method 2 using bidistilled water as eluent (Tab. 3.2-2). Due to the occurrence of pipework blockades, samples of MCTCurc-NE, TMCurc-NE, TMCurc-NS and TSCurc-NS were diluted 1:500 with an aqueous 0.1 % (w/v) poloxamer 188 solution and a 0.1 % (w/v) poloxamer 188 solution was applied as alternative eluent. Separation Method 3 was used for these experiments (Tab. 3.2-3). The evaluation of the MALLS data was done with the Astra software 4.90 (Wyatt) using the particle mode and the relative errors of the calculated  $r_{\text{RMSZ}}$  and  $r_{\text{RMSW}}$  were between 1 % and 3 % for all measurements. In addition, eluting fractions were collected every 1 min into glass vials and subsequently measured by PCS. The settings and procedure of the PCS measurements are described in chapter 3.2.2. For the measurement of samples, collected during AF4 runs with poloxamer as eluent, the dispersant viscosity of the poloxamer solution was calculated according to Augsten et al. (122).

Table 3.2-2 AF4 separation method 2.

<b>Eluent:</b>		<i>Bidistilled water preserved with 0.02 % (m/v) sodium azide</i>			
<b>Detector Flow:</b>		<i>1 ml/min</i>	<b>Inject Flow:</b> <i>0.20 ml/min</i>		
<b>Spacer height:</b>		<i>350 <math>\mu\text{m}</math></i>			
Step	$\Delta t$ [min]	Mode	X start [ml/min]	X end [ml/min]	Focus Flow [ml/min]
1	2	Elution	2	2	-
2	1	Focus	-	-	2
3	2	Focus + Injection	-	-	2
4	1	Focus	-	-	2
5	4	Focus + Injection	-	-	2
6	5	Elution + Injection <sup>a</sup>	2	0.3	-
7	20	Elution + Injection <sup>a</sup>	0.3	0.05	-
8	10	Elution + Injection <sup>a</sup>	0.05	0.05	-
9	10	Elution + Injection <sup>a</sup>	0.05	0	-

<sup>a</sup> Injection mode was additionally initialized to remove sample residues out of the injection loop

**Table 3.2-3 AF4 separation method 3.**

<b>Eluent:</b>		<i>0.1 % Poloxamer (w/v) in bidistilled water preserved with 0.02 % (m/v) sodium azide</i>			
<b>Detector Flow:</b>		<i>0.50 ml/min</i>			
<b>Spacer height:</b>		<i>490 μm</i>			
<b>Inject Flow:</b>	<i>0.20 ml/min</i>				
Step	Δ t [min]	Mode	X start [ml/min]	X end [ml/min]	Focus Flow [ml/min]
1	1	Elution	2	2	-
2	1	Focus	-	-	2
3	2	Focus + Injection	-	-	2
4	1	Focus	-	-	2
5	5	Elution	2	0.5	-
6	40	Elution	0.5	0	-
7	10	Elution + Injection <sup>a</sup>	0	0	-

<sup>a</sup> Injection mode was additionally initialized to remove sample residues out of the injection loop

### 3.3 Physicochemical characterization

#### 3.3.1 Zeta potential measurements

The zeta potential of the lipid nanoparticles was determined at 20 °C with a Zetamaster S (Malvern Instruments, UK). The particle velocity was measured by laser Doppler anemometry and the electrophoretic mobility was converted into the zeta potential using the Helmholtz-Smoluchowski equation (123). The lipid nanoparticles were diluted 1:1000, if not stated otherwise, with TRIS buffer (pH 7.4) of different concentrations (0 - 100 mM). Three aliquots of every diluted sample were measured performing three runs per aliquot. The mean and standard deviation were calculated from the single runs of the respective samples.

#### 3.3.2 Differential scanning calorimetry

Calorimetric measurements were performed by a Netzsch DSC 200 apparatus (Netzsch, Germany). Samples were accurately weighed in dotted aluminum pans (approximately 15 mg). Nitrogen was used as flush gas. The scans were recorded with a heating rate of 5 K/min for the bulk lipid and 2 K/min for the nanoparticles, if not stated otherwise. The respective cooling rate was 10 K/min and 5 K/min for the preparations. Besides constant heating some samples were also heated discontinuously by bringing the samples to 40 °C, holding this temperature for one hour and subsequently heating them to 80 °C.

### 3.3.3 X-ray diffraction

The patterns of the TM and TS bulk material and the patterns of the TM-NE, TM-NS and TS-NS preparations were recorded in transmission with a stationary linear position sensitive detector ( $2\theta = 0 - 40^\circ$ ) on a stage including a curved primary Ge (111) monochromator and high temperature attachment (STOE & CIE GmbH, Germany). The samples were sealed into glass capillaries. Cu  $K\alpha_1$  radiation was used and the scattering pattern of the powder samples was corrected by means of an empty capillary and the pattern of the nanoparticles was corrected against a capillary filled with distilled water. The resulting patterns were combined in one diagram to present both SAXS and WAXS region ( $2\theta = 0 - 40^\circ$ ,  $s = 0 - 4.7 \text{ nm}^{-1}$ ) (124).

### 3.3.4 Nuclear magnetic resonance spectroscopy

800  $\mu\text{l}$  of the respective formulation were mixed with 200  $\mu\text{l}$   $\text{D}_2\text{O}$  containing 0.75 % (v/v) of a TMS derivate as internal standard (see chapter 2).  $^1\text{H}$  NMR was performed at a temperature of 27  $^\circ\text{C}$  and a frequency of 400 MHz with a Gemini 2000 (Varian, France).

### 3.3.5 Raman spectroscopy

The Raman spectra were recorded by a Fourier transform Raman spectrometer RFS 100/S (Bruker, Germany). The solid bulk materials were brought into the cavity of an aluminum pan. Liquid samples were placed in glass tubes. The excitation source was a diode pumped Nd:YAG laser operating at a wavelength of 1064 nm. Spectra were detected at an angle of  $180^\circ$  relative to the incident beam. Every sample was analyzed with 200 scans at a laser power of 350 mW. The spectra were processed by the Bruker OPUS software (91).

The temperature dependence of the spectra of the TMCurc-NE and TMCurc-NS preparations was investigated in the range between 0  $^\circ\text{C}$  and 70  $^\circ\text{C}$ . After each temperature adjustment, the temperature was equilibrated for 10 min and subsequently the spectra were recorded.

### 3.3.6 Fluorescence spectroscopy

Fluorescence measurements were accomplished by a Hitachi F-4500 spectrophotometer (Hitachi Ltd., Japan). A xenon lamp was used as the light source. The excitation wavelength was set to 420 nm and the spectra were recorded in a range of 430 - 620 nm. The width of the slit was 5 nm and the speed of the scan was set to 60 nm per minute.

The fluorescence intensity was measured in an angle of 90°. The cuvette holder was connected to a thermostat to set the desired temperature during measurement.

Fluorescence anisotropy measurements were used to determine the mobility of the curcuminoids within organic solvents and the lipid nanoparticles, namely TMCurc-NE and TMCurc-NS. The dye is excited with polarized light and the emitted light can either be polarized or depolarized. Polarized light was generated by inserting a polarization filter (Hitachi Ltd., Japan) into the incoming light path. A second polarization filter was placed in front of the light detector. The polarization filters were moved into appropriate parallel and perpendicular position. The excitation wavelength was set to 430 nm and the recorded range was 470 - 540 nm for the experiments with polarized light. The scan speed was reduced to 15 nm per minute for these experiments. The steady-state anisotropy  $r$  is defined as:

$$\langle r \rangle = (I_{\parallel} - GI_{\perp}) / (I_{\parallel} + 2GI_{\perp}) \quad (2)$$

$I_{\parallel}$  is the fluorescence intensity parallel to the excitation polarization (polarized light) and  $I_{\perp}$  is the fluorescence intensity perpendicular to excitation polarization (depolarized light) (125).  $I_{\parallel}$  and  $I_{\perp}$  of the curcuminoid-loaded nanoparticles were corrected for light scattering by subtracting a background spectrum of a curcuminoid-free preparation.  $G$  is a factor which corrects the bias of the detection system on the emitted polarized light and is obtained by:

$$G = I_{hv} / I_{hh} \quad (3)$$

$I_{hv}$  is the detected light intensity when the first polarization filter is in horizontal position and the second polarization filter in vertical position.  $I_{hh}$  is the detected light intensity when both polarization filters are in horizontal position. The  $G$  factor was determined with a diluted TM-NS sample as light scatterer.

If the mobility of the investigated fluorescent dye, e.g. curcuminoids, is not restricted, the excitatory polarized light is depolarized by the movement of the fluorescence molecule and depolarized light is emitted. Thus, the resulting fluorescence anisotropy is close to 0 in this case. In contrast, an immobile fluorescent dye emits a high fraction of polarized light and the anisotropy increases accordingly.

## **3.4 Curcuminoid stability**

### **3.4.1 Loading efficiency & storage stability**

The amount of incorporated drug was determined with UV/Vis spectroscopy (Spekol 1200, Analytik Jena, Germany). A calibration curve was established, using six concentrations of the curcuminoids in a mixture of chloroform and methanol (1:1 v/v). The maximum absorption of the samples was at 429 nm. Each concentration was analyzed in triplicate. For the evaluation of the loading efficiency, three samples of 100  $\mu$ l were withdrawn from every produced formulation and were added to 10 ml of the chloroform/methanol mixture (1:1 v/v). The resulting solution was examined in triplicate by UV/Vis spectroscopy and the curcuminoid concentration was calculated by applying the aforementioned calibration curve. The curcuminoid content of the MTCurc-NE, TMCurc-NS and TSCurc-NS preparations was assessed few hours after the production and after one, two, three and twelve months of storage at 8 °C and protected from light.

### **3.4.2 Curcuminoid stability in physiological media**

The stability of the incorporated curcuminoids was determined in SGF, Sørensen phosphate buffer pH 6.8 and in enzyme-free FaSSIF. The investigated TMCurc-NE and TMCurc-NS preparations contained 0.01 % (w/w) curcuminoids. The preparations were diluted with the respective medium to a final curcuminoid concentration of 0.002 % (w/v) and put into glass vials. Every formulation was investigated in triplicate in the particular medium. The samples were placed into an orbital shaker which was vibrating with 800 rpm and heating the samples to 37 °C. At predefined time points (0, 1, 2, 4, 6 and 8 h), 200  $\mu$ l of the sample were withdrawn and given into 1.8 ml of a mixture of chloroform and methanol (1:1 v/v). The organic extracts were centrifuged at 1,100 x g for 5 minutes and afterwards quantified by UV/Vis spectroscopy as described above.

## **3.5 Biological in vitro characterization**

### **3.5.1 In vitro release**

The drug release of the TMCurc-NE and TMCurc-NS preparations was determined in SGF without enzyme, Sørensen phosphate buffer pH 6.8, in FaSSIF without enzyme and in FeSSIF without enzyme. Both formulations contained 0.01 % curcuminoids (w/w). The

preparations were diluted with the respective release medium to gain a drug concentration of 0.002 % (w/v). Samples of 200  $\mu$ l of the diluted sample were placed into the three cavities of an acryl block (Fig. 3.5-1 I). A dialysis membrane (regenerated cellulose,  $M_w$  cut-off: 6,000-8,000 Da, Spectrum Labs, USA) was gently put onto the cavities (Fig. 3.5-1 II). A second acryl block with holes congruent to the cavities was placed onto the membrane and the two blocks were screwed together tightly (Fig. 3.5-1 III). The block was put into the release medium, which was already heated to 37 °C (Fig. 3.5-1 IV).

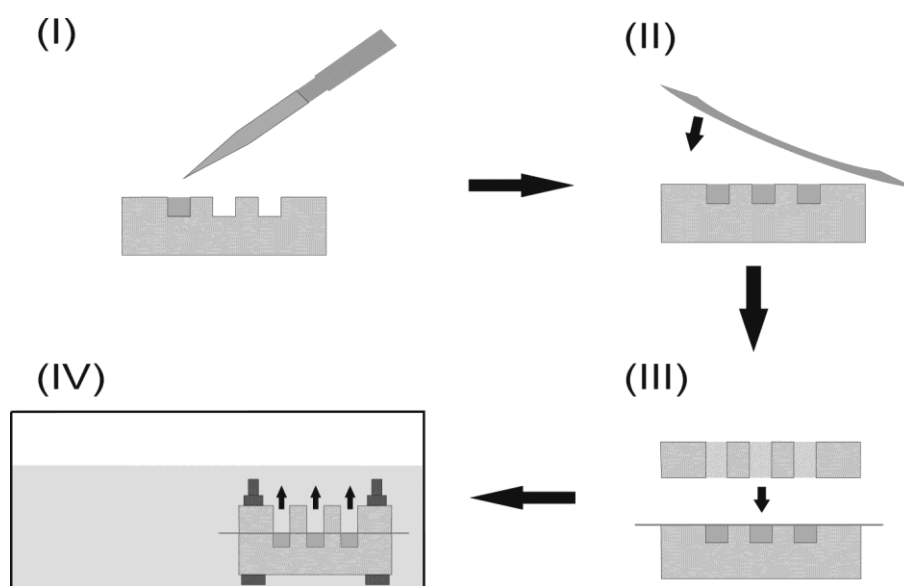


**Figure 3.5-1** Scheme of the preparation of the *in vitro* release model: (I) samples filled in cavities of the lower acryl block; (II) dialysis membrane placed onto filled cavities; (III) upper acryl block with congruent holes placed onto the lower block; (IV) chamber fixed with screws and placed in the tempered release medium.

The volume of release medium in the acceptor compartment provided sink conditions for the curcuminoids ( $c < c_s \cdot 0.1$ ). The vessel, containing the medium and the acryl block, was placed into an incubation shaker which was heated to 37 °C and shook with 30 rpm. At predefined time points (0, 15, 30, 60, 120, 180, 240, 360, 480 min) the block was removed from the medium and placed upside down in the Maestro™ *in vivo* fluorescence imaging system (Cambridge Research & Instrumentation, USA). The light source was a Cermax®-type 300 Watt Xenon lamp with 5600 K. A blue filter set (excitation: 445-490 nm, emission: 515 nm longpass) was used to detect the curcuminoid fluorescence. The Maestro™ software (Version 2.10) acquired multispectral image cubes in 10 nm steps in the range of 500 to 720 nm and the exposure time was set automatically (126). The fluorescence of the undiluted curcuminoid-loaded lipid nanoparticles was recorded prior



to the release experiments. Additionally, the autofluorescence of the curcuminoid-free medium and of the acryl block was determined. Thereby, the autofluorescence of the background and the curcuminoid fluorescence were distinguished in the obtained image cubes of the release model. For the result evaluation, the fluorescence of a single cavity at the named time points was related to the initial fluorescence of this cavity. The adsorption of the curcuminoids on the applied membrane was also investigated to verify the potential influence of this effect on the measurement. For this purpose, small pieces of the dialysis membrane were incubated in the different media supplemented with curcuminoid-loaded nanoparticles. After 0 h, 2 h, 4 h and 8 h the membranes were removed from the medium, rinsed with distilled water and the fluorescence was measured as described above.

### **3.5.2 *In vitro* digestion**

#### **3.5.2.1 *Applied media***

The effect of the gastric conditions on the nanoparticles was simulated by incubating the formulations in simulated gastric fluid (SGF, USP 31). Experiments were carried with enzyme-free medium and with medium containing 0.32 % (w/v) pepsin. The intestinal conditions were simulated with Sørensen phosphate buffer pH 6.8 (53.4 % (v/v)  $\text{KH}_2\text{PO}_4$  0.067 mol/l, 46.6 % (v/v)  $\text{Na}_2\text{HPO}_4 \cdot 2 \text{H}_2\text{O}$  0.067 mol/l) supplemented with 5 mmol/l bile extract and 1.25 mmol/l phospholipids for the fasted state (FaSSIF) and 15 mmol/l bile extract and 3.75 mmol/l phospholipids for the fed state (FeSSIF). Further, 150 mmol/l sodium chloride and 5 mmol/l calcium chloride were added and 450 U/ml of porcine pancreatin was used as enzyme source (127).

#### **3.5.2.2 *pH-stat method***

The digestion experiment was carried out under fasted and fed state conditions. The respective intestinal medium was heated to  $37 \text{ }^\circ\text{C} \pm 1 \text{ }^\circ\text{C}$  in a water bath and stirred with 1.200 rpm. The degradation velocity of MCTCurc-NE, TMCurc-NE, TMCurc-NS and TSCurc-NS was investigated. The respective lipid formulation was added to the digestion medium until a lipid concentration of 1 % (w/v) was obtained in the sample. For the blank samples the lipid preparation was replaced by the respective volume of phosphate buffer pH 6.8. A pH electrode connected to an autotitrator (DL 21, Mettler, Germany) was put into the liquid. The start-pH was manually adjusted to pH 6.8. By adding the aforementioned amount of pancreatin the digestion was started. The autotitrator kept the pH at 6.8 throughout the experiment by adding 0.1 mol/l sodium hydroxide (128). The experiment ran for 120 minutes and the cumulative consumption of sodium hydroxide was recorded.

Every formulation was investigated in triplicate under fasted and fed state conditions, respectively.

### **3.5.2.3 HPTLC/spectrodensitometry**

#### *Digestion under gastric conditions*

The digestion medium was filled into glass tubes and placed into an end-over-end shaker rotating with 10 rpm around its horizontal axis and heating the samples to  $37\text{ }^{\circ}\text{C} \pm 1\text{ }^{\circ}\text{C}$ . The investigated media were enzyme-free SGF and SGF containing pepsin (0.32 % (w/v)). TMCurc-NE or TMCurc-NS, respectively, were added to the medium until a lipid concentration of 1 % (w/v) was obtained. Both formulations were investigated in triplicate in each of the media. For the blank samples, the lipid preparation was replaced by the respective volume of SGF. After the lipid nanoparticles were added, the pH of the SGF was adjusted to pH 1.2 and placed in to the end-over-end shaker again. At predefined time points (0, 5, 10, 20, 30, 45, 60, 120 min) a sample of 100  $\mu\text{l}$  was withdrawn from the medium and added to 900  $\mu\text{l}$  of a mixture of chloroform and methanol (1:1 v/v). The organic extract was centrifuged for 5 min at 11,400 x g and the supernatant was filled into glass vials and stored in the dark at  $-20\text{ }^{\circ}\text{C}$  for further investigation. The samples were applied on silica gel plates (HPTLC Silica gel 60 F<sub>254</sub> GLP, Merck KGaA, Germany) and the fractions of free fatty acids, mono- di- and triglycerides were separated by HPTLC (AMD 2, CAMAG, Switzerland) employing an 11-step gradient based on hexane and ethyl acetate. Subsequently, the plates were submerged in a copper sulfate solution (15 % (w/v) copper sulfate pentahydrate, 8 % (w/v) phosphoric acid (85 % w/v), 5 % (v/v) methanol) for 20 seconds. Residual liquid was removed and the plates were heated in an oven at  $150\text{ }^{\circ}\text{C}$  for 50 minutes. The stains of the lipid derivatives were quantified by spectrodensitometric measurements at 675 nm [CAMAG TLC Scanner 3, (129)]. The quantitative amount of the respective lipid fraction was calculated from the calibration standards which were applied in a range of 0.25  $\mu\text{g}$  to 5  $\mu\text{g}$  on every plate. The detected lipids were standardized to myristic acid and its glycerol esters because the investigated lipid nanoparticles were solely built of trimyristin.

#### *Digestion under intestinal conditions*

FaSSIF or FeSSIF was filled into glass tubes and placed into an end-over-end shaker rotating with 10 rpm about its horizontal axis and heating the samples to  $37\text{ }^{\circ}\text{C} \pm 1\text{ }^{\circ}\text{C}$ . TMCurc-NE or TMCurc-NS was added to the medium until a lipid concentration of 1 % (w/v)

was obtained. Both formulations were investigated in triplicate in every medium. For the blank samples, the lipid preparation was replaced by the respective volume of phosphate buffer pH 6.8. After the addition of the adequate amount of lipid nanoparticles, the pH was adjusted to 6.8. Subsequently, the digestion was started by adding the pancreatin portion (450 U/ml). Thereafter, the samples were placed in the end-over-end shaker again. At predefined time points (0, 5, 10, 20, 30, 45, 60, 120 min) the pH of the medium was re-adjusted to 6.8 by the dropwise addition of a sodium hydroxide solution (1 mol/l). At the same time a sample of 100  $\mu$ l was withdrawn from the medium and added to 900  $\mu$ l of a mixture of chloroform and methanol (1:1 v/v). The organic solvents stopped the enzyme reaction and extracted the lipid fragments. The organic extract was centrifuged for 5 min at 11,400 x g and the supernatant was filled into glass vials and stored in the dark at -20 °C for further investigation. The application, development and analysis with HPTLC/spectrodensitometry were examined as described above.

#### **3.5.2.4 Drug solubilization**

A digestion experiment was carried out with TMCurc-NE and TMCurc-NS as described in chapter 3.5.2.2. Additionally, a blank sample supplemented with 0.01 % curcuminoid powder was also digested. The solubilized amount of curcuminoids was determined after the respective experiment was finished. Therefore, the remaining liquid was filled into a 15 ml plastic tube and centrifuged at 1,100 x g for 20 min. The supernatant was removed and again centrifuged for 10 min at 1,100 x g. Thereafter, three samples of 1 ml of the supernatant were transferred into 1.5 ml tubes and centrifuged for 5 min at 11,400 x g. 200  $\mu$ l of the clear supernatant were withdrawn and added to 1.8 ml of a mixture of chloroform and methanol (1:1 v/v). Again, the solution was centrifuged at 1,100 x g for 10 min and then examined by UV/Vis spectroscopy. The respective curcuminoid concentration was calculated by using the aforementioned calibration curve (see chapter 3.4.1).

### **3.5.3 Cell culture experiments**

A summary of the theory of the cell experiments is given in the Appendix.

#### **3.5.3.1 Cell culture and cell passaging**

Caco-2 cells were cultured with minimum essential medium (MEM) containing Earle's salts supplemented with 10 % (v/v) fetal bovine serum (FBS), 1 % (w/v) non-essential amino acids, 1 % (w/v) L-glutamine and 50  $\mu$ g/ml gentamicin at 37 °C in a humidified 5 % CO<sub>2</sub>/95 % air atmosphere. The cells were grown in cell culture flasks with 25 cm<sup>2</sup> surface

area and a filter screw cap, containing a PET filter with a pore size of 0.2  $\mu\text{m}$  (Greiner Bio-One, Germany).

Cells were harvested at a confluency of 80-90 %. First, the medium was removed and the cells were washed two times with 5 ml sterile PBS (2.7 mmol/l KCl, 137 mmol/l NaCl, 1.4 mmol/l  $\text{KH}_2\text{PO}_4$ , 4.3 mmol/l  $\text{Na}_2\text{HPO}_4$ , pH 7.4). Thereafter, the cells were treated with 1 ml of a 0.25 % (w/v) trypsin/0.02 % (w/v) EDTA solution for 5 min at 37 °C to detach the cells from the flask surface. The reaction was stopped by the addition of 5 ml MEM containing 10 % (v/v) FBS (130). The cell suspension was transferred into a tube and centrifuged for 10 min at 250 rpm (Z400K, Hermle, Germany). After centrifugation, the supernatant was removed and 900  $\mu\text{l}$  medium was added. The cell pellet was suspended in the medium until no aggregates were visible anymore. The cell suspension was further diluted with medium and the cells were counted using a Neubauer counting chamber.  $8 \times 10^5$  cells were seeded into a new culture flask and incubated as described above.

### 3.5.3.2 QBlue viability assay

The cytotoxicity of curcuminoid-free lipid nanoparticles, curcuminoid-loaded lipid nanoparticles and of free, crystalline curcuminoids was investigated. The respective formulations were diluted with serum-free MEM to the respective test concentration, shown in Table 3.5-1.

**Table 3.5-1 Overview of the examined formulations and the applied concentrations of the components.**

Sample	Initial lipid concentration	Applied lipid concentration	Initial curcuminoid concentration	Applied curcuminoid concentration
Curcuminoid-free preparations <sup>a</sup>	100 mg/ml	250 $\mu\text{g}/\text{ml}$ and 25 mg/ml	-	-
Curcuminoid-loaded preparations <sup>b</sup>	100 mg/ml	250 $\mu\text{g}/\text{ml}$ and 25 mg/ml	1 mg/ml	250 $\mu\text{g}/\text{ml}$ (680 $\mu\text{mol}/\text{l}$ ) and 25 $\mu\text{g}/\text{ml}$ (68 $\mu\text{mol}/\text{l}$ )
Curcuminoid stock solution (in DMSO)	-	-	25 mg/ml - 1 mg/ml	250 - 5 $\mu\text{g}/\text{ml}$ (680 - 14 $\mu\text{mol}/\text{l}$ )
<b>Additional tested samples</b>				
Poloxamer solution in serum-free MEM	Test concentration: 6.25 mg/ml			
DMSO in serum-free MEM	Test concentration: 1 % (v/v)			

<sup>a</sup> tested formulations: MCT-NE, TM-NE, TM-NS, TS-NS

<sup>b</sup> tested formulations: MCTCurc-NE, TMCurc-NE, TMCurc-NS, TSCurc-NS

The Caco-2 cells were harvested as previously described. The gained cells were subsequently seeded into a colorless 96-well plate reaching a concentration of 5,000 cells per well. The well-plate was incubated for 2 days at 37 °C in a humidified 5 % CO<sub>2</sub>/95 % air atmosphere to allow attachment and growth of the cells. Afterwards, the old medium was removed and 100 µl of the mentioned test solutions, containing the particular formulation, were given onto the cells (Table 3.5-1). The cells were incubated for another 24 h at the aforementioned conditions. Every formulation was investigated in triplicate. Cells incubated with pure serum-free MEM were used as control. After the incubation time of 24 h, the test solutions were removed and the cells were washed two times with serum-free MEM. After washing, 100 µl MEM and 10 µl of pre-warmed QBlue reagent (0.08 % w/v resazurin, BioChain, USA) were added to every well. The well plate was incubated for 3 h at 37 °C. Thereafter, 100 µl medium were removed from every well and transferred to a black 96 well plate. The fluorescence intensity of the wells was measured with a plate reader [excitation: 544 nm, emission: 590 nm, FLUOstar, BMG Labtech, Germany, (130)]. The median and the span of the fluorescence intensity values of the corresponding wells were determined. The relative cell viability was calculated by dividing the fluorescence intensity of the samples with the fluorescence intensity of the control.

## 4. Results and Discussion

### 4.1 *Critical parameters of the particle production*

The major objective of the homogenizing process was the fabrication of a stable formulation with a narrow particle size distribution. Furthermore, no particles with a diameter larger than 1  $\mu\text{m}$  should be present in the final product. The course of the homogenizing cycles was therefore tailored to the aforementioned aims. A small mean particle size was seen as a desirable attribute of the formulations, because small particles present a higher surface for the interaction with mucosal tissue in the gastro-intestinal tract. However, the presence of a small quantity of bigger particles e.g. > 1  $\mu\text{m}$ , was not seen as critical, because the preparations were intended for oral use and not for intravenous administration. The applied homogenizing regime resulted in a distinct reduction of the size, which was subsequently followed by a decreasing size distribution. Hence, the attainment of a narrow size distribution was closely connected with a small particle size.

The resulting product characteristics were found to be influenced by different parameters, such as applied lipid, applied emulsifier and temperature. Three of these parameters and their influence on the end product are discussed in the following:

#### *Lipid*

The present work focused on the formulation of lipid nanoparticles, based on triglycerides. Both, oils and high melting lipids, were tested. The application of different oils resulted in huge differences of the resulting particle size distribution of the nanoemulsions (Fig. 4.1-1). The particle size distribution of castor oil based emulsions was much broader compared to the MCT nanoemulsions, although the same homogenizing regime was applied. The soy bean nanoemulsion exhibited a particle size between castor oil and MCT. The different viscosities of the oils were thought to be the main reason for the observed size differences. Castor oil is a highly viscous oil ( $\eta \sim 1000 \text{ mPa}\cdot\text{s}$ ), whereas MCT and soy bean oil are low viscous ( $\eta \sim 30 \text{ mPa}\cdot\text{s}$  and  $\sim 60 \text{ mPa}\cdot\text{s}$ , respectively). Thus, the disruption of the castor oil droplets within the homogenizing valve is more difficult compared to the other oils. As a consequence, the castor oil formulations should have been processed with higher pressures and at higher temperatures to attain particle sizes comparable with, e.g. MCT. However, a further increase of pressure and temperature was not possible, due to constructional limitations of the homogenizer. MCT was chosen as model for the further investigation of curcuminoid-loaded nanoemulsions, because it was

the most suitable oil, providing an unproblematic production, a narrow size distribution and a sufficient stability.

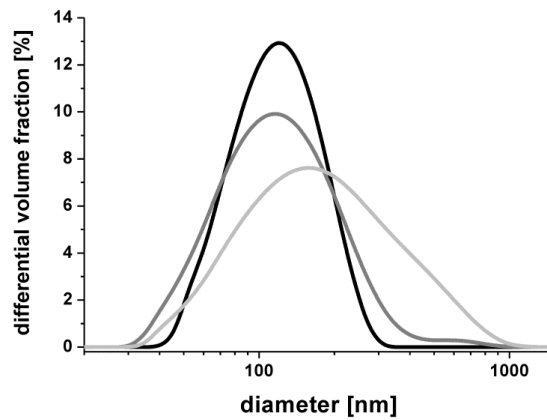


**Figure 4.1-1** Size distribution curves, recorded by LD, of nanoemulsions containing MCT (black curve); soy bean oil (grey curve) and refined castor oil (light grey curve). The emulsifier was 2.5 % (w/v) poloxamer 188. The given distribution curves are the average results of five measurements of one sample.

As solid lipids, TM and TS were evaluated. The resulting nanoparticles exhibited a broader particle size distribution than the MCT-based nanoemulsions (see chapter 4.2.1). The processing of solid lipids to nanoparticles affected the melting and crystallization behavior of the triglycerides, the drug incorporation and the *in vitro* digestability (see chapters 4.3.2, 4.3.5, 4.5.2).

The maintenance of a temperature above the melting point of TM and TS was of crucial relevance for the successful production of the particles. Hence, the process was executed under constant heating of the beaker, containing the preparation, the pump and the homogenizing valve. As a rule of thumb, the temperature during homogenization was set 5 °C above the actual melting point of the lipid. An insufficient heating of the formulation resulted in some cases in an unwanted recrystallization of the lipid. This, in turn, caused a blockade of the machine, which necessitates a time consuming dismantling and cleaning. The homogenizing process was especially sensitive to lipid recrystallization at the beginning of the production, when the particles were sufficiently large to block the homogenizer pipes.

## Emulsifier

The influence of emulsifiers on various properties of lipid nanoparticles, e.g. melting point, modification, morphology, digestability, was discussed in literature before (100,121,131,132). Furthermore, the particle size distribution can also be influenced by the applied emulsifier. The use of two different emulsifiers for the production of castor oil nanoemulsions resulted in considerably different size distributions (Fig. 4.1-2 A). Solutol<sup>®</sup> HS 15 in combination with lecithin (Lipoid S45) was directing the droplets to smaller particle sizes and a narrower distribution, in comparison to the poloxamer-stabilized formulations. Though, the differences between the particle size distributions of MCT-NE, processed with different emulsifiers, were only negligible (Fig. 4.1-2 B).

From all tested emulsifiers, poloxamer 188 was chosen as stabilizer for all further experiments, because of the following reasons:

- easy preparation of the stock solution
- hydrolytic stability
- up to 85 °C no clouding phenomena observed (phase inversion temperature)
- narrow particle size distribution of the lipid nanoparticles (MCT, TM and TS)
- good long-term stability of the produced formulations
- no gelation of the solid nanoparticles during storage

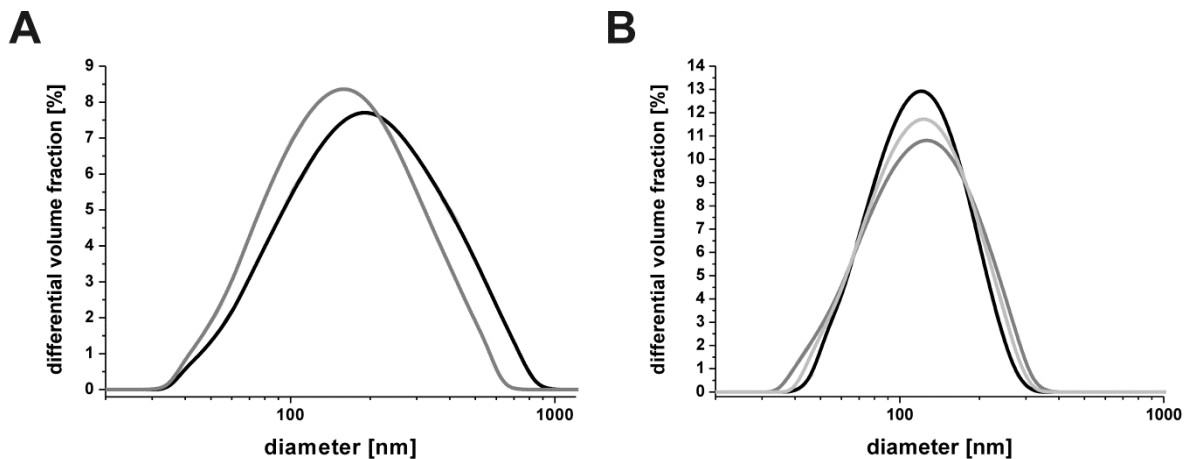


Figure 4.1-2 Size distribution curves, recorded by LD, of samples of (A) RCO-NE stabilized with 2.5 % (w/v) poloxamer 188 (black curve) and 2 % (w/v) Solutol<sup>®</sup> HS 15/0.5 % (w/v) lecithin (grey curve) and (B) MCT-NE stabilized with 2.5 % (w/v) poloxamer 188 (black curve), 2.5 % (w/v) poloxamer 407 (grey curve) and 2.5 % Cremophor<sup>®</sup> RH 40 (light grey curve). The given distribution curves are the average results of five measurements of one sample.



### *Homogenizing regime*

The particle reduction by a high pressure homogenizer is mainly dependent on the applied pressure as well as on the number of homogenizing cycles. Different homogenizing regimes have been tested in preliminary studies and the process protocol described in chapter 3.1 was found to be the most suitable one. The decrease of the particle size during the production process can be seen in Fig. 4.1-3. The droplet size of the crude emulsion, formed by the Ultra Turrax, was between 5  $\mu\text{m}$  - 50  $\mu\text{m}$ . Moreover, the emulsion droplets showed rapid creaming and the shearing with the Ultra-Turrax caused foaming. At the beginning, the crude emulsion, formed by the Ultra-Turrax, was processed with one cycle (pre-cycle) at low pressure. The first cycle turned the crude emulsion into a more stable intermediate product (Fig. 4.1-3 A). In addition, the foam was removed successfully. During the next nine cycles the pressure was increased stepwise and the particle size decreased continuously (Fig. 4.1-3 B-D). The gradual increase of the pressure spared the homogenizing equipment and the particle size distribution was decreased evenly. The application of three cycles for every pressure step assured the complete processing of the whole sample. The final cycle at 50 MPa removed the residual fraction of larger particles and a monomodal size distribution was gained (Fig. 4.1-3 E). The removal of this side fraction between 500 nm and 800 nm was not achieved for all preparations (see chapter 4.2.1). Actually, the occurrence of this phenomenon could not be finally explained. It was suggested that a partial blockade of the second stage pressure by the high melting lipid, resulting in a dysfunction of this part, was the underlying cause. The filtration step, which followed the homogenizing process, did not alter the particle size distribution (Fig. 4.1-3 F). The filtration was seen as necessary to remove particles larger than 1  $\mu\text{m}$ , which probably escaped appropriate size reduction during homogenizing. The presence of such particles within the preparation might cause stability problems during long-term storage by accelerating particle agglomeration.

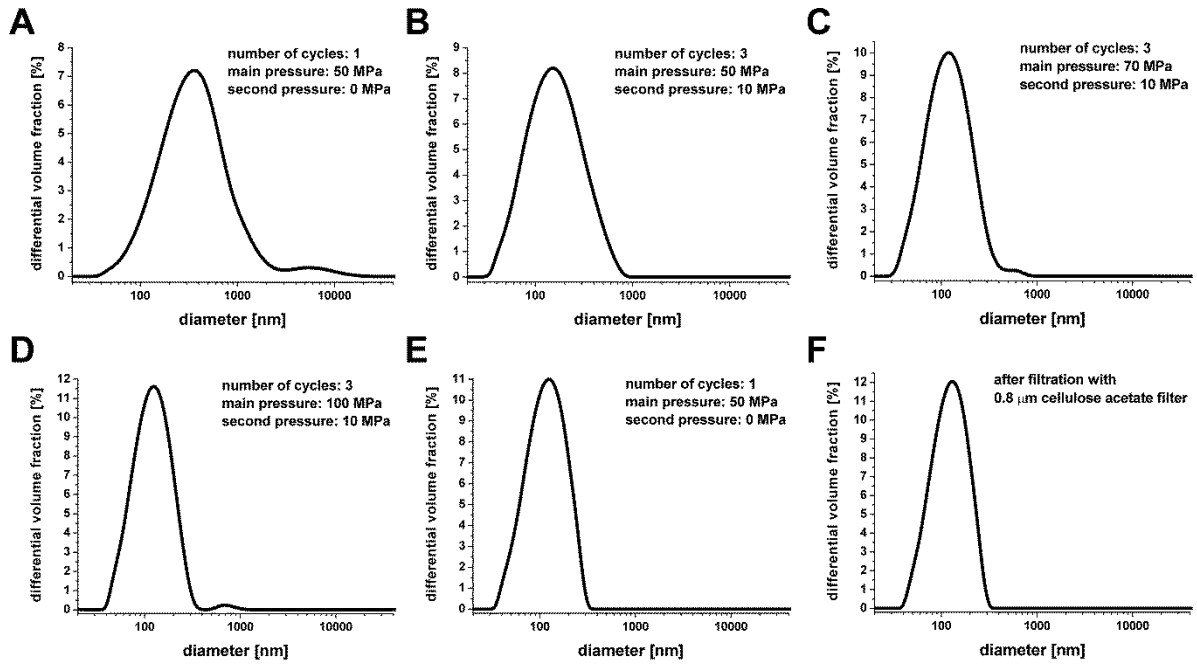


Figure 4.1-3 Size distribution curves, recorded by LD of samples of TM-NE after the (A) 1<sup>st</sup> stage (“pre-cycle”), (B) 2<sup>nd</sup> stage, (C) 3<sup>rd</sup> stage, (D) 4<sup>th</sup> stage and the (E) 5<sup>th</sup> stage (“end cycle”) of the homogenizing process and after the (F) filtration step. The given distribution curves are the average results of five measurements of one sample.

## 4.2 Particle characteristics

### 4.2.1 Particle size distribution

The MCT-NE preparations had a small and narrow size distribution (Fig. 4.2-1). The mean particle size was found to be approximately 130 nm. The TM nanoparticles exhibited mean particle sizes of up to 161 nm and had a broader distribution compared to MCT. The particle size distributions of the TS preparations were similar to the TM formulations. The  $d_{90}$  was below 300 nm for every formulation (Tab. 4.2-1). The incorporation of the curcuminoids did not alter the particle size distribution of the drug-loaded nanoparticles in comparison to the drug-free preparations. Besides the broader main peak, TM and TS nanoparticles also showed a small side peak between 600 - 800 nm (Fig. 4.2-1, arrow). The investigation of these formulations in a light microscope revealed no particles bigger than 1  $\mu\text{m}$ .

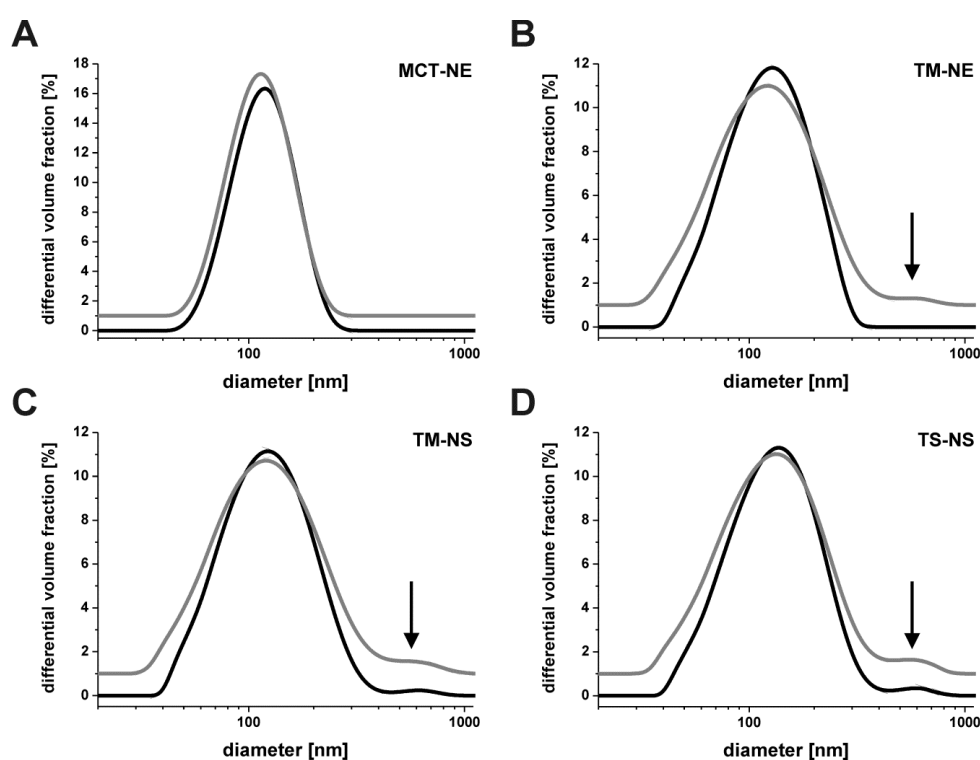


Figure 4.2-1 Size distribution curves recorded by LD of a sample of (A) MCT-NE; (B) TM-NE; (C) TM-NS and (D) TS-NS. Black curves are the drug-free preparations. Grey curves are the curcuminoid-loaded nanoparticles. The grey curves were shifted along the ordinate by 1 % for better visualization. The arrows point to the small side fraction exhibited by some preparations. The given distribution curves are the average results of five measurements of one sample.

The z-average diameters of MCT-NE and MCTCurc-NE were 130 and 137 nm respectively and the PDI was 0.07. The respective mean values of PCS and LD were in good agreement for these samples which pointed to a narrow and monomodal size distribution of the MCT based nanoemulsions. The other formulations exhibited z-average diameters in the range of 153 - 205 nm with a PDI below 0.12. The side peak of the TM and the TS preparations, which was detected by LD was not found with PCS. The calculated mean diameters of the PCS and LD measurements differed distinctly for these samples (Tab. 4.2-1). Generally, the z-average diameter estimated by PCS tended to be higher compared to the mean diameter estimated by LD. It was concluded that the aforementioned side fraction between 600 and 800 nm of the TM and TS formulations was causing the discrepancies between the applied particle sizing techniques. Furthermore, the anisometric shape of the particles in the crystalline samples (TM-NS and TS-NS) must be taken into account as well (see chapter 4.2.3 and 4.2.4). One should keep in mind that it remains difficult for light scattering techniques, like PCS and LD to describe the size of non-spherical particles properly. In contrast to a sphere, the size of an anisometric particle cannot be described with one single size parameter, like the diameter, because the dimensions of anisometric particles are different in the respective spatial orientation. The applicability of the light scattering techniques, potential pitfalls during result calculation and suggestions for the correct interpretation of the gained results were discussed in literature recently (133,134).

**Table 4.2-1 Particle size distribution of the developed formulations, determined by LD and PCS. Z-averages are given as mean  $\pm$  standard deviation of three measurements of one sample. The given PDI is the mean of three measurements. The LD values are given as average results of five measurements of one sample.**

Sample	PCS		LD			
	<i>z</i> -Av. (nm)	PDI	<i>d</i> <sub>10</sub> (nm)	Median (nm)	Mean (nm)	<i>d</i> <sub>90</sub> (nm)
MCT-NE <sup>a</sup>	137.7 $\pm$ 0.6	0.07	83	125	130	185
MCTCurc-NE <sup>b</sup>	130.0 $\pm$ 1.7	0.07	80	120	126	179
TM-NE <sup>a</sup>	153.7 $\pm$ 0.6	0.1	73	130	139	220
TMCurc-NE <sup>b</sup>	165.0 $\pm$ 0	0.1	67	132	152	258
TM-NS <sup>a</sup>	170.7 $\pm$ 0.6	0.12	71	130	146	235
TMCurc-NS <sup>b</sup>	185.0 $\pm$ 1.0	0.12	66	130	157	266
TS-NS <sup>a</sup>	194.3 $\pm$ 1.5	0.07	75	140	156	246
TSCurc-NS <sup>b</sup>	205.0 $\pm$ 1.0	0.11	69	137	161	267

<sup>a</sup>composition: 10 % (w/w) lipid, 2.5 % (w/w) poloxamer 188

<sup>b</sup>composition: 10 % (w/w) lipid, 2.5 % (w/w) poloxamer 188, 0.05-0.1% (w/w) curcuminoid

In summary, the evaluation of a particle size distribution strongly depends on the applied method and on the properties of the examined particles. However, it is vital that the applied particle measuring technique is capable of detecting fractions of larger particles (> 700 nm), because these particles may influence the stability of the preparation. The prepared TM- and TS-based nanoparticles showed a broad distribution and a distinct particle fraction bigger than 700 nm. Therefore, the LD measurements should be seen as more applicable for the evaluation of the particle size distribution TMCurc-NS and TSCurc-NS, because fractions of particles > 700 nm are estimated more reliable with this technique. A determination of the particle size distribution solely with PCS measurements was seen as insufficient for the characterization of the formulations.

#### **4.2.2 Particle long-term stability**

The batches of MCTCurc-NE, TMCurc-NE, TMCurc-NS and TSCurc-NS, investigated for 12 months, exhibited the same particle size characteristics as the batches presented in chapter 4.2.1. The mean diameters of all preparations were well below 200 nm (Tab. 4.2-2). The MCT-based nanoparticles had a narrow size distribution and the smallest mean diameter. The TM nanoparticles showed a larger mean particle size and a slightly broader size distribution. The TS-based nanoparticles exhibited the broadest distribution and the largest mean diameter. The differences between drug-free and curcuminoid-loaded preparations were again negligible, and were not attributed to the presence of the curcuminoids. In general, the long-term observation revealed a variation of the characteristic particle size values of  $\pm 10$  nm for almost all preparations, which was seen as normal fluctuation. However, for MCT-NE, MCTCurc-NE and TSCurc-NS an increasing  $d_{90}$  value was recorded indicating a growing fraction of bigger particles. On the contrary, the mean diameter of these preparations increased only slightly. The appearance of bigger particles within the MCT and TSCurc-NS preparations pointed to a partial agglomeration or coalescence, respectively, of the nanoparticles. There was found no satisfying explanation for the occurrence of the described particle agglomeration in the MCT and TS-based samples, only. However, the increase of the particle size was thought to be non-serious for the overall stability of these preparations. Moreover, the investigation of the mentioned samples with a light microscope (Axiolab, Zeiss, Germany) revealed no agglomerates larger than  $1 \mu\text{m}$ .

Table 4.2-2 Particle size distribution of the developed formulations, determined by LD. The size distribution was determined few hours after production and after 6 months and 12 months of storage at 8 °C or 22 °C, respectively. The LD values are given as average results of five measurements of one sample.

Sample	$d_{10}$ [nm]	Median [nm]	Mean [nm]	$d_{90}$ [nm]
MCT-NE <sup>a</sup> fresh	83	125	130	185
MCT-NE <sup>a</sup> 6 months	79	131	138	208
MCT-NE <sup>a</sup> 12 months	79	136	143	216
MCTCurc-NE <sup>b</sup> fresh	80	120	126	179
MCTCurc-NE <sup>b</sup> 6 months	82	132	137	200
MCTCurc-NE <sup>b</sup> 12 months	77	131	138	208
TM-NE <sup>a</sup> fresh	73	130	139	220
TM-NE <sup>a</sup> 6 months	69	133	143	235
TM-NE <sup>a</sup> 12 months	76	136	145	226
TMCurc-NE <sup>b</sup> fresh	65	127	147	246
TMCurc-NE <sup>b</sup> 6 months	65	129	148	253
TMCurc-NE <sup>b</sup> 12 months	69	132	144	236
TM-NS <sup>a</sup> fresh	71	130	146	235
TM-NS <sup>a</sup> 6 months	64	121	134	223
TM-NS <sup>a</sup> 12 months	68	128	139	227
TMCurc-NS <sup>b</sup> fresh	66	130	157	256
TMCurc-NS <sup>b</sup> 6 months	63	123	147	246
TMCurc-NS <sup>b</sup> 12 months	65	125	150	241
TS-NS <sup>a</sup> fresh	75	140	156	246
TS-NS <sup>a</sup> 6 months	74	138	157	250
TS-NS <sup>a</sup> 12 months	74	136	156	247
TSCurc-NS <sup>b</sup> fresh	69	137	161	267
TSCurc-NS <sup>b</sup> 6 months	68	140	179	333
TSCurc-NS <sup>b</sup> 12 months	67	137	176	319

<sup>a</sup>composition: 10 % (w/w) lipid, 2.5 % (w/w) poloxamer 188

<sup>b</sup>composition: 10 % (w/w) lipid, 2.5 % (w/w) poloxamer 188, 0.05-0.1% (w/w) curcuminoid

### 4.2.3 Transmission electron microscopy

The detailed geometry of the nanoparticles was investigated by preparing TEM micrographs. Images of the MCT and TM nanoemulsions prepared by the negative stain technique exhibited the expected round droplets (Fig. 4.2-2). The droplet size of the MCT nanoemulsion was between 60 nm and 150 nm. The droplets of the TM nanoemulsion had diameters between 110 nm and 500 nm. Thus, the TM nanoparticles had a much broader particles size distribution compared to the MCT droplets. However, the droplet sizes, estimated in the micrographs, were overall bigger compared to the values obtained by LD and PCS, which was caused by the spreading of the droplets on the copper grid during the preparation. In addition, a coalescence of the droplets has probably occurred during the preparation, too. This effect was thought to be the reason for the large diameters of the TM droplets in the TEM micrographs. Therefore, the values determined in the micrographs were not regarded as correct droplet diameters of the nanoemulsions.

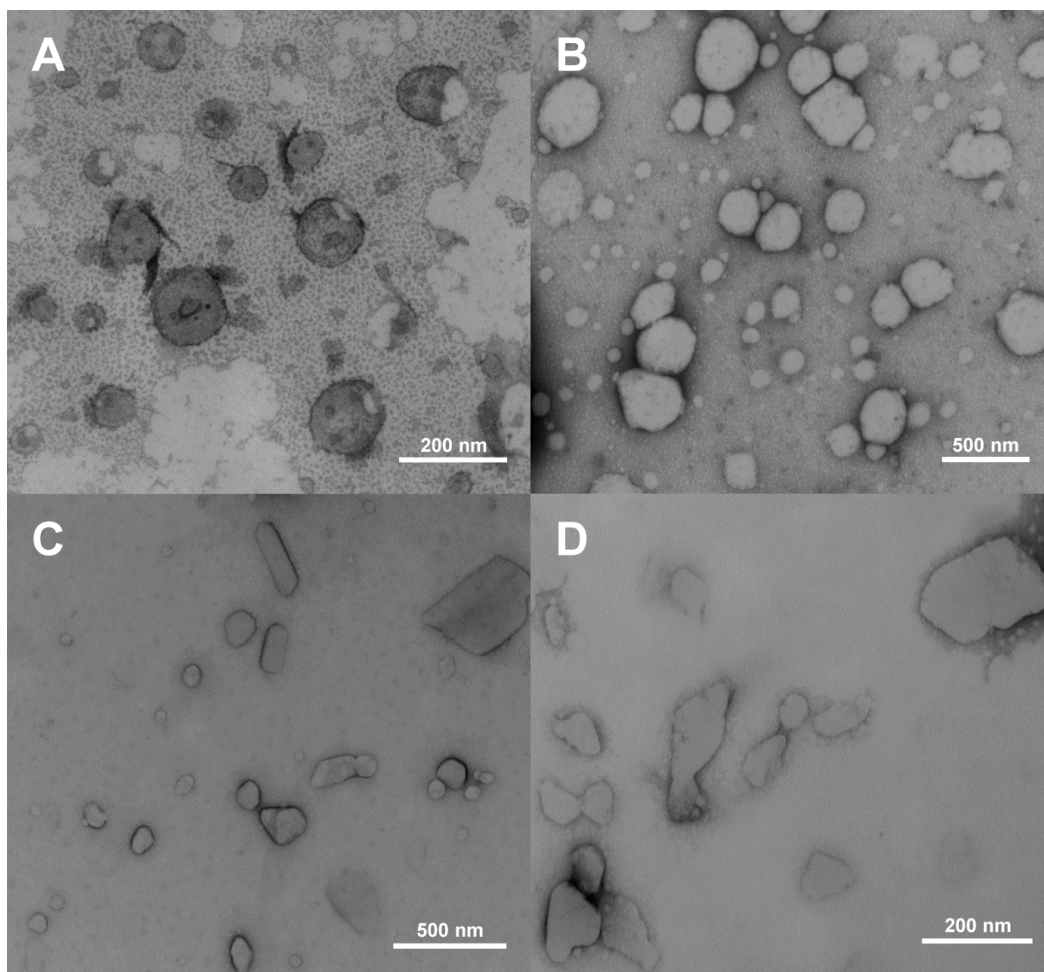


Figure 4.2-2 TEM micrographs of (A) MCTCurc-NE; (B) TMCurc-NE; (C) TMCurc-NS and (D) TSCurc-NS. The samples were prepared by negative staining. The obtained images were corrected for brightness and contrast.

The solid lipid nanoparticles revealed an anisometric structure with a huge diversity in shape (Fig. 4.2-2 C & D). The observed geometries were rotund, rhombic or completely irregular. Generally, smaller particles appeared more round or oblong, whereas the bigger particles revealed a platelet structure typical for lipid particles in  $\beta$ -modification (100). The size determination of the crystalline particles was omitted, because of the huge geometric diversity of the particles. A plain position of the particles on the used copper grid was further not verifiable. If the particles were not located plainly on the copper grid, a size determination via the micrographs would have resulted in erroneous values. The nanoparticles were also sticking together and overlapping, due to the drying of the sample during the staining procedure. A distinction between the particles was therefore often not possible.

From the freeze-fractured samples a lamellar structure of the lipid matrices could be suggested (Fig. 4.2-3). The overall thickness of the examined particles was between 50 to 70 nm. The thickness of one single molecular layer inside the TM and the TS particles was determined by X-ray diffraction to be 3.5 and 4.5 nm respectively. Therefore, these particles consisted of approximately fifteen single layers.

The TEM micrographs were of great value for the verification of the geometric structure of the solid nanoparticles. The form of the SLN was shown to be dependent on the actual size of particle. Generally, the particle appearance was turning into a platelet form with increasing particle size. However, the images, obtained by freeze-fracture, illustrated that the combination of poloxamer and triglyceride resulted in a compact, block-like structure of the nanoparticles. In contrast, it was reported by other research groups that the application of phospholipids as emulsifier was leading to much thinner platelets with a thickness 10 molecular layers or less (132).



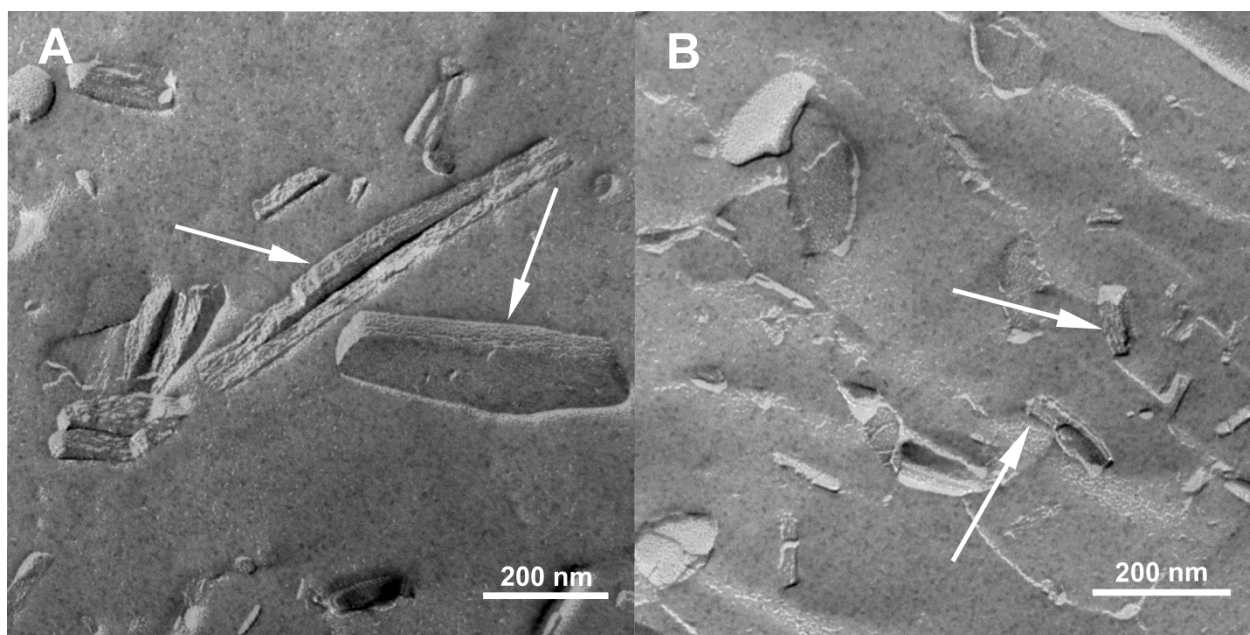


Figure 4.2-3 TEM micrographs of (A) TMCurc-NS and (B) TSCurc-NS. The samples were prepared by freeze-fracture. The obtained images were corrected for brightness and contrast. The arrows highlight the lamellar surface of fractured particles.

## 4.2.4 Asymmetric flow field-flow fractionation

### 4.2.4.1 Particle size analysis

The investigation of the lipid nanoparticles with AF4 provided information about the particle size distribution of the samples. A first impression of the size distribution was gained by the diameter versus time-curves (d-vs-t). Their size interval appeared different for the respective formulations (Fig. 4.2-4). The size interval of the d-vs-t curve was between 80 nm and 300 nm for MCTCurc-NE (Fig. 4.2-4 A). The respective intervals of the d-vs-t curves got broader for TMCurc-NE, TMCurc-NS and TS Curc-NS, which pointed to a larger mean particle size and a broader size distribution of these samples (Fig. 4.2-4 B-D). The calculated mean diameters (z-average and mass weighted mean) are presented in Table 4.2-3. It was found that the mean particle sizes were increasing in the order MCTCurc-NE < TMCurc-NE < TMCurc-NS < TS Curc-NS.

The calculation of the mass weighted distribution curves confirmed the narrow and monomodal size distribution of MCTCurc-NE (Fig. 4.2-5 A, grey curves). The peak maximum of the differential mass weighted distribution curve was at around 110 nm for MCTCurc-NE. The differential distribution curve of TMCurc-NE revealed a broader distribution than MCTCurc-NE with a small peak at approximately 100 nm (Fig. 4.2-5 A, black curves). The slope of the cumulative distribution curves was steeper for MCTCurc-NE

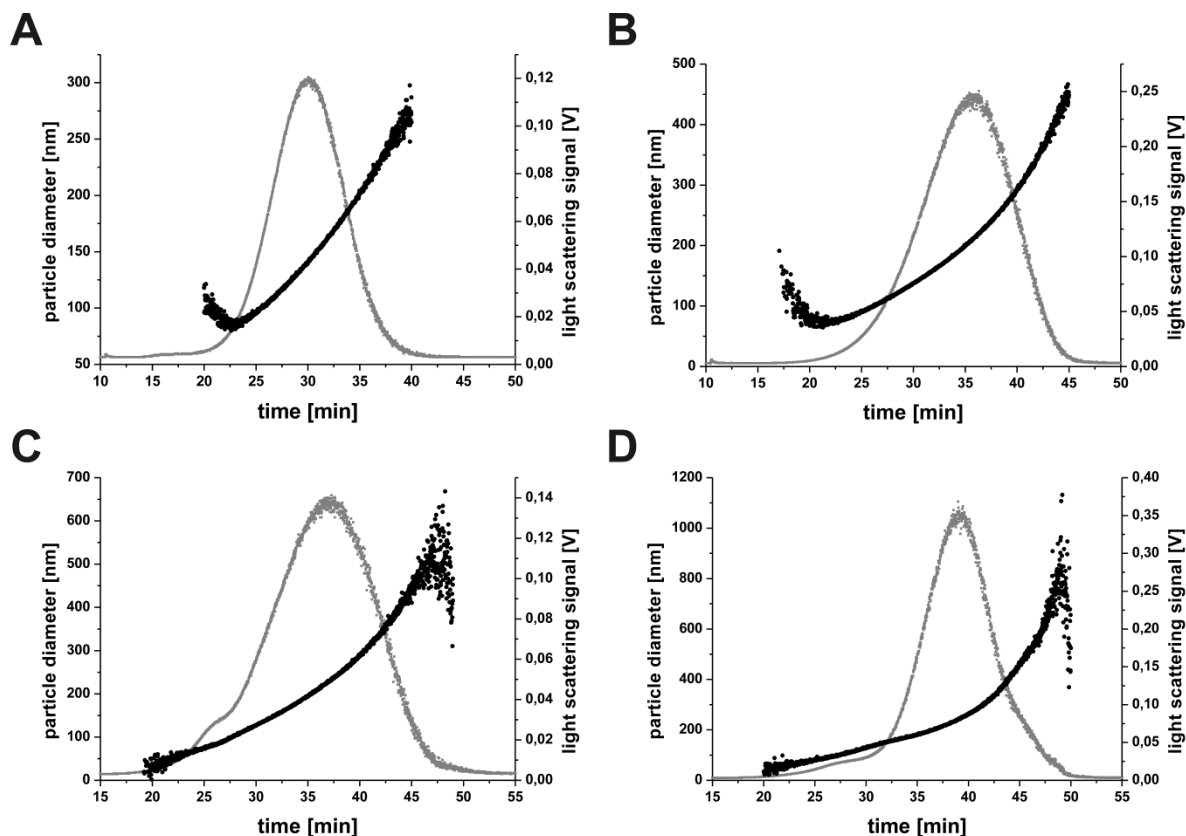


Figure 4.2-4 AF4/MALLS elution profiles of a sample of (A) MCTCurc-NE, (B) TMCurc-NE, (C) TMCurc-NS and (D) TSCurc-NS. (●)  $d_{RMS}$ , (●) scattered light intensity at a detector angle ( $\theta$ ) of  $90^\circ$ .

than for TMCurc-NE, which further verified the narrower size distribution of the MCT-based nanoemulsion. The crystalline TMCurc-NS and TSCurc-NS preparations had a broad and multimodal mass weighted size distribution (Fig. 4.2-5 B). The peak maximum of the differential distribution curves was at around 230 nm for both samples. Additionally, there was a peak at smaller particle sizes fraction ( $< 150$  nm) in both samples. This fraction appeared to be larger for TMCurc-NS than for TSCurc-NS. On the contrary, TSCurc-NS showed a distinct fraction of particles  $> 450$  nm. The characteristic particle sizes  $d_{10}$ ,  $d_{50}$  and  $d_{90}$ , obtained from the cumulative distribution curves, of all investigated samples are summarized in Table 4.2-3.

The comparison of the AF4/MALLS data with the LD data revealed both concordant and divergent results. The primary size results,  $d_{GEOMZ}/d_{RMSZ}$  and  $d_{GEOMW}/d_{RMSW}$ , calculated from the MALLS raw data, were much larger than the mean diameter obtained by LD (Tab. 4.2-3 and Tab. 4.2-4). This discrepancy was explained by the influence of larger particles on the size calculation from the MALLS data. The z-average diameter and the mass weighted mean diameter, gained by AF4/MALLS, are calculated over the whole peak area and therefore the

Table 4.2-3 Characteristic diameters of the curcuminoid-loaded preparations, determined by AF4/MALLS.  $d_{GEOmz}/d_{RMSz}$ : z-average diameter.  $d_{GEOmw}/d_{RMSw}$ : mass weighted diameter. Given size values are the mean  $\pm$  standard deviation ( $n=3$ ).

Sample	$d_{GEOmz}$ [nm]	$d_{GEOmw}$ [nm]	$d_{10}$ [nm]	$d_{50}$ [nm]	$d_{90}$ [nm]
<i>MCTCurc-NE</i>	158.1 $\pm$ 3.5	192.7 $\pm$ 4.2	91.3 $\pm$ 5	121.7 $\pm$ 1.6	172.4 $\pm$ 6.7
<i>TMCurc-NE</i>	291.1 $\pm$ 5.1	279.4 $\pm$ 6.3	86.3 $\pm$ 3.3	154.2 $\pm$ 1.7	263.3 $\pm$ 1.3
Sample	$d_{RMSz}$ [nm]	$d_{RMSw}$ [nm]	$d_{10}$ [nm]	$d_{50}$ [nm]	$d_{90}$ [nm]
<i>TMCurc-NS</i>	379.1 $\pm$ 2.2	329.6 $\pm$ 2.4	138.3 $\pm$ 3.6	270.5 $\pm$ 1.8	480.2 $\pm$ 3.6
<i>TSCurc-NS</i>	492.8 $\pm$ 10.7	316.9 $\pm$ 6.9	180.7 $\pm$ 1.1	300.9 $\pm$ 12.5	621.5 $\pm$ 12.2

presence of a small quantity of larger particles has a huge impact on the resulting mean diameter. Especially *TMCurc-NS* and *TSCurc-NS* had a distinct fraction of particles larger than 400 nm, as it can be seen from the differential distribution curves. Therefore, the largest differences between AF4/MALLS and LD are also found for these samples. An overestimation of particles larger than 500 nm during size calculation from the AF4/MALLS raw data has been reported before (133). Kuntsche and co-workers suggested that the requirements of the RGD approximation were not fulfilled anymore for these particles and size calculation was therefore erroneous (133).

On the contrary, the curves of the differential mass weighted size distributions correspond overall well to the recorded LD curves (Fig. 4.2-5 and Fig. 4.2-1) and the tendency of an increasing particle size from *MCTCurc-NE* to *TSCurc-NE* was also confirmed by all other

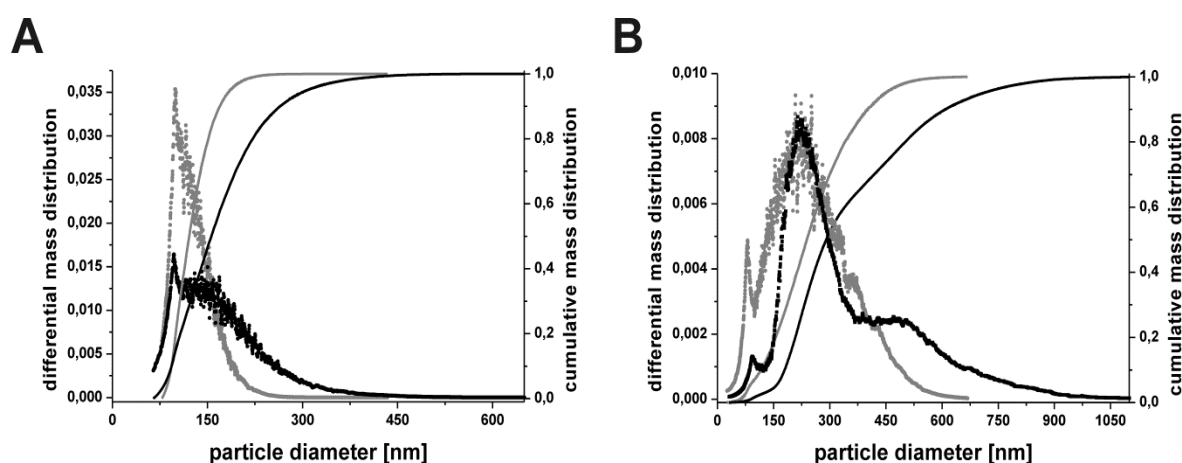


Figure 4.2-5 Mass weighted size distributions of (A) black curves: *TMCurc-NE*, grey curves: *MCTCurc-NE* and (B) black curves: *TSCurc-NS* and grey curves: *TMCurc-NS*. Dots represent the differential distributions. Lines represent the cumulative distributions. Size distributions were calculated from the raw data of the samples presented in Fig. 4.2-4.

applied particle sizing techniques. The small particle size and narrow size distribution of MCTCurc-NE was shown consistently by all methods, too. In addition, the fraction of particles larger than 500 nm in the TMCurc-NS and TSCurc-NS preparations was detected by AF4/MALLS and LD. However, the particle fraction < 150 nm of TMCurc-NS and TSCurc-NS was only revealed by AF4/MALLS.

The characteristic size values  $d_{10}$ ,  $d_{50}$ , derived of the cumulative distribution curves were comparable with the corresponding LD values for MCTCurc-NE and TMCurc-NE (Tab. 4.2-3 and Tab. 4.2-4). In contrast, the MALLS-derived  $d_{90}$  was much larger than the  $d_{90}$  estimated by LD. This finding further emphasizes the aforementioned fact that AF4/MALLS weights larger particles higher than LD and as a consequence a broader size distribution and a higher  $d_{90}$  is assessed.

The  $d_{10}$ ,  $d_{50}$  and  $d_{90}$  of TMCurc-NS and TSCurc-NS, calculated on the basis of the AF4 data, were much larger than the values determined by LD (Tab. 4.2-3 and Tab. 4.2-4). The median ( $d_{50}$ ) of TMCurc-NS and TSCurc-NS was determined to be twice as large by AF4/MALLS compared to LD. These discrepancies might be caused by the aforementioned different size weighting of LD and AF4/MALLS. A further reason for the huge size differences was thought to be the different mathematical models applied by LD and AF4/MALLS for the calculation of the particle size distribution. This was suggested to have a special impact on the characterization of non-spherical particles. A brief summary of AF4/MALLS result calculation has been given in chapter 3.2.4.2. The used analytical software considers the particle shape during the evaluation of the MALLS data. A detailed overview of the evaluation of the LD data was already given by other authors (135). Briefly, the software of the LD apparatus (Mastersizer 2000, Malvern) calculates a volume weighted size distribution from the raw data. This size distribution can be seen equal to

**Table 4.2-4 Particle size distribution of samples of curcuminoid-loaded lipid nanoparticles, determined by LD. The same batch of the respective formulation was used for LD and AF4/MALLS measurements (see Tab. 4.2-3). Given LD values are the average result of five runs of one sample.**

Sample	$d_{10}$ [nm]	Median [nm]	Mean [nm]	$d_{90}$ [nm]
<i>MCTCurc-NE</i>	81	128	133	193
<i>TMCurc-NE</i>	65	128	147	246
<i>TMCurc-NS</i>	66	130	157	266
<i>TSCurc-NS</i>	76	142	159	256

the mass weighted size distribution, calculated by the Astra software. The particle size distribution of MCTCurc-NE and TMCurc-NE was calculated from the LD raw data by applying a spherical model. For the calculation of the size distribution of TMCurc-NS and TSCurc-NS, a spherical and a non-spherical calculation model were applied. Interestingly, no difference in size distribution and characteristic diameters, like  $d_{10}$ ,  $d_{50}$  and  $d_{90}$ , between spherical and non-spherical model was found for TMCurc-NS and TSCurc-NS. Unfortunately the mathematical basics of the applied models are not accessible to the software user. Thus, the reasons of the aforementioned discrepancies of the characteristic particle sizes  $d_{10}$ ,  $d_{50}$  and  $d_{90}$  between LD and AF4/MALLS could not be clarified.

AF4/MALLS was seen as a valuable tool for the determination of the particle size distribution. The setup of suitable separation methods was more time-consuming at the beginning, compared to other applied particle sizing techniques. However, when an adequate method was found, the samples could be examined quickly and reproducible results with an acceptable standard deviation were obtained. One advantage of the applied analytical software was the direct access to the raw data of the particular measurement. A more or less individual fit of the raw data was possible. The evaluation of the MALLS data was therefore more comprehensible, compared to the result evaluation of LD and PCS measurements. However, the free choice of parameters during evaluation of the MALLS data can easily result in false interpretation and incorrect results. One further has to keep in mind that larger particles may be overestimated by MALLS and especially the mean diameters  $d_{RMSz}$  and  $d_{RMSw}$  should be interpreted carefully.

#### **4.2.4.2 Particle shape analysis**

Besides the determination of the particle size distribution, the particle shape was also investigated by AF4/MALLS. For this purpose, higher particle concentrations (0.1 mg lipid absolute) were fractionated by AF4. The fractions were collected and subsequently examined with PCS. The actual estimation of the particle shape was done by calculating the ratio of the AF4-derived  $d_{RMS}$  and the z-average diameter  $d_{H(PCS)}$  obtained by PCS. The  $d_{RMS}$  and geometric diameter  $d_{GEO}$  are directly proportional for compact spheres with a geometric ratio  $d_{RMS}/d_{GEO}$  of 0.775 (chapter 3.2.4.2; Eq. 1). This ratio increases for non-spherical particles, e.g. for rigid rods the value is approximately 2 (119). For compact spheres the  $d_{GEO}$  complies with the  $d_{H(PCS)}$  and this parameter was therefore replaced by the PCS-derived z-average diameter in the aforementioned equation of the geometric ratio.

In a first experimental series, samples of TMCurc-NE and TMCurc-NS were investigated and the geometric ratio was calculated accordingly. The hydrodynamic diameter  $d_{H(PCS)}$  (z-average) of the single fractions increased with collection time and the PDI was below

0.15 for all samples. For TMCurc-NE, the  $d_{H(PCS)}$  complies well with the  $d_{GEOM}$ -curve obtained from the MALLS data (Fig. 4.2-6). The ratio  $d_{RMS}/d_{H(PCS)}$  was between 0.8 and 0.87 and the supercooled particles of TMCurc-NE were confirmed to be of spherical shape. The  $d_{H(PCS)}$  of the TMCurc-NS fractions was smaller than the  $d_{RMS}$  values obtained by AF4/MALLS (Fig. 4.2-6). The  $d_{RMS}/d_{H(PCS)}$  ratio for the crystalline TMCurc-NS particles was between 1 and 1.4, indicating a non-spherical particle shape, which was already demonstrated by the TEM micrographs (chapter 4.2.3).

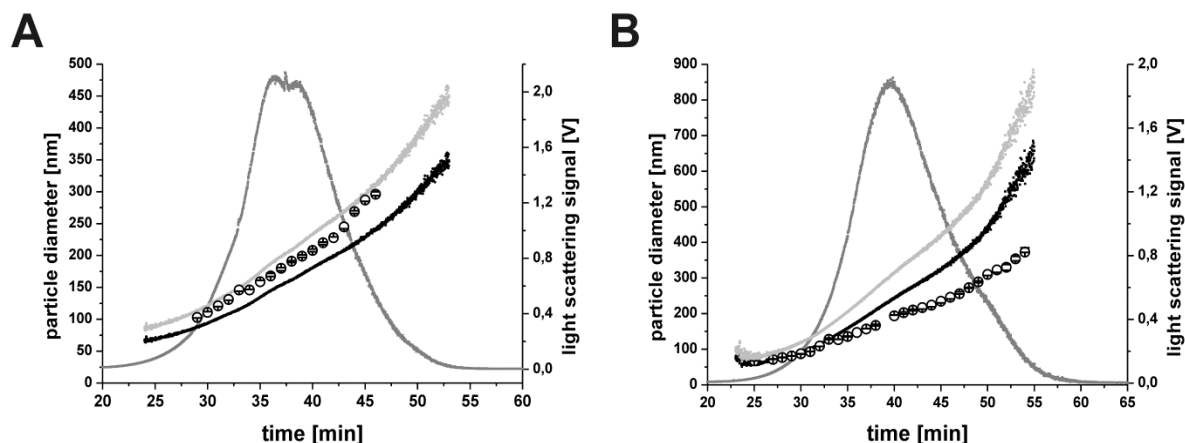


**Figure 4.2-6** AF4/MALLS elution profiles of a sample of (A) TMCurc-NE and (B) TMCurc-NS. (●)  $d_{RMS}$ , (○)  $d_{GEOM}$ , (●) scattered light intensity at a detector angle ( $\theta$ ) of  $90^\circ$ , (○) hydrodynamic diameter  $d_H$  (z-average), determined by PCS. The (○) dots represent the mean of three runs of one sample and the error bars their respective standard deviation.

The aforementioned experiments with the injection of a high lipid concentration (0.1 mg absolute) into the channel resulted in some cases in a blockade of the system. It was suggested that the particles might form aggregates within the machine, probably causing the blockade. A similar agglomeration phenomenon was sometimes observed during LD measurements of the SLN preparations, too. Though, the nanoparticles did not tend to form aggregates during long-time storage at  $8^\circ\text{C}$  or  $22^\circ\text{C}$  respectively. The dilution of the nanoparticles with bidistilled water, as it was done for the PCS measurements, did also not result in a detectable agglomeration. One potential explanation for the observations in LD and AF4 is that a part of the emulsifier layer on the particle surface is washed off due to the high shear forces and dilution in these systems. It is reasonable, that the partial removal of the emulsifier makes the particles more prone to aggregation.

As a consequence of the AF4 system blockade, the eluent was changed to an aqueous 0.1 % (m/v) poloxamer 188 solution and a smaller lipid amount (0.05 mg absolute) was injected. Indeed, the changes of the experimental setup reduced the incidence of system blockades. Though, the decreasing width and the overall appearance of the elution peak

indicated a decreasing separation quality when poloxamer 188 was added to the eluent (Fig. 4.2-7).

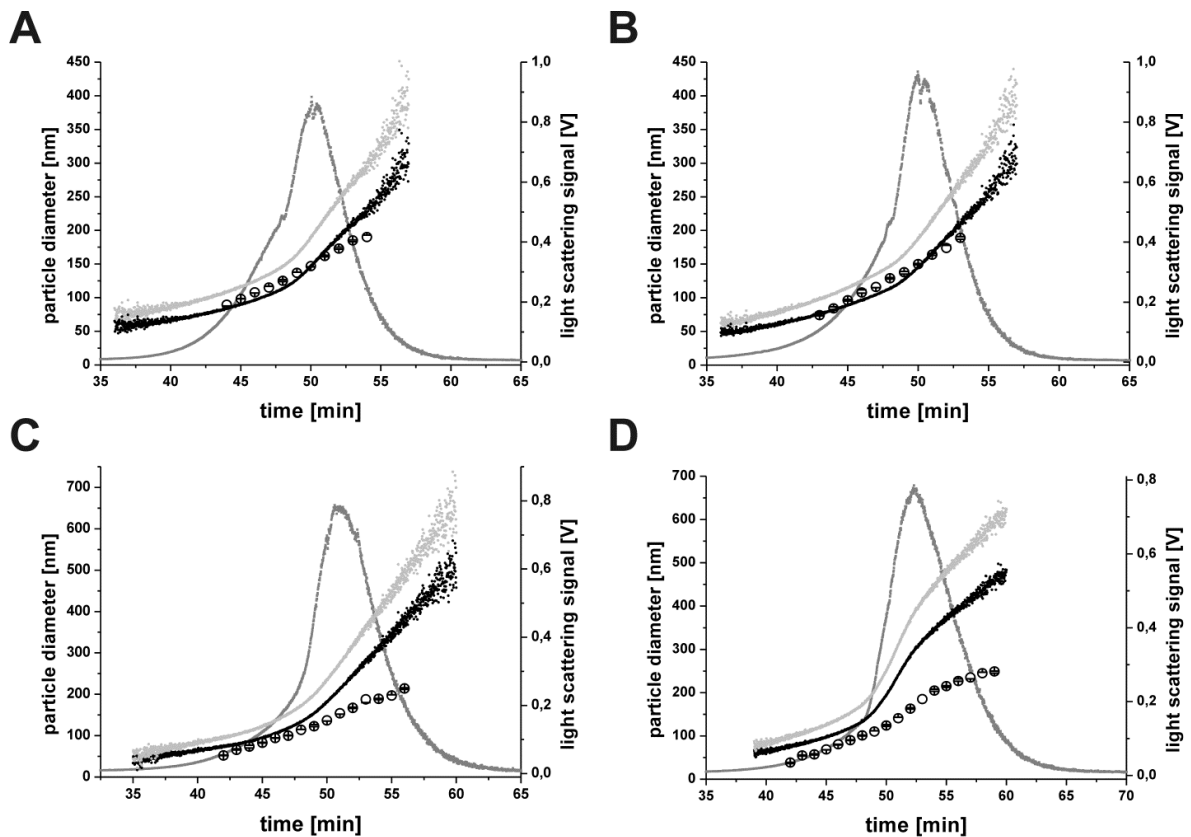


Figure 4.2-7 AF4/MALLS elution profiles of a sample of (A) MCTCurc-NE, (B) TMCurc-NE, (C) TMCurc-NS and (D) TSCurc-NS. (●)  $d_{RMS}$ , (○)  $d_H$ , (●) scattered light intensity at a detector angle ( $\theta$ ) of  $90^\circ$ , (○) z-average determined by PCS. The (○) dots represent the mean of three runs of one sample and the error bars their respective standard deviation.

The progression of d-vs-t curves was also different from the curves obtained in poloxamer-free eluent. The curves showed a rather flat slope at the beginning, followed by a steep increase of the curve after 50 minutes, indicating a rapid increase of the particle size. Thus, a good fractionation of the particles was probably not provided in the latter stage of the experiment. However, the characteristic particle sizes of the investigated formulations were thought to be reliable (Tab.4.2-5). The differences of the particle sizes between the formulations examined with an aqueous eluent and the formulations examined with a poloxamer-based eluent were attributed to normal batch-to-batch fluctuations (Tab.4.2-3 and Tab.4.2-5). Thus, the presence of poloxamer 188 in separation method 3 was thought to alter the fractionation quality, but the calculated particle sizes were overall comparable to the poloxamer-free methods.

Table 4.2-5 Characteristic diameters of the curcuminoid-loaded preparations, determined by AF4/MALLS.  $d_{GEOmz}/d_{RMSz}$ : z-average diameter.  $d_{GEOmw}/d_{RMSw}$ : mass weighted diameter. Given MALLS values were calculated from elution profile of one sample.

Sample	$d_{GEOmz}$ [nm]	$d_{GEOmw}$ [nm]	$d_{10}$ [nm]	$d_{50}$ [nm]	$d_{90}$ [nm]
<i>MCTCurc-NE</i>	267.6	259.8	95.8	138.5	241.8
<i>TMCurc-NE</i>	264.2	238.4	79.6	136	239.8
Sample	$d_{RMSz}$ [nm]	$d_{RMSw}$ [nm]	$d_{10}$ [nm]	$d_{50}$ [nm]	$d_{90}$ [nm]
<i>TMCurc-NS</i>	332.2	308.4	105.4	243.6	421
<i>TSCurc-NS</i>	377.2	341	179.7	345.8	458.6

As it was described for TMCurc-NE and TMCurc-NS before, the fractions of the investigated samples were again collected and subsequently examined with PCS. The hydrodynamic diameter  $d_{H(PCS)}$  of the collected fractions increased with collection time. However, the PDI of the samples was always above 0.18, pointing to a broad distribution of the single fraction. Moreover, the  $d_{H(PCS)}$  did not fit the  $d_{GEOm}$  or  $d_{RMS}$  curves, respectively, as it was expected from the previous experiments conducted with poloxamer-free eluent (Fig. 4.2-7 and Fig. 4.2-6). Generally, the  $d_{H(PCS)}$  was concluded to be too small in comparison to the  $d_{GEOm}$  or  $d_{RMS}$ , respectively.

As a consequence, the determined ratios  $d_{RMS}/d_{H(PCS)}$  were tending to higher values, indicating to an erroneous particle shape. For example, the  $d_{RMS}/d_{H(PCS)}$  ratio of MCTCurc-NE was between 0.9 and 1.1, which pointed rather to anisometric particles, than to compact spheres, which are actually present in the MCT-based nanoemulsion. Moreover, the estimated particle shapes of TMCurc-NE and TMCurc-NS were found to be distinctly different for the experiments conducted with a poloxamer-containing eluent compared to the data obtained with a poloxamer-free eluent. Therefore, an appropriate estimation of the particle shape by AF4/MALLS in combination with PCS was concluded to be not possible, when the eluent contained higher amounts of poloxamer 188. The fractionation quality of AF4 was shown to be decreased by the presence of poloxamer 188, but the gained particle sizes were altogether seen as correct values. Hence, the presence of poloxamer 188 in the samples was thought to influence the PCS measurement in an unfavorable way. One possible reason might be the changed viscosity of the samples, containing poloxamer, although this was regarded by adjusting the samples viscosity within the PCS software (see chapter 3.2.2). Another reason might be the formation of ordered structures by excessive poloxamer, which would also have influenced the light scattering of the sample. Moreover, the injected amount of lipid was thought to be too



low, resulting in a low particle concentration within the single fractions. The high PDI of the fractionated samples was seen as the consequence of the low particle concentration and of the disturbing effect of poloxamer 188. Thus, the results, obtained by PCS, were thought to be inappropriate for the comparison with the MALLS data and for an assessment of the of the particle shape. It was concluded that the injected lipid amount has to be increased in future experiments, to achieve better conditions for the PCS measurements. Furthermore, the influence of poloxamer 188 on the PCS measurement has to be evaluated thoroughly.

#### 4.2.5 Conclusion

The applied analytical techniques provided a good overview of the particle size distribution and the particle morphology. The produced formulations were shown to have a mean particle size below 200 nm and a narrow size distribution, although some formulations exhibited a fraction of particles larger than 500 nm. All formulations revealed a good long-term stability and only a minor increase of the particle size distribution was found for the MCT and TS nanoparticles. The incorporation of the curcuminoids did not influence the particle size distribution of the nanoparticles. The minor differences between the drug-free and curcuminoid-loaded nanoparticles were rather attributed to normal batch-to-batch variations of the production process.

The anisometric particle shape of the solid nanoparticles was revealed by the TEM micrographs and the AF4/MALLS experiments. The TEM micrographs illustrated the huge geometric diversity of the crystalline particles very well. The lipid nanoparticles were shown to be of an irregular and heterogeneous shape. Smaller particles had a rotund or oblong form, whereas bigger particles were square-cut and in some cases of almost rhombic shape. A difference of the particle shape between the crystalline TM and TS nanoparticles was not verifiable by the TEM micrographs. Information on the particle geometry was also gained indirectly from the AF4/MALLS measurements. The irregular particle shape of the crystalline TMCurc-NS preparation was revealed by the comparison of the diameters, determined by MALLS, and of the corresponding z-averages from the PCS measurements. The ratio  $d_{\text{RMS}}/d_{\text{H(PCS)}}$  was found to be higher for a crystalline TMCurc-NS preparation compared to a supercooled TMCurc-NE preparation, containing liquid droplets. In accordance with different literature reports, this was considered to be evidential for the anisometric particle form of TMCurc-NS (119,136). Thus, an estimation of the particle shape was also achievable by AF4/MALLS measurements. The advantage of AF4/MALLS was the evaluation of a bigger particle population and the obtainment of a general impression of the particle geometry. However, the particles cannot be

investigated individually by this method and a clear idea of the particle shape is not attainable. Therefore, the preparation of TEM micrographs is essential, because a detailed insight and description of the geometric form of individual particles can be gained with this technique.

The comparability of the results obtained by the respective techniques was different with regard to the investigated formulation. The mean particle size and the distribution width, determined by PCS, LD and AF4/MALLS, were overall comparable for the MCT-NE and TM-NE preparations. The spherical droplets within these preparations can be easily described by one single parameter, the diameter. It was shown in chapter 4.2.1 and 4.2.4 that the diameters calculated by PCS or AF4/MALLS, respectively, were similar to the corresponding values determined by LD, although different mathematical models were applied for the evaluation of the raw data by the particular techniques. In contrast, the calculated mean diameters for the TM-NS and TS-NS formulations, containing flat and anisometric particles, were dependent on the applied analytical technique. A comprehensive size characterization of an anisometric particle was shown to be challenging, because for irregular shaped particles there is simply not one “correct” diameter. The particular analytical techniques use different mathematical approaches and assumptions for the calculation of the particle size, each resulting in different size values for one and the same particle population. PCS and LD, for example, are assuming spherical bodies for the calculation of the mean particle size and only AF4/MALLS regarded the potential anisometric particle shape of a sample during result calculation. Thus, the characteristics of anisometric particles have to be interpreted with care and the declaration of a mean particle size must always be followed by the description of the applied analytical method and the used parameters for the result calculation.

## **4.3 Physicochemical characteristics**

### **4.3.1 Zeta potential**

The placement of a particle into a liquid results in the appearance of an electrical double layer on the surface of this particle. This layer is caused by the surface charge of the particle. The electrical double layer is comprised of an inner layer, called Stern layer, and an outer, so called diffuse layer (123). If an electrical field is applied on the sample, the particle will migrate towards the electrode of opposite charge. The migration of the particles causes a slipping plane between medium attached to the surface of the moving particle and immobile fluid. The electric potential at the slipping plane of a particle and the surrounding bulk solution is defined as the zeta potential [ $\zeta$ , (123)]. The zeta potential can be used to describe the surface charge of a particle within a certain liquid. It is further an important indicator of the stability of colloidal dispersions. If the zeta-potential is high (in a negative or positive way), the particles repulse each other and do not aggregate. In contrast, particles with low zeta-potential are more prone to aggregation. However, the zeta-potential is no fixed value, but dependent on a variety of parameters, e.g. solvent, electrolyte concentration, nature of electrolyte, pH of the solvent and temperature. The surface charge of the particle is directly influenced by the pH, due to protonation and deprotonation of the used particle matrix. The used solvent should contain a minimum of electrolytes (conductivity ~ 1 mS/cm), to assure the correct formation of an electrical double layer (137). Both, constant pH and minimum electrolyte concentration, is provided by measuring the zeta-potential in a diluted buffer solution. In consideration of the multiple influencing factors, the presented potentials of the lipid nanoparticles should not be seen as absolute values, but rather as approximations indicating a tendency of the surface charge.

The determined zeta potentials are shown in Table 4.3-1. The poloxamer-stabilized formulations had zeta potentials between -3 mV and -9 mV and thus an almost neutral surface. Poloxamer 188 is an uncharged emulsifier, consisting of lipophilic polypropylene oxide (PPO) and hydrophilic polyethylene oxide (PEO/PEG). Hence, a zeta potential near to 0 mV was already expected in advance, because the surface of the nanoparticles was assumed to be enveloped by an emulsifier carrying hardly any charge. The stabilizing effect of poloxamer 188 is caused by the steric repulsion of the hydrophilic PEG chains (138). The hydrated PEG chains form a shell around the lipid nanoparticles that sterically prevents the particles from aggregation. The zeta potential of the nanoparticles was not affected by the applied buffer concentration, emphasizing that the PEG chains of poloxamer 188 were not sensitive to the electrolyte concentration of the solution. When a

MCT-NE sample was investigated in bidistilled water, the zeta potential was determined to be too low and the obtained value was seen as incorrect (Tab. 4.3-1). Though, the presence of a certain amount of ions is concluded to be essential for the reliable determination of the zeta potential. The influence of the electrolyte concentration on the zeta potential was further investigated with MCT nanoemulsions, stabilized with Solutol® HS 15 and lecithin (Lipoid S45) (Tab. 4.3-1). Solutol® HS 15 is a nonionic emulsifier, but Lipoid S45 contains negatively charged phospholipids and therefore the surface of the emulsion droplets also exhibited a negative charge. The examination of these samples revealed that an increasing electrolyte concentration was followed by a decrease of the zeta-potential (Tab. 4.3-1). In contrast to the poloxamer-stabilized systems, the buffer concentration clearly influenced the resulting zeta potential of the nanoemulsions stabilized with Solutol® HS 15 and Lipoid S45. Thus, the measurement conditions, especially the electrolyte concentration, for samples with a distinct surface charge have to be constant throughout all measurements to assure comparable results. Furthermore, the stability of these preparations is probably influenced by the presence of electrolytes. It was suggested that the preparations stabilized with Solutol® HS 15/Lipoid S45 were more prone to aggregate in highly concentrated salt solutions, than the poloxamer-stabilized systems.

Table 4.3-1 Zeta potential of different nanoparticles preparations at 20 °C. The given values are the mean of nine runs  $\pm$  standard deviation.

Sample	Emulsifier	Dilution	Diluent	$\zeta$ -potential [mV]
<i>MCT-NE</i>	Poloxamer 188 <sup>a</sup>	1:1000	Tris buffer 100 mM	-4.73 $\pm$ 1.47
<i>MCT-NE</i>	Poloxamer 188 <sup>a</sup>	1:1000	Tris buffer 50 mM	-5.28 $\pm$ 1.98
<i>MCT-NE</i>	Poloxamer 188 <sup>a</sup>	1:1000	Tris buffer 20 mM	-3.98 $\pm$ 0.19
<i>MCT-NE</i>	Poloxamer 188 <sup>a</sup>	1:1000	Tris buffer 10 mM	-4.3 $\pm$ 0.79
<i>MCT-NE</i>	Poloxamer 188 <sup>a</sup>	1:200	Tris buffer 10 mM	-3.82 $\pm$ 0.39
<i>MCT-NE</i>	Poloxamer 188 <sup>a</sup>	1:1000	bidistilled water	-38.47 $\pm$ 0.74
<i>MCT-NE</i>	Solutol HS 15/ Lipoid S45 <sup>b</sup>	1:1000	Tris buffer 100 mM	-10.96 $\pm$ 1.96
<i>MCT-NE</i>	Solutol HS 15/ Lipoid S45 <sup>b</sup>	1:1000	Tris buffer 50 mM	-15.97 $\pm$ 1.39
<i>MCT-NE</i>	Solutol HS 15/ Lipoid S45 <sup>b</sup>	1:1000	Tris buffer 20 mM	-22.36 $\pm$ 0.54
<i>MCT-NE</i>	Solutol HS 15/ Lipoid S45 <sup>b</sup>	1:1000	Tris buffer 10 mM	-29.36 $\pm$ 0.5
<i>MCT-NE</i>	Solutol HS 15/ Lipoid S45 <sup>b</sup>	1:1000	bidistilled water	-43.6 $\pm$ 1.92
<i>TM-NE</i>	Poloxamer 188 <sup>a</sup>	1:1000	Tris buffer 10 mM	-8.68 $\pm$ 0.44
<i>TM-NE</i>	Poloxamer 188 <sup>a</sup>	1:200	Tris buffer 10 mM	-4.81 $\pm$ 0.33
<i>TM-NS</i>	Poloxamer 188 <sup>a</sup>	1:1000	Tris buffer 10 mM	-6.34 $\pm$ 1.48
<i>TM-NS</i>	Poloxamer 188 <sup>a</sup>	1:200	Tris buffer 10 mM	-5.03 $\pm$ 0.32
<i>TS-NS</i>	Poloxamer 188 <sup>a</sup>	1:1000	Tris buffer 10 mM	-7.64 $\pm$ 0.79
<i>MCTCurc-NE</i>	Poloxamer 188 <sup>a</sup>	1:1000	Tris buffer 10 mM	-8.71 $\pm$ 1.03
<i>TMCurc-NE</i>	Poloxamer 188 <sup>a</sup>	1:1000	Tris buffer 10 mM	-6.93 $\pm$ 0.95
<i>TMCurc-NS</i>	Poloxamer 188 <sup>a</sup>	1:1000	Tris buffer 10 mM	-5.36 $\pm$ 0.24
<i>TSCurc-NS</i>	Poloxamer 188 <sup>a</sup>	1:1000	Tris buffer 10 mM	-3.09 $\pm$ 0.32

<sup>a</sup> concentration: 2.5 % (w/v) Poloxamer 188

<sup>b</sup> concentration: 2 % (w/v) Solutol HS 15/0.5 % (w/v) Lipoid S45

### 4.3.2 Differential scanning calorimetry

The melting and the recrystallization point of the TM and TS nanoparticles were lower compared to the bulk material. The melting points of the bulk material were found to be 58 °C for TM and 72 °C for TS (Fig. 4.3-1). Lutton published approximately the same melting points for these triglycerides (139). The TM-based nanoparticles had a melting point of approximately 53 °C and the TS preparations were melting at around 68 °C (Fig. 4.3-1).

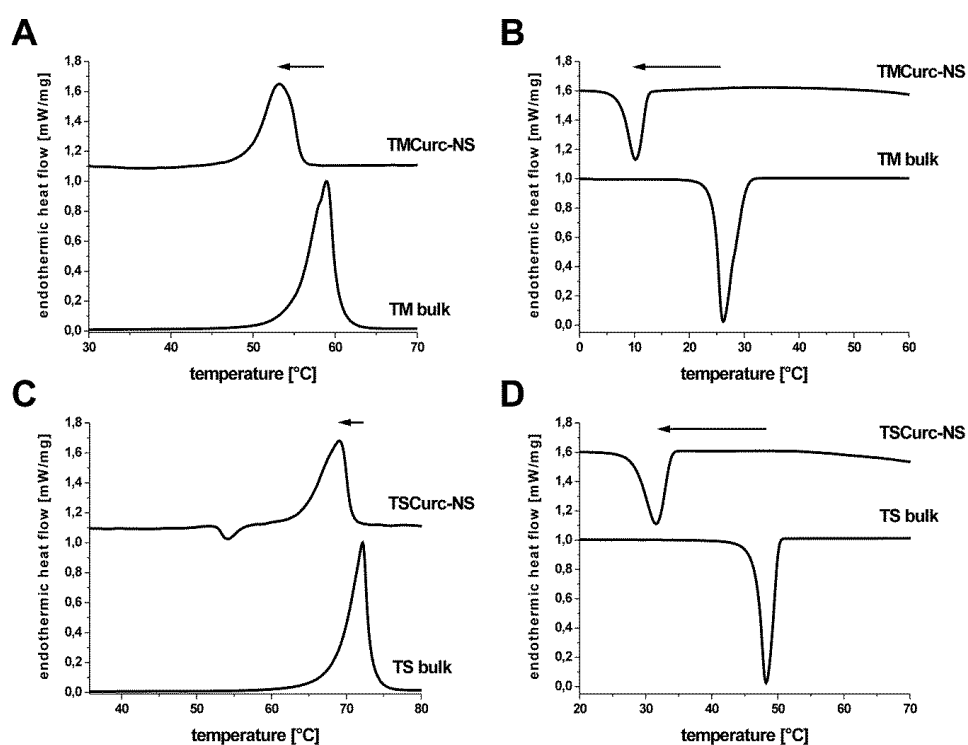


Figure 4.3-1 DSC thermograms of heating and subsequent cooling of bulk lipid and lipid nanoparticles. (A) heating curves (2 K/min) of TM bulk and TMCurc-NS a few hours after production and storage at 8 °C; (B) cooling curves (5 K/min) of previously molten TM samples presented in (A); (C) heating curves (2 K/min) of TS bulk and TSCurc-NS a few hours after production and storage at 8 °C; (D) cooling curves (5 K/min) of previously molten TS samples presented in (C). The thermograms were normalized to the maximum/minimum of the respective curve and the upper thermograms were shifted along the ordinate for better visualization.

As Bunjes *et al.* reported earlier, the shift of the melting peaks can be explained by the colloidal nature of the samples (115). Despite the melting point depression, it was concluded that TM and TS existed predominantly in  $\beta$ -modification within the particles, because the obtained melting points were in agreement with the literature data reporting

on the melting points of TM- and TS-based nanoparticles in the  $\beta$ -modification (99). Additionally, the melting peaks of the nanoparticles were broader than the peaks of the raw materials. A size-dependent melting of the particles is seen as the underlying reason for this observation (132). The existence of different particle fractions in the investigated samples was confirmed by the light scattering experiments and by the TEM-micrographs (chapters 4.2.1 and 4.2.3).

The crystallization point of the preparations was shifted dramatically to lower temperatures. The molten particles did solidify around 15 °C below the crystallization point of the bulk lipid (Fig. 4.3-1). This shift must not be seen as absolute, because crystallization is a complex process which is influenced by a variety of parameters, e.g. particle size, cooling rate and presence of foreign substances. Nevertheless, it shows that a small particle size is one key parameter for the delay of the lipid crystallization. The big depression of the crystallization point resulted in a non-solidification of the curcuminoid-loaded TM particles when cooled down to 22 °C after production (Fig. 4.3-2).

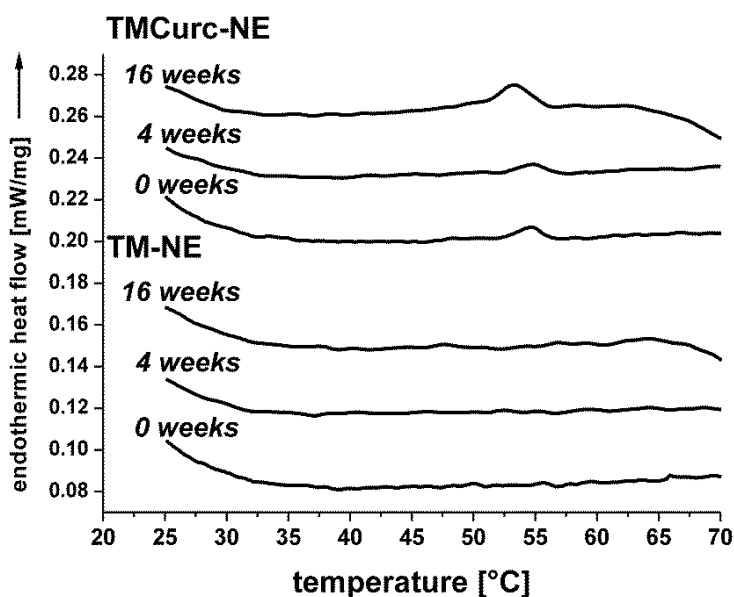


Figure 4.3-2 DSC thermograms of heating samples of TM-NE and TMCurc-NE. The DSC scans were recorded a few hours, four weeks and sixteen weeks after preparation and storage at 22 °C. The thermograms were shifted along the ordinate for better visualization.

The occurrence of supercooling behavior was reported for several formulations of lipid nanoparticles (140). This effect made it possible to investigate the lipid either in the crystalline or in the liquid state. The DSC curves of the TM particles, stored at 22 °C showed no melting event during the observation period of sixteen weeks. In several

curcuminoid-loaded preparations a minor melting event at 54 - 55 °C was detected (Fig. 4.3-2). Hence, a small fraction of lipid did crystallize in these samples. The peak was getting more pronounced over sixteen weeks. The observed behavior of the curcuminoid loaded TM formulations emphasized the metastable character of supercooled lipid nanoparticles. The presence of the curcuminoids seemed to induce crystallization of the lipid matrix. It was suggested that the drug precipitated after the production in the cold lipid matrix. The precipitated curcuminoids might, in turn, induce the partial solidification of the lipid carrier. At least for pure triglyceride matrices the supercooled state is concluded to be not suitable as a drug carrier, because uncontrolled recrystallization can take place. This may result in drug expulsion from the particles or other unpredictable effects. However, for other lipid systems more stable supercooled preparations have been described (84).

Crystalline TM particles were only obtained when the formulation was cooled below 8 °C (Fig. 4.3-1). Under these conditions, the TM particles transformed rapidly into the  $\beta$ -modification so that the unstable, intermediate  $\alpha$ - or  $\beta'$ -modifications were not detected. The melting enthalpy was 19 J/g, being about 10 % of the enthalpy of the bulk lipid. The content of lipid in the samples was 10 % (w/w). It was therefore concluded that the TM matrix did crystallize completely.

Freshly prepared TS nanoparticles showed an exothermal peak at around 55 °C additionally to the melting of the  $\beta$ -modification at 68 °C (Fig. 4.3-3 A).

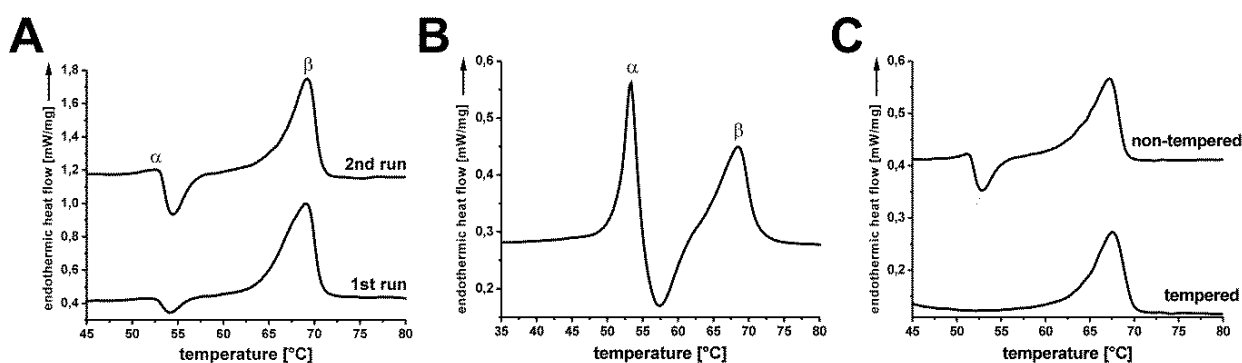


**Figure 4.3-3** DSC thermogram of: (A) two consecutive heating runs of a TSCurc-NS sample with an intermediate cooling step (not shown). Greek letters indicate the melting point of the respective modification; (B) heating curve (5 K/min) of a TSCurc-NS sample recorded after previous melting and subsequent rapid cooling (10 K/min, not shown); (C) heating curves of two TSCurc-NS samples after melting and subsequent cooling (not shown). *Non-tempered sample*: continuous heating. *Tempered sample*: discontinuous heating. The thermograms were shifted along the ordinate for better visualization.



The small endothermic peak and the subsequent exothermic peak were related to the melting of the  $\alpha$ -lipid modification and the subsequent crystallization in the  $\beta$ -modification. Comparable results have been reported for nanoparticles consisting of pure triglycerides (121). The transition was getting even more intense if the samples were heated a second time after previous cooling (Fig. 4.3-3 A). A higher cooling rate was further enforcing the formation of the  $\alpha$ -phase in the TS particles (Fig. 4.3-3 B). Unprocessed TS exhibited the same behavior as the nanoparticles. The  $\alpha$ -fraction of the TS nanoparticles was decreasing over the observation period of 16 weeks (Fig. 4.3-4).

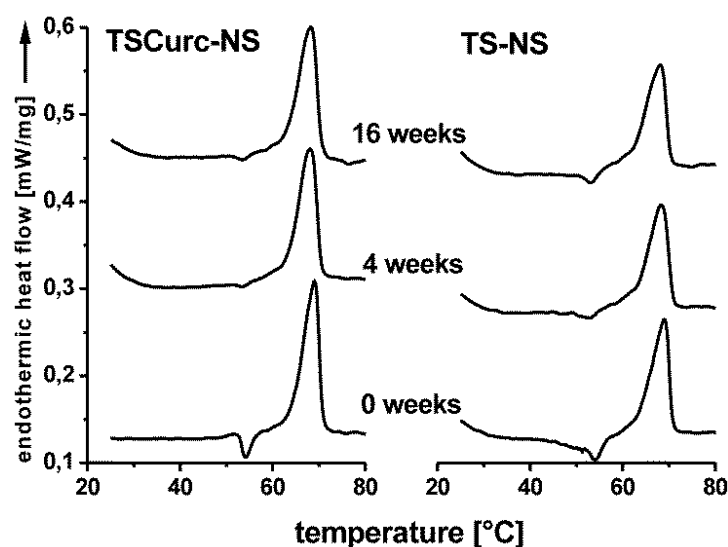


Figure 4.3-4 DSC thermograms of heating samples of TSCurc-NS and TS-NS. The DSC scans were recorded a few hours, four weeks and sixteen weeks after production and storage at 22 °C. The thermograms were shifted along the ordinate for better visualization.

The effect of discontinuous heating on the occurrence of the  $\alpha$ -modification was also investigated. For this purpose, two samples of TSCurc-NS were heated above the melting temperature and subsequently cooled down to induce crystallization. Now, one sample was continuously heated and the recorded DSC thermogram exhibited a small peak at around 52 °C, indicating the melting of a small fraction of TS with  $\alpha$ -modification (Fig. 4.3-3 C, upper curve). The second sample was heated to 40 °C, kept at this temperature for one hour and was subsequently heated to final 80 °C. The tempering of this sample at a temperature close to the melting point of the  $\alpha$ -modification resulted in the disappearance of the lipid fraction with  $\alpha$ -modification (Fig. 4.3-3 C, lower curve). Thus, the lipid crystals ordered fast to the  $\beta$ -modification without any detectable residues of the  $\alpha$ -phase. Tempering was concluded to accelerate the transition of the lipid

modifications. The melting enthalpy of the TS nanoparticles in  $\beta$ -modification was 21.6 J/g, being almost 10 % of the respective bulk enthalpy. Hence, the lipid matrix in the TS nanoparticles was concluded to be also fully crystallized. The comparison of the drug-free and the curcuminoid-loaded lipid nanoparticles revealed no influence of the drug on the melting behavior. The presence of curcuminoids did not have any impact on the occurrence or the sequence of the phase transition of the lipids during solidification. In accordance with the results of Bunjes *et al.*, the ordering of the TM chains during recrystallization was very fast, so that the unstable  $\alpha$ -phase was not verifiable in these preparations under the applied experimental conditions (99). In contrast, the solidification of the TS melt takes place in part via the  $\alpha$ -modification, because the chain ordering process to a stable modification is slower due to the higher chain length. It was shown that this transition was accelerated when the sample is stored at higher temperatures, e.g. 40 °C for a short time.

### 4.3.3 X-ray diffraction

The crystalline modification of the lipid matrix was elucidated in more detail with X-ray scattering. The small angle and wide angle area and the respective reflexes were recorded simultaneously. The supercooled TM particles showed no sharp reflexes, but two broad halos which pointed to a low long range order usually found in amorphous or fluid systems. This result confirmed the non-solidification of the TM nanoparticles at a storage temperature of 22 °C. They remained in a metastable liquid state.

When the cold stored TM-NS and TS-NS preparations were examined, three main peaks were observed in the wide angle finger-print area at  $2.2 \text{ nm}^{-1}$ ,  $2.6 \text{ nm}^{-1}$  and  $2.7 \text{ nm}^{-1}$  respectively (Fig. 4.3-5). The pattern of the bulk showed the same reflexes. The described peaks in the wide angle area are typical for a triclinic subcell occurring in the  $\beta$ -modification (141). In agreement with the DSC measurements it was confirmed that the nanoparticles contained either TM or TS in  $\beta$ -modification.

The sharp single reflexes in the small angle domain further confirmed the crystalline structure of the TM-NS and TS-NS nanoparticles. The recorded values for the long and the short spacing and the respective literature data were summarized in Table 4.3-2.

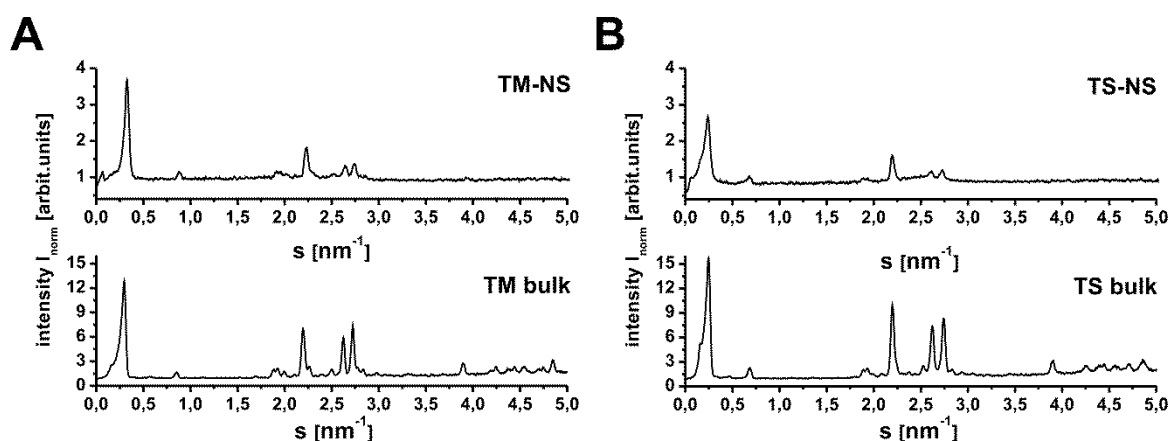


Figure 4.3-5 X-ray diffraction pattern of samples of (A) TM-NS nanoparticles and TM bulk and of (B) TS-NS nanoparticles and TS bulk. Small and wide angle area were recorded simultaneously.

Table 4.3-2 Short and long spacings of the recorded pattern and the corresponding values of the  $\beta$ -modification found in the literature.

Sample	Short spacing $d^*$ (nm)	Short spacing $d$ (nm) $\beta^{**}$	Long spacing $d^*$ (nm)	Long spacing $d$ (nm) $\beta^{**}$
<i>TM bulk</i>	0.46, 0.38, 0.37	0.46, 0.38, 0.37	3.51	3.55
<i>TM-NS SLN</i>	0.46, 0.38, 0.37		3.44	
<i>TS bulk</i>	0.45, 0.38, 0.36	0.46, 0.38, 0.37	4.42	4.51
<i>TS-NS SLN</i>	0.45, 0.38, 0.36		4.42	

\* values were calculated by  $d=1/s$ ,  $s$ = reciprocal spacing ( $\text{nm}^{-1}$ )

\*\* data obtained from Lutton et al. (139)

#### 4.3.4 Nuclear magnetic resonance spectroscopy

$^1\text{H}$  NMR spectroscopy is an analytical method which is commonly applied in pharmaceutical sciences (142). It was also used for the characterization of lipid nanoparticles, but it still has not reached the same impact as DSC and X-ray diffraction, because basic parameters, like melting point and lipid modification, are not estimable by  $^1\text{H}$  NMR spectroscopy (114,143). However,  $^1\text{H}$  NMR spectroscopy can help to obtain further information about the properties of the lipid phase and the emulsifier, e.g. mobility and interfacial characteristics. In contrast to DSC, the  $^1\text{H}$  NMR experiments can be performed using constant temperature conditions. This is a special advantage for the investigation of colloidal systems, because some nonionic surfactants are subjected to transformations, e.g. clouding or gelation under the influence of heat (144). Disadvantages of standard

$^1\text{H}$  NMR spectroscopy are the inaccessibility of solid materials and the comparably low sensitivity of the method. Thus, an investigation of the incorporated drug was not possible, because of its low concentration in the formulations. With regard to the curcuminoid-loaded nanoparticles, a detailed analysis of the lipid matrix and of the emulsifier was carried out.

An overview of the detected peaks and their assignment to a certain structure is given in Figure 4.3-6. The good separation of the lipid and the emulsifier signals enabled the characterization of both compounds without interference by the other one. The spectra of the lipid nanoparticles were evaluated in terms of peak appearance and line width at the half amplitude of the respective peak. This parameter is an indicator of the mobility of the fluid component. A highly viscous or solid matrix leads to a broadening or complete disappearance of the peaks.

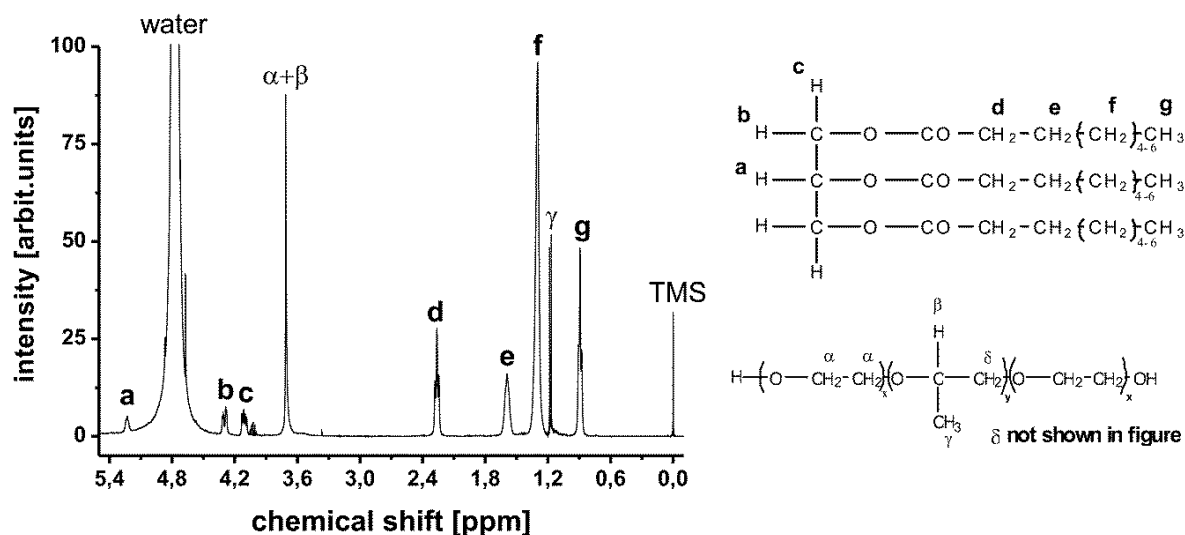


Figure 4.3-6  $^1\text{H}$  NMR spectrum of MCTCurc-NE. The latin letters assign the signal in the  $^1\text{H}$  NMR spectrum to the protons in the triglyceride formula. The greek letters assign the signals in the  $^1\text{H}$  NMR spectrum to the protons in the formula of poloxamer 188 [according to (114)].

A comparison of the spectra of MCTCurc-NE and TMCurc-NE preparation revealed only minor differences (Fig. 4.3-7 A). The presence of the peaks a-g in the supercooled TM nanoemulsion clearly showed the fluid state of the lipid matrix. The line width of peak f (1.6 ppm) of the TM nanoemulsions was 10 Hz. The line width of the same peak was 13 Hz for the MCT nanoemulsion. The line width of peak e (1.6 ppm) was approximately 20 Hz for MCTCurc-NE and TMCurc-NE. The higher intensity of peak e in TM-NE compared to MCT-NE was caused by the longer alkyl chain of the myristic acid. The line width of peak g

(0.9 ppm) was not determinable because of the triplet structure. The similar peak appearance of both formulations indicated a high mobility of the fatty acid chains in the respective emulsion droplets. Therefore, the state of the lipid chains in the supercooled TM nanoemulsions was comparable with the state of the MCT-based emulsion. The shape and the line width of the peaks of the supercooled TM preparation were not changing over an observation period of three weeks (Fig. 4.3-7 B).

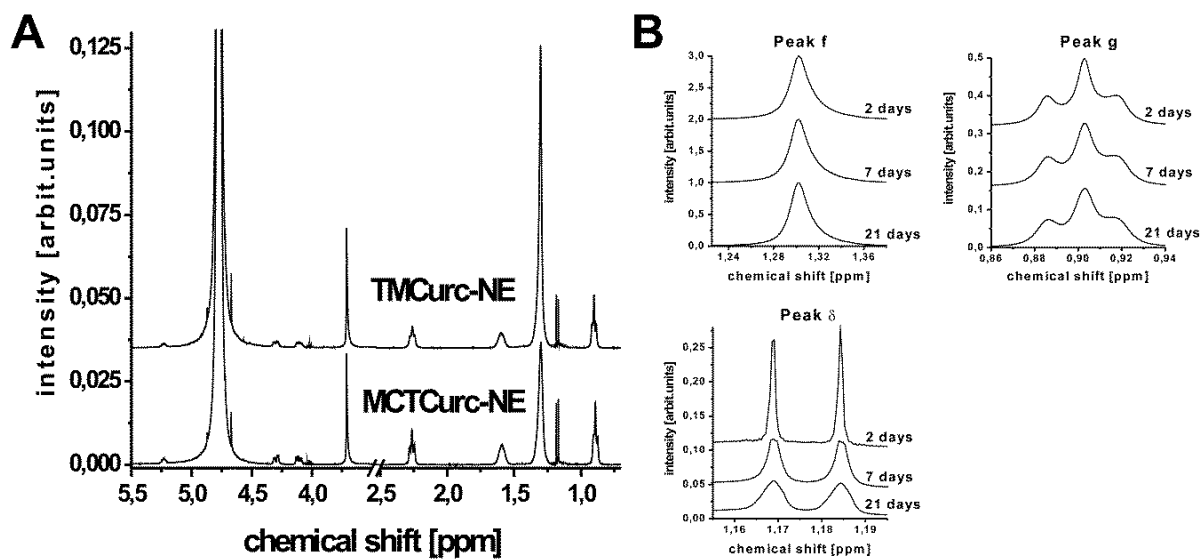


Figure 4.3-7 (A)  $^1\text{H}$  NMR spectra of TMCurc-NE and MCTCurc-NE. The spectra were recorded 48 h after production. The original spectra were normalized to the respective water signal (4.75 ppm). (B)  $^1\text{H}$  NMR spectra of peak f,  $\delta$  and g of a TMCurc-NE sample recorded 48 hours, 7 days and 21 days after preparation and storage at 22 °C. The original spectra were normalized to peak f (1.3 ppm). The spectra were shifted along the ordinate for better visualization.

Thus, the conditions in the emulsions droplets were not changing with time and no further ordering of the lipid chains was detected. The sharp poloxamer 188 peaks proved the high mobility of the emulsifier in the preparation. The poloxamer 188 duplet (1.15 ppm) was broadening within three weeks and the partition of the two peaks was less sharp compared to the beginning. The singlet at 3.7 ppm was also slightly broadening from 3 Hz to 5 Hz during the observation period. The time-dependent change of the line width was probably caused by a further ordering of the polymer chains during storage.

The spectrum of the crystalline TM nanoparticles showed signals of protons of the fatty acid chain (Fig. 4.3-8 A). The detected peaks were attributed to the protons of the terminal methyl group (Peak g, 0.9 ppm, Fig. 4.3-8 B) and to the methylene protons belonging to the distal carbons of the fatty acid chain (Peak f, 1.3 ppm, Fig. 4.3-8 B).

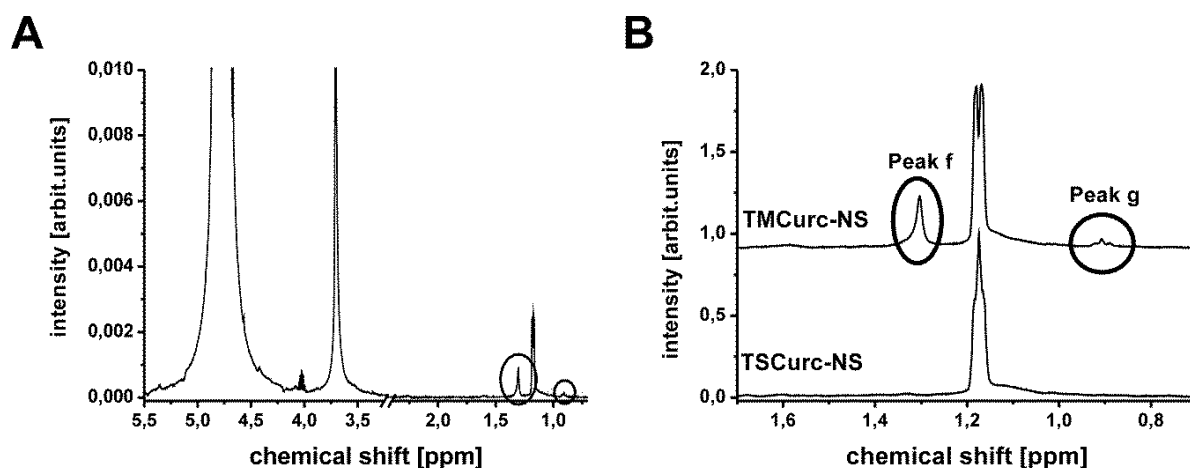


Figure 4.3-8 (A) <sup>1</sup>H NMR spectrum of a TMCurc-NS sample recorded 48 hours after preparation and storage at 8 °C. (B) <sup>1</sup>H NMR spectra of TSCurc-NS and TMCurc-NS (detail of Fig.4.3 -8 A) recorded 48 hours after production and storage at 8 °C. The circles highlight the peaks f and g caused by lipid protons. The spectra were normalized to the respective water signal (4.75 ppm) and shifted along the ordinate for better visualization.

The signals a-e representing the proximal protons of the triglyceride were not detectable (Fig. 4.3-8 A, for position of peak a-e see Fig. 4.3-6). The line width of peak f was 6-7 Hz. Thus, the protons were as mobile as in the emulsion droplets of the supercooled nanoemulsions. Peak f was still detectable but less strong after five months of storage at 8 °C and its line width was not changed significantly. In contrast peak g vanished with time and could hardly be detected after 150 days. The appearance of the mentioned peaks was unexpected, because the protons in the chains of the solid lipid matrix cannot give any signal. Hence, the remaining signals were assigned to mono- and diglycerides and free fatty acids of TM. These molecules can be inherent in the used lipid as a residue of the production process (see Certificate of Analysis in the Appendix). A partial saponification during the production of the nanoparticles was also possible, because the lipid was exposed to heat and wetness over a longer period of time. Due to their increased hydrophilic properties, the partial glycerides and free fatty acids were likely to be located in the interface between water and lipid phase. So these molecules were either situated on the surface of the particles or were solubilized by the emulsifier in the water phase. In contrast, the spectra of the TS nanoparticles revealed no peaks associated to the lipid

protons (Fig. 4.3-8 B). On the one hand the concentration of stearic acid and partial glycerides might have been too low to give a signal. On the other hand these substances are more lipophilic and therefore they may have crystallized together with the triglyceride instead of residing in the amphiphilic interface.

### 4.3.5 Raman spectroscopy

Raman spectroscopy is detecting molecular vibrations after the excitation with infra-red light. In contrast to IR-spectroscopy, aqueous samples are well accessible by Raman spectroscopy. The basic principles of this technique have been reported in detail before (145). Raman spectroscopy is a non-destructive analytic method, but if the applied laser beam is too strong the sample can heat up considerably. This method is used for the investigation of lipids since many years (146,147). Amongst other information, the composition of the lipid, the physical state, the conformation of the lipid chain and the crystalline modification can be obtained from the recorded Raman spectra. However, only few reports exist about an application of Raman spectroscopy for the characterization of colloidal lipid systems (91).

The recorded Raman spectra allowed a clear differentiation between the crystalline and the supercooled state of the TM nanoparticles (Fig. 4.3-9 A).

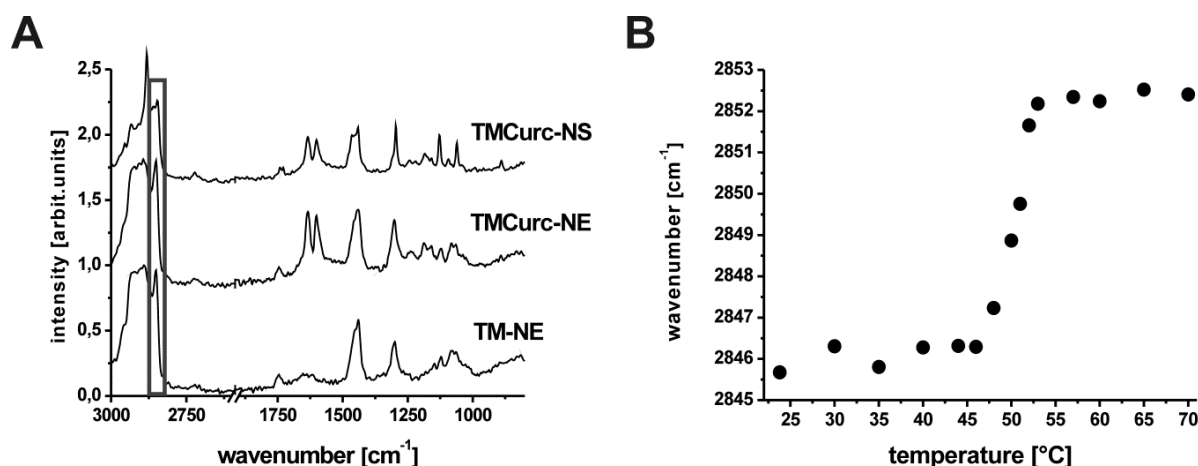


Figure 4.3-9 (A) Raman spectra of a crystalline TMCurc-NS, a supercooled TMCurc-NE and a supercooled TM-NE sample. The graphs were intercepted between 1900 cm<sup>-1</sup> and 2600 cm<sup>-1</sup>. The grey rectangle marks the symmetric CH<sub>2</sub>-stretching (position ~ 2850 cm<sup>-1</sup>). The spectra were shifted along the ordinate for better visualization. (B) Peak position of the symmetric CH<sub>2</sub>-vibration during the continuous heating of a sample of TMCurc-NS.

The crystalline matrix resulted in sharp peaks, whereas the peaks broadened and in some cases shifted to higher wavenumbers in the liquid state. The assignment of the peaks to specific molecular vibrations and the inherent information about the conformation of the lipid molecule has been described in detail before (91). The symmetric CH<sub>2</sub>-stretching caused a peak at around 2842 cm<sup>-1</sup> in the TMCurc-NS sample, indicating a *trans*-conformation of the lipid chain. The peak at 2880 cm<sup>-1</sup> was attributed to the asymmetric CH<sub>2</sub>-stretching and the sharp peak of the TMCurc-NS sample pointed to an ordering of 3 or more methylene groups of the fatty acid chain in *trans*-conformation. In addition, the sharp bands at 1130 cm<sup>-1</sup> and 1060 cm<sup>-1</sup> also indicated a highly ordered lipid chain. Thus, an ordered crystalline matrix of the lipid in TMCurc-NS was confirmed by the Raman spectra. In contrast, the peaks at 2880 cm<sup>-1</sup>, 1130 cm<sup>-1</sup> and 1060 cm<sup>-1</sup> were not detectable in the supercooled formulations, TM-NE and TMCurc-NE. Moreover the position of the CH<sub>2</sub>-stretching shifted to higher wavenumbers and was found at around 2853 cm<sup>-1</sup>. These findings verified a low order of the TM lipid chains and the liquid state of TM within the supercooled nanoemulsions was therefore confirmed. The peak position of the symmetric CH<sub>2</sub>-vibration of the fatty acid chain was used to monitor the melting of the solid nanoparticles (Fig. 4.3-9 B). The rapid increase of the wavenumber at 50 °C was marking the melting event of the lipid. So the actual melting point found by Raman spectroscopy was 3 °C - 4 °C lower compared to the values determined by DSC.

The spectra of the pure curcuminoids exhibited several sharp and intensive bands. The strongest were situated at 1601 cm<sup>-1</sup> (phenol rings, Peak A) and at 1630 cm<sup>-1</sup> (CO-C=C, Peak B), (148). The recorded spectra showed a clear difference with respect to peak position and peak ratio between crystalline substance, curcuminoids amorphously embedded in Kollidon 12 PF and an ethanolic solution of the drug (Fig. 4.3-10 A). Whereas the position of peak A was not changing, peak B was dependent on the physical state of the curcuminoids (Fig. 4.3-10 A). For crystalline curcuminoids, peak B was at 1627 cm<sup>-1</sup> and shifted to 1632 cm<sup>-1</sup> when the substance was dissolved in ethanol. As it was already explained for the lipid bands, the peak position characterized the degree of order of a molecule. The shift of peak B, caused by dissolution of the curcuminoids, indicated a lower order of the CO-C=C-group of the substance in a solution compared to the crystalline state. The insensitivity of peak A to a change of the physical state was explained by the rigid conformation of the phenol ring, which was thought to be more or less independent from the environmental conditions. The intensity ratio Peak A/Peak B was higher in the crystalline state compared to the dissolved curcuminoids (Fig. 4.3-10 B). The peak shift, as well as the peak ratio, was used to determine the state of the curcuminoids within the lipid nanoparticles.



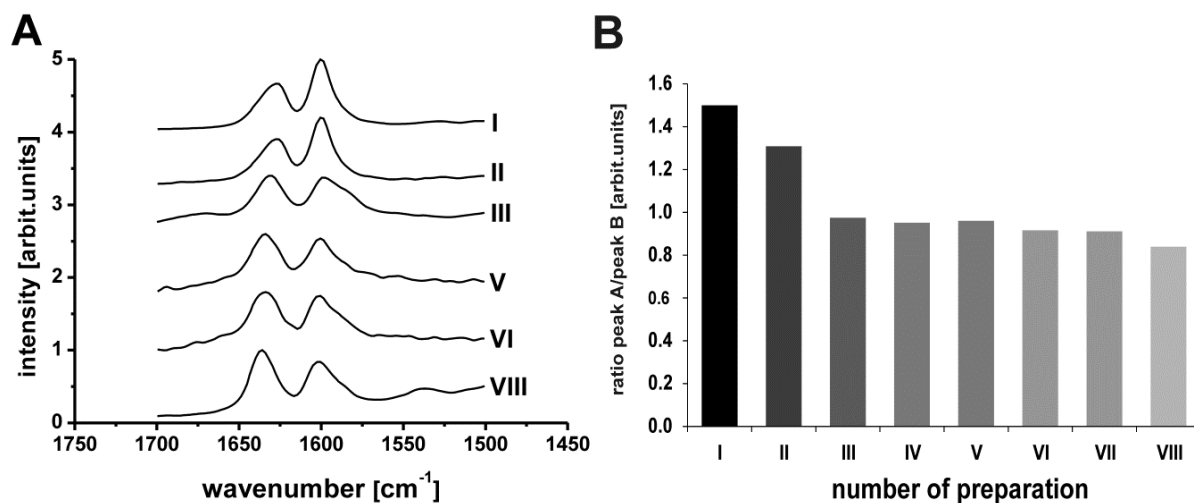


Figure 4.3-10 (A) Raman spectra of the curcuminoid double band in dependence of the physical state of the drug. The spectra were shifted along the ordinate for better visualization. (B) Intensity ratio Peak A/Peak B of the curcuminoid double band (Peak A:  $1600\text{ cm}^{-1}$ , Peak B:  $1633\text{-}1627\text{ cm}^{-1}$ ) in different physical states of the substance. Investigated samples: [I] crystalline curcuminoid powder, [II] aqueous curcuminoid suspension (0.1 % w/v), [III] curcuminoid embedment in Kollidon PF12 (0.1 % w/w), [IV] TSCurc-NS (only Fig. 4.3-10 B), [V] TMCurc-NS, [VI] TMCurc-NE, [VII] MCTCurc-NE (only Fig.4.3-10 B), [VIII] curcuminoid solution in ethanol (0.2 % w/v).

The curcuminoid double band was well separated from the lipid signals (Fig. 4.3-9 A). The signals of the incorporated curcuminoids were notably intensive, although the drug concentration in the preparation was at 0.1 % (w/w). The curcuminoids were still detectable at a concentration of 0.025 % (w/w) within the nanoparticles. When the signals of the curcuminoids loaded onto the nanoparticles were compared to the spectra of the free curcuminoids, it was assessed that they were more alike the spectrum of non-crystalline curcuminoids (Fig. 4.3-10 A). The maximum of peak B of the curcuminoid-loaded nanoparticles was at the same wavenumber as it was for the amorphous curcuminoid embedding and the curcuminoid solution. The ratio Peak A/Peak B of the formulations was similar to the ratio of the amorphous embedding (Fig. 4.3-10 B). Moreover, the curcuminoid ratios of the liquid and the solid nanoparticles were almost identical. Therefore, it was concluded that the major fraction of the drug remained in an amorphous or solubilized state when the formulation was cooled down after production. No substantial change in the physical condition of the drug occurred when the lipid matrix was solidifying again. Mulik et al. suggested an amorphous state of the incorporated curcumin for their SLN preparation (118).

The direct incorporation of the curcuminoids into the highly ordered lipid matrix was rather improbable. The fate of the drug in the formulations was suggested to be as follows: (I) the curcuminoids are dissolved in the hot lipid, (II) the curcuminoids precipitate in the liquid droplets during cooling, (III) the lipid matrix recrystallizes and the curcuminoids are expelled, (IVa) the drug is attached on the surface of the fully crystalline particles or (IVb) the curcuminoids are located in a solubilized state in the interface between water, emulsifier and solid lipid.

### 4.3.6 Fluorescence spectroscopy

The fluorescence spectrum of the curcuminoids in pure MCT showed an asymmetric peak with two maxima at 464 nm and 485 nm (Fig. 4.3-11 A). The spectra of the respective lipid nanoparticles were asymmetric, too, but their shape and position appeared to be very different from that of the bulk material. The maxima of MCTCurc-NE, TmCurc-NE, TMCurc-NS and TSCurc-NS were at 491 nm, 495 nm, 502 nm and 504 nm respectively (Fig.4.3-11 A). No second maximum was detected in the nanoparticles, but a shoulder at smaller wavelengths. This shoulder was expressed intensely in the spectrum of MCTCurc-NE, got weaker for TMCurc-NE and could hardly be seen in the spectra of the crystalline nanoparticles.

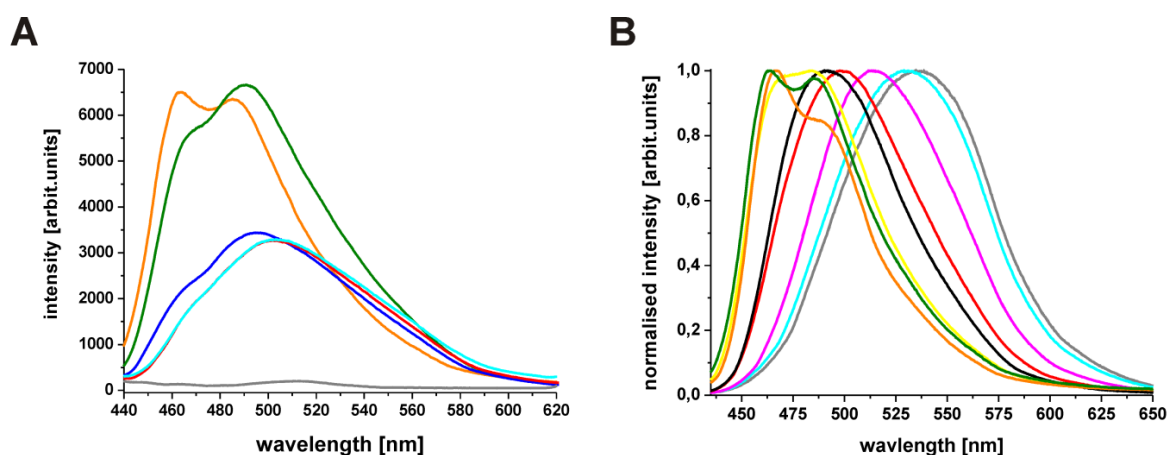


Figure 4.3-11 (A) Fluorescence spectra of curcuminoids dissolved in MCT (●) [0.5  $\mu\text{g}/\text{ml}$ ], curcuminoids incorporated in MCTCurc-NE (●), TmCurc-NE (●), TMCurc-NS (●) TSCurc-NS (●) nanoparticles [2.0  $\mu\text{g}/\text{ml}$ ] and a curcuminoid-free TM-NS (●) sample. Excitation wavelength: 420 nm. (B) Fluorescence spectra of curcuminoids dissolved in methanol (●), ethanol (●), tert.-butanol (●), acetone (●), chloroform (●), ethyl acetate (●), dioxane (●) and MCT (●). Curcuminoid concentration: 1  $\mu\text{g}/\text{ml}$  in methanol and ethanol, 0.5  $\mu\text{g}/\text{ml}$  in all other solvents. The spectra were normalized to their respective maximum intensity.

The shift of the maximum was attributed to a polarity change in the environment of the curcuminoids. The correlation between peak maximum and environmental polarity was demonstrated by dissolving the curcuminoids in different organic solvents. The maximum of the curcuminoid fluorescence in the most apolar solvents, MCT and dioxane, was at around 465 nm (Fig. 4.3-11 B). The spectra showed a distinct red shift when the solvent polarity increased. The maximum in the most polar solvent methanol was at 530 nm. In addition, the curcuminoid intensity was also dependent on the solvent. The intensity increased with decreasing polarity. This phenomenon was reported for curcumin in literature before (149,150).

In contrast to the apolar environment in bulk MCT, the curcuminoids will have more contact to polar regions within the emulsion droplets and the crystalline particles. Due to the small size of the particles, a considerable part of the drug will also be situated at the interface between water and lipid. Furthermore, the Raman data supported the idea that the curcuminoids were mainly attached to the surface of the crystalline particles. Thus, the fluorescence maxima were shifted to higher wavelengths, because the majority of the drug was residing on the more polar surface of the particles.

The structured shape of the different fluorescence spectra of the curcuminoid-loaded nanoparticles indicated the existence of several single species of the drug in the preparations (Fig. 4.3-11 A). A similar peak form with two maxima was also occurring in aprotic and apolar solvents, like MCT, dioxane and ethyl acetate, although the partition of the maxima was more pronounced in the solvents than in the nanoparticles (Fig. 4.3-11 B). In contrast, the dissolution of curcuminoids in polar solvents resulted in an unstructured and almost symmetric fluorescence spectrum. A fit of the fluorescence spectra of the lipid nanoparticles with Gaussian functions was calculated to determine the number of single curves of which the recorded spectrum may be composed of. It was found that a stable fit was possible with four Gaussian functions. However, an assignment of the gathered fitting curves to a certain state of the curcuminoids was not possible. One reason for the special shape of the spectra in the presence of lipids and apolar solvents could be the keto-enol tautomerism of the curcuminoids. It was reported that the proton migration of the tautomeric forms of the curcuminoids caused structured bands in the fluorescence spectrum, when the substance was dissolved in aprotic and non-polar solvents (150). However, possible regions of different polarity within the particles can be seen as another reason for the structured shape of the spectrum. In addition, scattered light from the particles may also influence the aspect of the fluorescence peak, although the light scattering of an unloaded TM-NE preparation was only weak (Fig. 4.3-11 A).

The fluorescence intensity of the curcuminoids was much lower when they were incorporated in the lipid nanoparticles compared to the MCT solution. The ratio of the fluorescence intensity to the concentration of the curcuminoids was determined. The

lowest ratio was calculated for the crystalline TMCurc-NS and TSCurc-NS preparations. This value was related to the ratios of the other formulations. Compared to the crystalline nanoparticles, the fluorescence/concentration ratio was almost equal for TMCurc-NE, but four times higher for MCTCurc-NE and eight times higher for the MCT solution of the curcuminoids. Therefore, the fluorescence intensity of the curcuminoids was dependent on the kind of lipid phase and on the dispersity of this phase. The reduced curcuminoid fluorescence of the nanoparticles was explained by the quenching effect of water. It was reported by Jasim *et al.* that the presence of water effectively quenched the fluorescence of curcuminoids (151). The authors postulated that the water molecule and the fluorescent dye build a complex which is not fluorescent. Due to the big surface/volume ratio of the nanoparticles, an intense interaction of the drug in the particle and the surrounding water was possible. The smaller intensity of the crystalline nanoparticles was caused by the presence of the majority of the curcuminoids on the surface of the particles, where they were distinctly quenched by the present water. In contrast, the curcuminoids were allowed to diffuse freely within the oil droplets of the emulsion which reduced the quenching effect. Though, the different fluorescence intensity of TMCurc-NE and MCTCurc-NE was not explainable by the quenching effect of water. The different solubility of the curcuminoids in the respective lipid may be the basic reason for the differences between the two emulsions. The curcuminoids were dissolved under constant heating in the respective lipid before homogenization. It was found that the drug was dissolved better in MCT compared to TM or TS. Curcuminoids might have precipitated, in part, within the emulsion droplets, during the cooling step after preparation. The non-dissolved fraction may have exhibited a less intense fluorescence compared to the dissolved curcuminoids. The fraction of dissolved curcuminoids is thought to be bigger in MCTCurc-NE, resulting in a higher fluorescence intensity. Conclusively, the fluorescence of the curcuminoids within the nanoparticles is amongst others influenced by the quenching effect of water and by its solubility in the respective lipid phase.

The heating and subsequent melting of a sample of TMCurc-NS had a big impact on the fluorescence properties of the incorporated drug (Fig. 4.3-12). The melting process influenced the maximum intensity, the peak position and the shape of the peak. The higher mobility and bigger thermal energy of the surrounding water caused an increased quenching at higher temperatures resulting in a smaller  $I_{\text{Max}}$  of the spectrum (Fig. 4.3-12 B). This phenomenon was also seen when MCTCurc-NE or TMCurc-NE were continuously heated. In these preparations the curcuminoid quenching was thought to be mainly caused by the increasing temperature of the liquid lipid within the droplets, because the major fraction of the curcuminoids was considered to be situated within the droplets and not at their surface. As a consequence, the surrounding water played probably only a minor role in quenching the curcuminoids during heating of the

nanoemulsions. The red shift of the fluorescence spectrum of TMCurc-NS pointed towards an increased polarity of the environment of the drug. This was explained by a better penetration of the water molecules onto the surface of the particles with rising temperature. At around 48 °C the fluorescence intensity of the TMCurc-NS sample was slightly increasing and the peak position was shifting to smaller wavelength (Fig. 4.3-12 A). This marked the beginning of the melting process. The maximum intensity and minimum peak position was reached at 51 °C (Fig. 4.3-12 B).

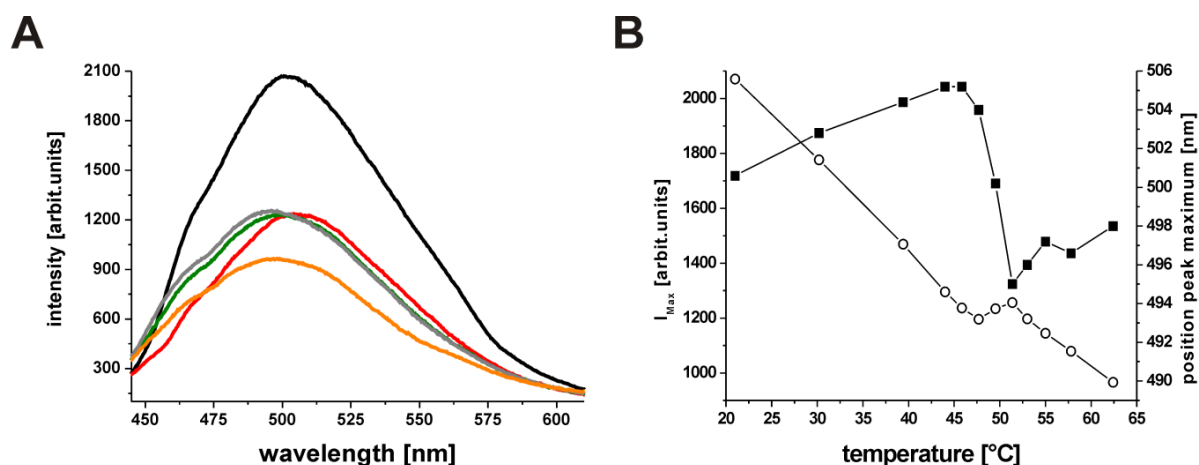


**Figure 4.3-12 (A)** Fluorescence spectra of a sample of TMCurc-NS at 21 °C (●), 46 °C (●), 49 °C (●), 51 °C (●) and 62 °C (●). Curcuminoid concentration: 2  $\mu\text{g}/\text{ml}$ . **(B)** Maximum intensity (-o-) and peak maximum (-■-) of the fluorescence spectra of TMCurc-NS during continuous heating.

At that point the lipid matrix was considered to be completely molten. The melting temperature was a bit lower compared to the temperature found by DSC, but coincided well with the temperature-dependent Raman measurements (see chapter 4.3.5.). Above 51 °C, the intensity fell again and the peak maximum was shifted to higher wavelength. Besides the changes of fluorescence intensity and peak position, the shape of the spectrum was changing, too. The shoulder at smaller wavelengths, typically found for liquid lipids, was appearing at 49 °C indicating a liquid fraction within the nanoparticles. The observed blue shift of the peak during the melting process was probably caused by a decreasing polarity, because the curcuminoids could diffuse from the surface of the particles in the liquid centre. The increasing fluorescence intensity was possibly caused by a partly solubilization of the curcuminoids in the lipid matrix.

The fluorescence anisotropy of the curcuminoids in the applied solvents and in the nanoparticles was clearly different (Fig. 4.3-13). Pure MCT had the highest anisotropy values, which proved that the curcuminoids are highly immobile within the oil. In

contrast, the anisotropy was only low for a solution of curcuminoids in acetone and the mobility of the drug appeared to be high within the organic solvent. The curcuminoid-loaded nanoparticles exhibited anisotropies of around 0.2 and were situated between acetone and MCT. The obtained results were explicitly lower compared to the anisotropy of curcumin associated to proteins or phospholipid micelles (118,152,153). Thus, the curcuminoids were still maintaining a considerable mobility within the nanoparticles. Interestingly, no clear difference in anisotropy between fluid and solid matrix was detectable. Hence, it is suggested that the curcuminoids are not adhered strongly on the lipid surface of the crystalline particles, but are rather enclosed loosely in the particles. With regard to the incorporated drug the anisotropy measurements confirmed that the solid lipid nanoparticles were not a static system, which immobilized the curcuminoids. On the contrary, the drug was still in a mobile state and in connection with the aforementioned fluorescence experiments, the aqueous environment of the nanoparticles, e.g. polarity and temperature, was shown to have a severe impact on the properties of the curcuminoids.

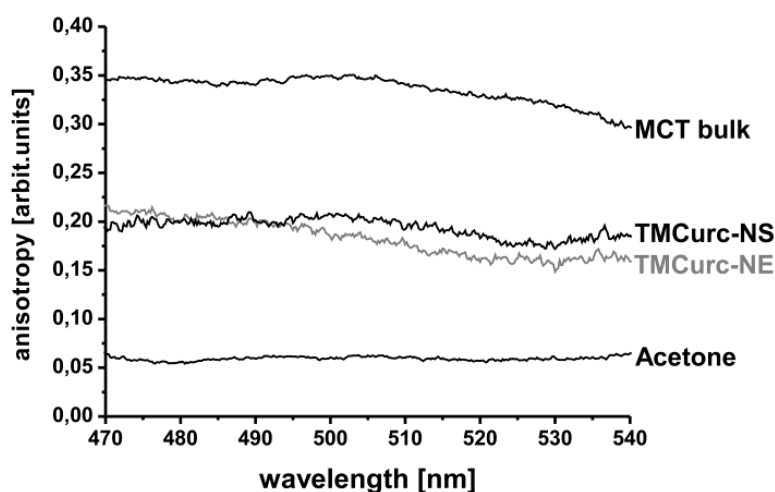


Figure 4.3-13 Fluorescence anisotropy of curcuminoid solutions in MCT and acetone (1.0  $\mu\text{g/ml}$ ) and of samples of TMCurc-NS and TMCurc-NE (2.0  $\mu\text{g/ml}$ ).

#### 4.3.7 Conclusion

The physicochemical properties of the produced lipid nanoparticles were elucidated by means of various techniques. The zeta potential was shown to be close to 0 mV for all poloxamer-stabilized systems, which confirmed the absence of a surface charge of the nanoparticles. The neutral surface was caused by the applied uncharged emulsifier,

poloxamer 188, whose PEG-chains build a hydrophilic shell around the nanoparticles. Hence, the stabilization of the preparations was not attained by electric repulsion of the nanoparticles, but sterical shielding was seen as major mechanism. The zeta potential was not affected by the physical state of the lipid or by the presence of curcuminoids. Furthermore, the buffer concentration did not influence the zeta potential. Thus, the poloxamer-stabilized formulations were suggested to be stable at higher electrolyte concentrations and in contrast to commercially available nanoemulsions (e.g. Lipidem) particle aggregation within salt solutions might be sustained.

The physical state of the lipid matrix was investigated by DSC, X-ray diffraction,  $^1\text{H}$  NMR and Raman spectroscopy. The supercooled state of the TM-NE and TMCurc-NE preparations was confirmed by the aforementioned techniques. The drug-free TM-NE nanoemulsions were widely stable over the observation period of 16 weeks, whereas the TMCurc-NE preparations showed some traces of recrystallization during this time. However, a direct impact of the incorporated drug on a spontaneous crystallization of the lipid matrix out of the supercooled state was not clearly verifiable. Thus, the supercooled state in general was thought to be metastable and not suitable as drug delivery system, because a partial recrystallization of the lipid during long-time storage cannot be surely excluded. Furthermore, the recrystallization of the supercooled melt might fundamentally change the properties of the formulation with unforeseen consequences for, amongst others, stability, drug release, particle degradation.

It was demonstrated that the TM nanoparticles were only crystallizing, when the preparation was cooled down to  $8^\circ\text{C}$ . The lipid crystallized solely in  $\beta$ -modification, as it was verified by DSC and X-ray diffraction. The crystallization of TM into the stable  $\beta$ -modification took place very fast, so that the  $\alpha$ - and  $\beta'$ -modification were not detectable by DSC. The TS nanoparticles solidified at higher temperatures than the TM nanoparticles and the phenomenon of a supercooled melt was not observed for these preparations. In contrast to the TM formulations, TS-NS and TSCurc-NS partially contained lipid with  $\alpha$ -modification beside a large lipid fraction in  $\beta$ -modification. The lipid fraction in  $\alpha$ -modification was subsequently converted into  $\beta$ -modification within sixteen weeks.

The  $^1\text{H}$  NMR investigations showed that the mobility of the liquid lipid phase of TMCurc-NE was not changing over a period of three weeks. The signals of the emulsifier were broadening over time which was explained with a further ordering of the polymer chains in the samples. In TMCurc-NS, a fraction of free fatty acids and partial glycerides was detected by  $^1\text{H}$  NMR.

The supercooled state of TM-NE and TMCurc-NE was further confirmed by Raman spectroscopy. The position and width of the bands indicated a low order of the fatty acid chains of TM, confirming the liquid state of the formulations. The peaks in the Raman spectra of the crystalline TM and TS nanoparticles pointed to a highly ordered crystalline

matrix, where the *trans*-conformation of the fatty acid chain was predominant. Furthermore, Raman spectroscopy gave unique information about the localization of the curcuminoids within the particle and their physical state. It was demonstrated that the ratio of the double band at  $1600\text{ cm}^{-1}$  and  $1630\text{ cm}^{-1}$  was depending on the physical state of the curcuminoids. The curcuminoid bands of the drug-loaded nanoparticles were similar in shape and ratio to the non-crystalline free substance. It was concluded that the curcuminoids were enclosed in an amorphous state within the particles. The present data suggested that the application of this method can help to elucidate the interaction of drug and lipid matrix, even at low concentrations of the drug. Further details of the drug-carrier interaction were gained by fluorescence spectroscopy. The intensity, position and shape of the fluorescence peak were influenced by the applied lipid, by the physical state of the lipid matrix and by the surrounding aqueous phase. The fluorescence intensity of the curcuminoids was lower for the nanoparticles compared to a solution of the drug in bulk lipid. The loss of intensity within the nanoparticles was explained by the quenching effect of the surrounding water. The curcuminoids, incorporated in the nanoparticles, exhibited a red shift of the spectrum compared to the solution in bulk lipid, which indicated a localization of the drug in a more polar environment, probably the particle surface.

Continuous heating of the nanoparticles resulted in pronounced decrease of the fluorescence intensity by water quenching, which further demonstrated the impact of the surrounding environment on the properties of the incorporated curcuminoids. The nanoparticles were therefore not separating the drug, but an interaction between drug and surrounding media took place. The properties of the lipid phase also influenced the fluorescence of the curcuminoids and thus the melting process was indirectly traceable by recording the curcuminoid fluorescence of the nanoparticles with increasing temperatures. From the results of the fluorescence and the Raman measurements, it was concluded that the curcuminoids were separated from the lipid matrix during crystallization and were attached to the surface of the particles.

The mobility of the curcuminoids within the nanoparticles was investigated by fluorescence anisotropy measurements. The curcuminoid mobility within the nanoparticles was shown to be decreased compared to a solution of the drug in an organic solvent, but still higher than in a viscous oil. Thus, the conditions within the particles were concluded to be fairly different from that in the lipid bulk material.



## 4.4 Curcuminoid stability

### 4.4.1 Loading efficiency & storage stability

The amount of incorporated curcuminoids was about 97 % for MCTCurc-NE, TMCurc-Ns and TSCurc-NS in relation to the initially applied quantity of drug, which was seen as a good drug loading efficiency (Fig. 4.4-1). The loss of 3 % of the drug was attributed to the complex production process. It was, for example, noticed that the curcuminoids were adsorbing on the used plastic hose. Moreover, the preparation had to be heated to 70 - 85 °C, which probably caused some hydrolytic degradation as well. The total curcuminoid content was decreasing by around 5 % over a period of 12 months, indicating a good long-term stability of the drug within the lipid particles under the applied storage conditions (Fig. 4.4-1). Normally, curcuminoids decompose rapidly in aqueous environment under neutral or basic pH conditions (32,154,155). In contrast, a noteworthy degradation of the curcuminoids was obviously not occurring when the drug was incorporated into or associated to the lipid nanoparticles. The good long-term stability of curcuminoids in SLN formulations has been recently confirmed by other research groups (70,156). With the sufficient stability of the curcuminoids within the lipid nanoparticles, one important requirement for the suitability of the developed system was fulfilled.

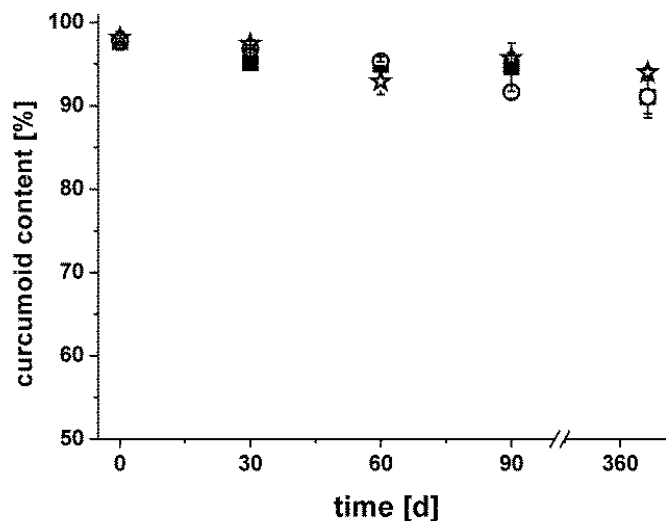


Figure 4.4-1 Curcuminoid content of the drug-loaded lipid nanoparticle preparations during long-time storage at 8 °C. (■) MCTCurc-NE, (○) TMCurc-NS, (★) TSCurc-NS. The symbols represent the mean of nine measurements. The error bars represent the respective standard deviation.

#### 4.4.2 Curcuminoid stability in physiological media

As it was mentioned in the previous chapter, curcuminoids are decomposing rapidly at a pH value > 7.0. Since the pH of the applied media was below 7 (SGF: pH 1.2, phosphate buffer: pH 6.8, FaSSIF: pH 6.8) the curcuminoid loaded TM nanoparticles exhibited a good drug stability throughout the experiment (Fig. 4.4-2).

The incubation of the preparations in SGF resulted in a decrease of the curcuminoids content to 92 % of the initial value. A slight degradation of the curcuminoids under comparable conditions was also reported by Wang *et al.* (154). On the contrary, phosphate buffer did not affect the curcuminoid stability distinctly. The good stability of the curcuminoids at pH 6.8 was in accordance to Tønnesen *et al.* who reported a half-life of around 15 h for an aqueous curcumin solution at this pH value (32). The curcuminoid content in the FaSSIF samples was somewhat lower compared to the phosphate buffer. The experiments proved the stability of the curcuminoids in the simulated physiological media.

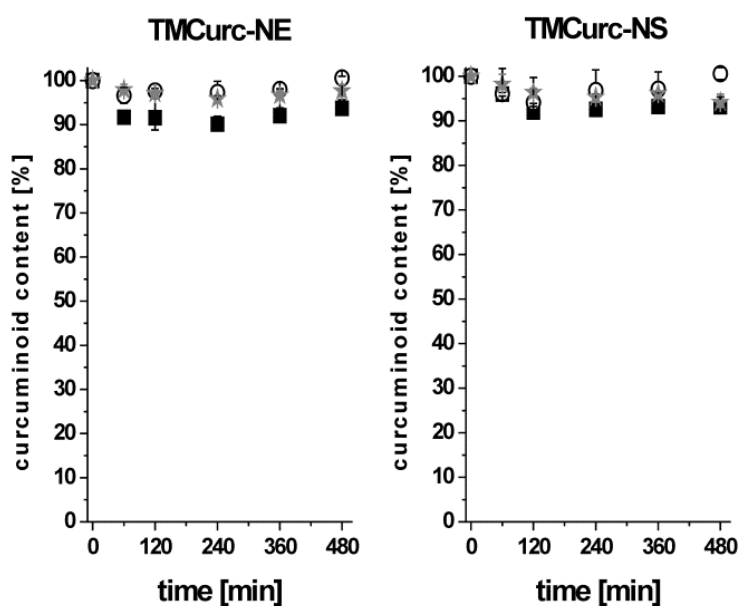


Figure 4.4-2 Curcuminoid content of samples of TMCurc-NE and TMCurc-NS incubated in (■) SGF, (○) Sørensen phosphate buffer pH 6.8 and (★) FaSSIF. The symbols represent the median value. The error bars represent the span of the single values.

## 4.5 Biological *in vitro* characteristics

### 4.5.1 *In vitro* release

The determination of the drug release from colloidal systems has been controversially discussed in the past years. A critical overview about this topic was provided by Washington (157). Various different techniques for the determination of the release have been reported so far (158-161). Major problems of such release measurements are the complicated separation of colloidal carrier and release medium as well as the warranty of sink conditions throughout the experiment. Normally, “perfect” sink conditions, meaning an infinite volume of release medium, are not attainable under *in vitro* conditions. In practice, the concentration of the released drug should not exceed 10 % of its saturation value in the respective medium. Colloidal carriers, like nanoparticles, are mostly used for the encapsulation of lipophilic, poorly water-soluble drugs (81,162). Thus, the volume of the release medium must be large for the investigation of such systems, because an oversaturation of the system must be avoided. Unfortunately, this results in a low concentration of the drug in the release medium, which demands a highly sensitive detection method. Curcuminoids are also poorly water-soluble substances. The release kinetics of curcuminoid formulations have already been described by other authors (70,73,74,163,164). The applied methods for release determination in the mentioned literature were either centrifugation or the dialysis-bag method. It is unclear, whether the centrifugation forces ensure the quantitative separation of released drug and colloidal carrier. Moreover, there are controversial reports about the localization of the released drug. Some authors located and quantified the drug in the pellet of the centrifuged sample (163,165). In contrast, the released amount of curcumin was determined in the supernatant of the centrifuged sample by another research group (164). The dialysis bag-method has been critically discussed by Benita *et al.* and by Washington (157,159). The authors claimed that actually the release rate of the drug from the carrier is not determined with this method, but rather the release rate of the drug from the dialysis bag. In addition, the insufficient water-solubility of the curcuminoids, for example, required the addition of solubilizers, like ethanol, to provide sink conditions as well as a detectable drug concentration in the acceptor compartment (73). The application of organic solvents as solubilizing agents is critical, because they can have a serious impact on particle stability and might influence drug release dramatically.

The aim of the presented release chamber was the examination of an alternative way for determining the release of curcuminoids from nanoparticles. One advantage of the presented model was the direct determination of the drug concentration in the donor compartment. Thus, the actual volume of the acceptor medium could be adjusted to sink

conditions regardless of the detectability of the substance in this compartment. The curcuminoids were fluorescent within the particles, but were quenched after the release into the aqueous media. Hence, the released drug did not impair the measurement. A quenching of the curcuminoid fluorescence within the particles was excluded by loading the particles with 0.01 % (w/w) drug only. Preliminary experiments showed that the curcuminoid fluorescence within the nanoparticles increased linearly in a range between 0.01 % and 0.05 % (Fig. 4.5-1).

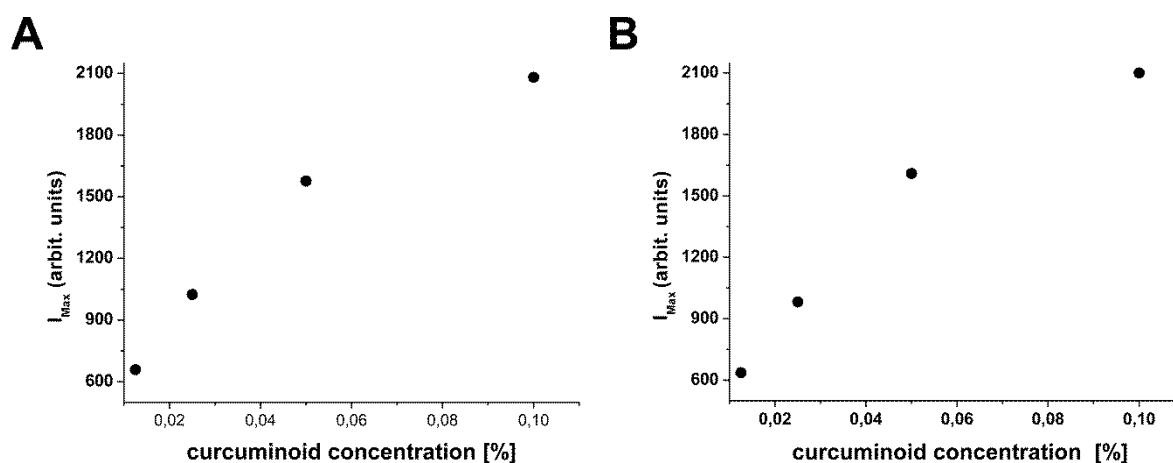


**Figure 4.5-1** Fluorescence of (A) TMCurc-NE and (B) TMCurc-NS loaded with different amounts of curcuminoids in the range of 0.0125 % (w/w) and 0.1 % (w/w). The fluorescence spectra were recorded with Hitachi F-4500 spectrophotometer. The settings of the instrument are described in schapter 3.3.6.

Furthermore, the applied fluorescence imaging method is a sensitive measurement technique and even low concentrations of the curcuminoids were well detectable. Though, it was found that the curcuminoids were slightly adsorbing on the dialysis membrane, which resulted in a detectable fluorescence. The extent of curcuminoid adsorption was equal for all investigated media. Hence, it was suggested that this effect did not influence the measurement in a critical way. The aforementioned observations, like auto-fluorescence of the release medium and drug adsorption on the membrane, illustrate the need for a careful evaluation of the experimental conditions.

The *in vitro* release profiles of the curcuminoids are shown in Figure 4.5-2. The release was investigated in SGF, phosphate buffer pH 6.8, FaSSIF and FeSSIF. The respective media were chosen, because they were imitating the compartments, which have to be passed when the curcuminoid-loaded nanoparticles are administered orally. It was found that the curcuminoids were released slightly in phosphate buffer pH 6.8 (Fig. 4.5-2 A). A bigger amount of curcuminoids was released in SGF. In TMCurc-NE, only about 15 % of the

drug was released in SGF, whereas almost 40 % of the curcuminoids were released from the TMCurc-NS samples. An even more intense release of the drug was observed during the incubation of the preparations in FaSSIF or FeSSIF, respectively (Fig. 4.5-2 B).

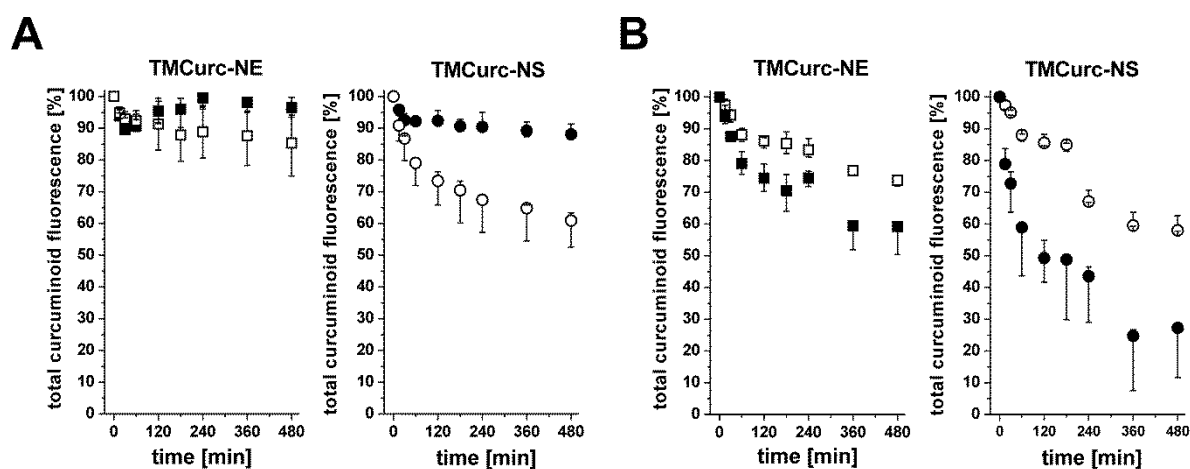


**Figure 4.5-2 Curcuminoid release profiles during examination of TMCurc-NE and TMCurc-NS. (A) release media: (□ ) and (○ ) SGF pH 1.2; (● ) and (■ ) Sørensen phosphate buffer pH 6.8. (B) release media: (□ ) and (○ ) FaSSIF; (● ) and (■ ) FeSSIF. The median of three values is presented. The error bars symbolize the span of the single values.**

The loss of fluorescence was more pronounced in FeSSIF than in FaSSIF. However, the bile salts, dissolved in the intestinal media, were fluorescing at approximately the same wavelength as the curcuminoids. The auto-fluorescence of a curcuminoid-free FaSSIF and FeSSIF sample was subtracted from the image cubes recorded during the release measurements in the simulated intestinal media. Although the method allowed the differentiation between curcuminoid and bile salt fluorescence, the presence of substances with a fluorescence maximum near the maximum of the investigated drug was concluded to be a potential error source and such an experimental setup should be avoided in future experiments.

The released amount of drug and the speed of the release were always higher for the crystalline TMCurc-NS samples compared to the liquid TMCurc-NE samples. The curcuminoids were thought to be mainly located at the surface of the crystalline TM nanoparticles, whereas they could freely diffuse in liquid droplets of the TM nanoemulsion. Thus, the drug attached on the solid particles was in incessant contact with the release medium, which resulted in a faster dissolution and subsequently in a faster release. The higher drug release in SGF was attributed to the increased solubility of the curcuminoids under acidic conditions (pH 1.2) compared to the almost neutral phosphate buffer (pH 6.8), (73). The presence of bile salts and phospholipids caused the pronounced

drug release in the artificial intestinal media, because these compounds solubilized the curcuminoids effectively. The higher concentration of bile salts and phospholipids in the fed state medium therefore entailed a faster release. However, a typical burst release, which was reported frequently for other drug-loaded nanoparticles, was not found for the curcuminoid-loaded lipid nanoparticles in any of the tested release media (158,160,166). It has to be verified in upcoming experiments whether the missing burst release is an inherent characteristic of the curcuminoid-loaded nanoparticles or whether it is caused by the experimental setup of the release determination.

The conducted experiments demonstrate the general applicability of the developed model for the determination of drug release from nanoparticles. The release observation, based on fluorescence imaging was capable to differentiate between various release patterns of the curcuminoids, which were dependent on the used release medium. The direct determination of the residual drug amount in the nanoparticles was concluded to be a clear advantage compared to other methods, which determine the amount of the released drug. However, the model needs to be further optimized and crucial parameters have to be further investigated. Potential side effects, like the aforementioned auto-fluorescence of the release medium or drug adsorption on the membrane, illustrate the need for a careful evaluation of the experimental conditions. Additionally, the influence of stirring speed, membrane surface and drug concentration within the block cavities on the release velocity needs further clarification.

## **4.5.2 *In vitro* digestion**

### **4.5.2.1 *Digestion in simulated gastric media***

The exposure of the TM nanoparticles to simulated gastric fluid (SGF) revealed no degradation of the lipid matrix and the amount of triglyceride was not decreasing throughout the whole observation period (Fig. 4.5-3 A-D). The presence of pepsin did not influence the stability of the triglyceride. However, the distribution of the data points was unsatisfactorily broad for some samples (Fig. 4.5-3 B & D). The flocculation of TMCurc-NE and TMCurc-NS during the incubation in the acidic medium was seen as main reason for this outcome, because the particle aggregation impaired the reproducible withdrawal of the samples. The unfavorable distribution of the data might have masked a minor degradation of the triglyceride matrix. However, the stability of the triglyceride matrix was proven indirectly because no relevant degradation products, like fatty acids or partial glycerides were detected by HPTLC/spectrodensitometry. The detection limit of the HPTLC/spectrodensitometry method for TM was below 0.005 % (w/v). Thus, small amounts of probable degradation products would have been detectable. The experiment

demonstrated the hydrolytic stability of the triglyceride under acidic conditions. However, *in vivo* the lipid particles are expected to be degraded partially by the gastric lipase. Additional experiments involving this enzyme will be necessary to further clarify the fate of the lipid nanoparticles during the passage of the stomach. Unfortunately, digestion tests for gastric lipase are currently not commercially available.

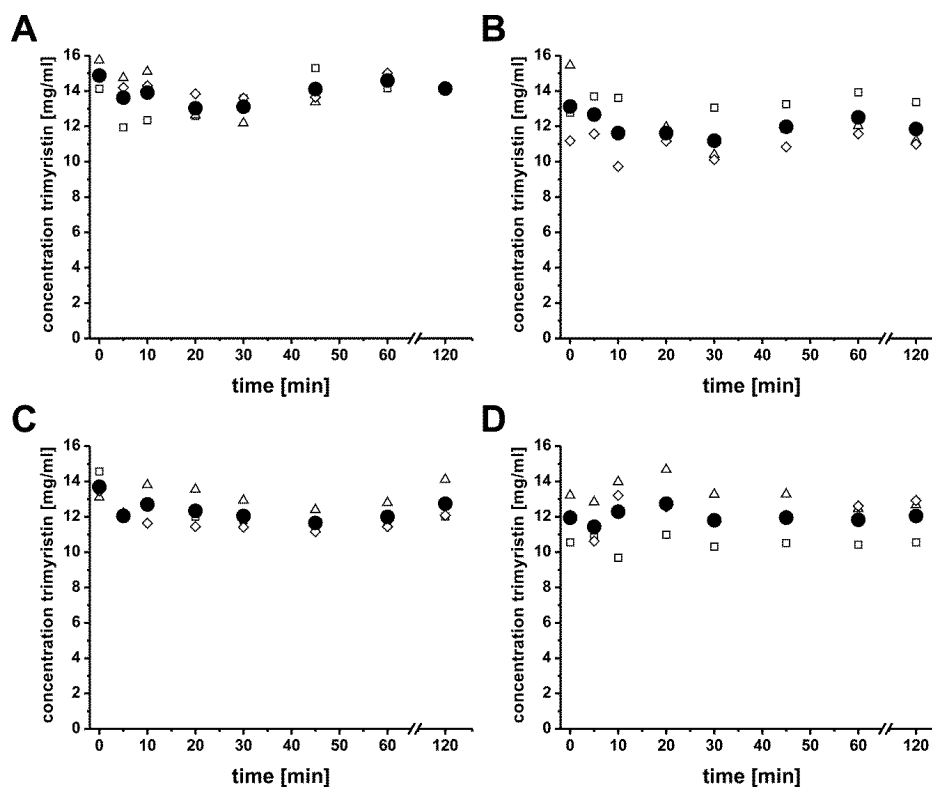
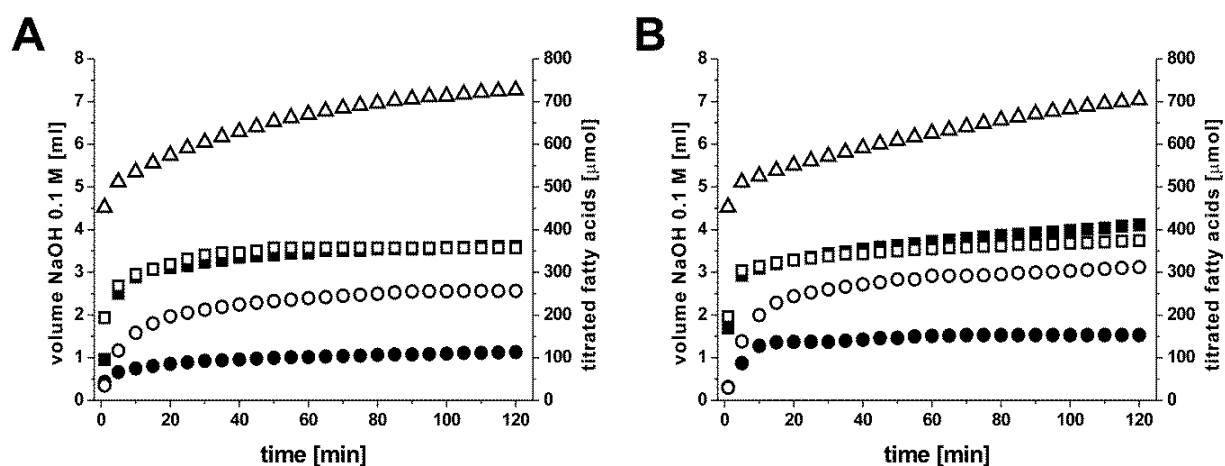


Figure 4.5-3 TM concentration curves during the *in vitro* digestion in SGF. (A) TMCurc-NE in SGF without pepsin; (B) TMCurc-NS in SGF without pepsin; (C) TMCurc-NE in SGF containing pepsin; (D) TMCurc-NS in SGF containing pepsin. (●) mean of three digestion runs, (Δ), (○), (□) concentration profiles of the respective samples.

#### 4.5.2.2 Digestion in simulated intestinal media (pH-stat method)

During the *in vitro* digestion of the different formulations in simulated intestinal media, free fatty acids are formed as a result of the degradation of the triglyceride matrix. The release of the fatty acids caused a drop of the pH value. Sodium hydroxide (0.1 mol/l) had to be added to keep the pH constantly at 6.8. As a result, the consumption of sodium hydroxide was used to illustrate the degradation velocity of the triglyceride particles by the pancreatic lipase (Fig. 4.5-4). The progression of the titration curves was almost similar in FaSSIF and FeSSIF (Fig. 4.5-4).



**Figure 4.5-4** Consumption of sodium hydroxide during the *in vitro* digestion of different lipid nanoparticle formulations in (A) FaSSIF and (B) FeSSIF. (● ) blank; (○ ) TSCurc-NS; (□ ) TMCurc-NE; (■ ) TMCurc-NS and (Δ) MCTCurc-NE. The median of three titrations is presented.

Generally, two phases could be distinguished from the titration curves. In the first five minutes, there was a high initial consumption of sodium hydroxide in all investigated samples, corresponding to a high output of free fatty acids (Fig. 4.5-4). The initial digestion speed appeared to be slower for TSCurc-NS compared to TMCurc-NS, which signified to a delay in degradation of the long-chain lipid. Interestingly, no clear difference between the supercooled TMCurc-NE nanoemulsion and the crystalline TMCurc-NS nanoparticles was recorded. After the high initial slope, the consumption curve of the TM- and TS-based preparations was getting flatter indicating little digestion activity. Thus, the major part of the triglyceride matrix was digested in the first ten to fifteen minutes. In contrast to TM and TS, the MCTCurc-NE samples were also showing considerable consumption of sodium hydroxide in the latter stage of the experiment. The reason for this outcome is discussed in detail in the following sections.

The titration curves indicated the digestion speed to be approximately the same in fasted and fed state conditions. However, the consumption of sodium hydroxide was higher for the blank FeSSIF compared to the blank FaSSIF, because the fed state medium contained more phospholipids, which were hydrolyzed during the experiment. These differences between FaSSIF and FeSSIF were not clearly verifiable for MCTCurc-NE, TMCurc-NE and TMCurc-NS.

The different consumption of sodium hydroxide of the particular formulations had various reasons. Firstly, the deployed molar amount of triglyceride in the digestion experiment was higher for MCT compared to TS, which resulted in a higher amount of free fatty acids and thus a higher consumption of sodium hydroxide. Secondly, the released fatty acids



were only ascertained by the pH-stat method when they were dissociated. The dissociation of an acid is determined by its  $pK_a$ . For fatty acids this value is dependent on the respective chain length but also on the composition of the environment (167). The  $pK_a$  values are getting smaller with decreasing chain length, but are generally in the range from 4 to 8 (168). Hence, the corresponding free fatty acids of MCT, TM and TS were probably not fully dissociated under the applied conditions of the digestion experiment (pH 6.8). The relative amount of ascertained free fatty acids was therefore calculated. For this purpose, the released amount of the respective fatty acid determined by the pH-stat method was divided by the actual amount of cleavable fatty acids of the triglyceride. The calculation revealed that about 45 % of the stearic acid, 60 % of myristic acid and almost 100 % of caprylic and capric acid were ascertained by the titration experiment. The incomplete titration of long-chain fatty acids by the pH-stat method was already reported by other research groups (128,169). In summary, the higher consumption of sodium hydroxide during the digestion of MCTCurc-NE compared to the TM- and TS-based nanoparticles was at least partially caused by the lower  $pK_a$  of caprylic and capric acid leading to a higher dissociation at pH 6.8. This might also explain the different progression of the titration curve of the MCT formulation compared to TM and TS (Fig. 4.5-4). The high initial consumption of sodium hydroxide marked the degradation of the triglyceride matrix of the particles, whereas in the second phase with a weaker curve slope the degradation of the diglycerides was recorded. The pH-stat method could visualize this process only for MCT, but not for TM or TS.

Besides the  $pK_a$ , the precipitation of the released fatty acids as insoluble calcium soaps and their incorporation into mixed micelles might also have influenced the detectable amount of fatty acids. In addition, the different water solubility and tendency to form liquid crystalline phases of the particular fatty acids also have to be considered. The incomplete titration of long chain fatty acids could be circumvented by a back titration at the end of the digestion experiment (170,171). However, this attempt implies the risk of an advanced hydrolytic decomposition of monoglycerides due to the elevated pH value. In addition, it is questionable if the fatty acids trapped in mixed micelles or calcium soaps can be determined by this approach.

The pH-stat method was seen as a fast and practicable method to monitor the digestion of the lipid nanoparticles. Nevertheless, the above mentioned drawbacks and limitations of this method have to be taken into account, e.g. when the results of two different lipids are compared.

### 4.5.2.3 Digestion in simulated intestinal media (HPTLC/spectrodensitometry)

The HPTLC analysis in combination with spectrodensitometry provided useful data of the fate of the triglycerides and of all related degradation products. The liquid triglyceride matrix of TMCurc-NE was degraded within five minutes (Fig. 4.5-5). A difference in the degradation speed between fasted state and fed state conditions was not verifiable. Due to the fast hydrolysis of the triglyceride the concentration of 1,2-diglyceride reached its maximum already five to ten minutes after the start of the experiment (Fig. 4.5-5).

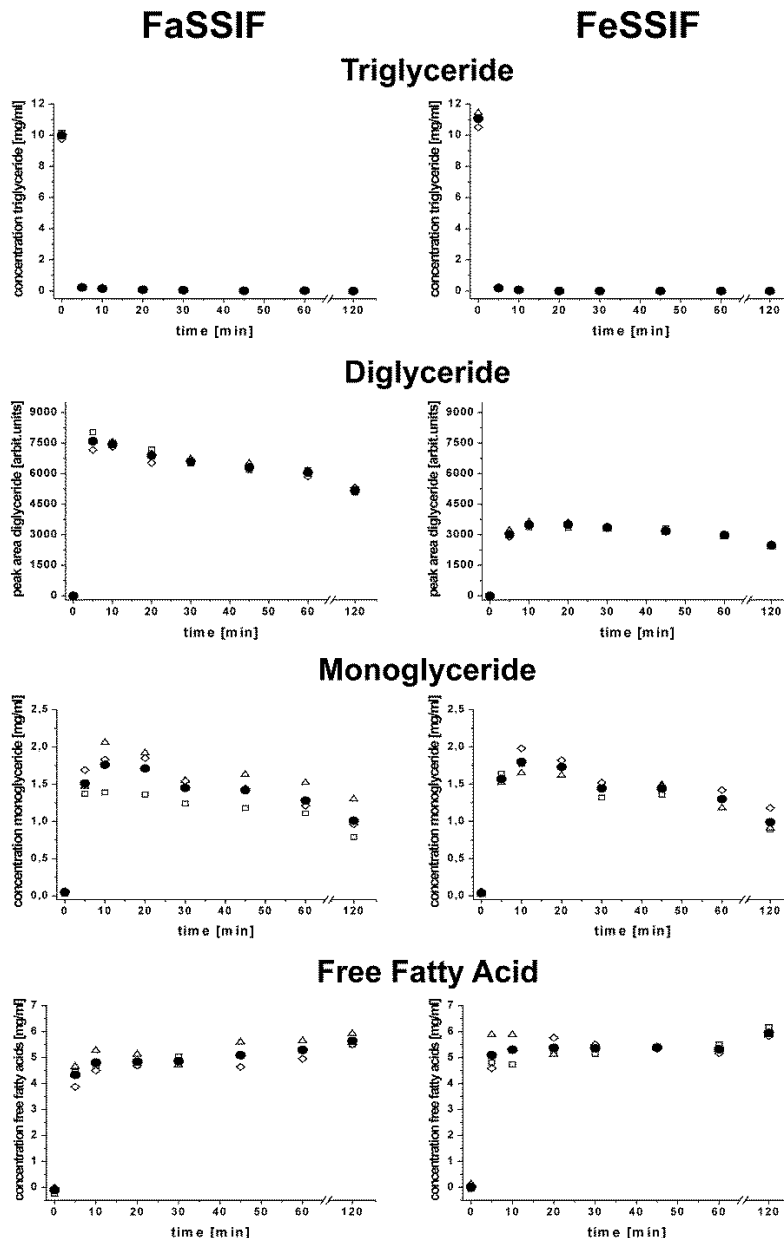


Figure 4.5-5 Concentration profiles of TM and its degradation products during the *in vitro* digestion of TMCurc-NE in simulated intestinal media. (● ) mean of three digestion runs; (Δ), (○ ), (□ ) concentration profiles of the respective samples.

The 1,2-diglyceride content was subsequently decreasing again, because of its further degradation to the 2-monoglyceride. The maximum concentration and the end concentration of 1,2-diglyceride was higher in FaSSIF than in FeSSIF. Hence, the digestion process of 1,2-diglyceride proceeded faster in the fed state medium. A considerable amount of 1,2-diglyceride also remained undigested after 120 minutes in FaSSIF as well as in FeSSIF. The concentration of 2-monoglyceride in the digestion medium was rapidly increasing within the first ten minutes of the experiment (Fig. 4.5-5). 2-monoglycerides are the end product of the digestion *in vivo*. They are absorbed by the enterocytes and are subsequently re-esterified to triglycerides. Subsequently, these triglycerides are transferred to the bloodstream or the lymphatic system. It was therefore expected that the concentration of the 2-monoglyceride reaches a plateau during the *in vitro* digestion. However, the concentration of the 2-monoglyceride was decreasing again after reaching its maximum concentration at 10 minutes. This outcome was attributed to a phenomenon called acyl-group migration (172,173). After the lipase hydrolyzed the fatty acids in sn-1 and sn-3 position 2-monoglyceride was left. Subsequently, the fatty acid in sn-2 position shifted spontaneously to the sn-1 position. The 1-monoglyceride was hydrolyzed by the lipase to a free fatty acid and glycerol. However, the complete decomposition of triglycerides to glycerol and free fatty acids occurs only *in vitro* (172).

There was no clear difference between FaSSIF and FeSSIF for the 2-monoglyceride curve profile. It was expected that the maximum concentration would be higher in the fed state medium, because of the faster degradation of 1,2-diglyceride. In contrast, both curve profiles show hardly the same progress and the maximum concentration was almost identical.

The characteristics of the concentration curve of the free fatty acids resembled the curves recorded by the pH-stat method (Fig. 4.5-4; Fig. 4.5-5). At the beginning the concentration increased steeply, followed by a slower release of fatty acids. The results of the HPTLC/spectrodensitometry analysis confirmed the assumption that the high initial consumption of sodium hydroxide during the pH-stat titration was caused by the degradation of the triglyceride. The weak slope of the consumption curve at the latter stage of the digestion was caused by the slow degradation of the mono- and diglycerides.

The digestion of the crystalline trimyristin particles is shown in Figure 4.5-6. Compared to the supercooled nanoemulsion, the degradation of the solid lipid nanoparticles was delayed (Fig. 4.5-6). Under fasted conditions, it took about 30 minutes until the triglyceride matrix of TMCurc-NS was completely hydrolyzed. In contrast to the digestion of TMCurc-NE, a difference in the digestion speed between fasted state and fed state was detectable for TMCurc-NS.

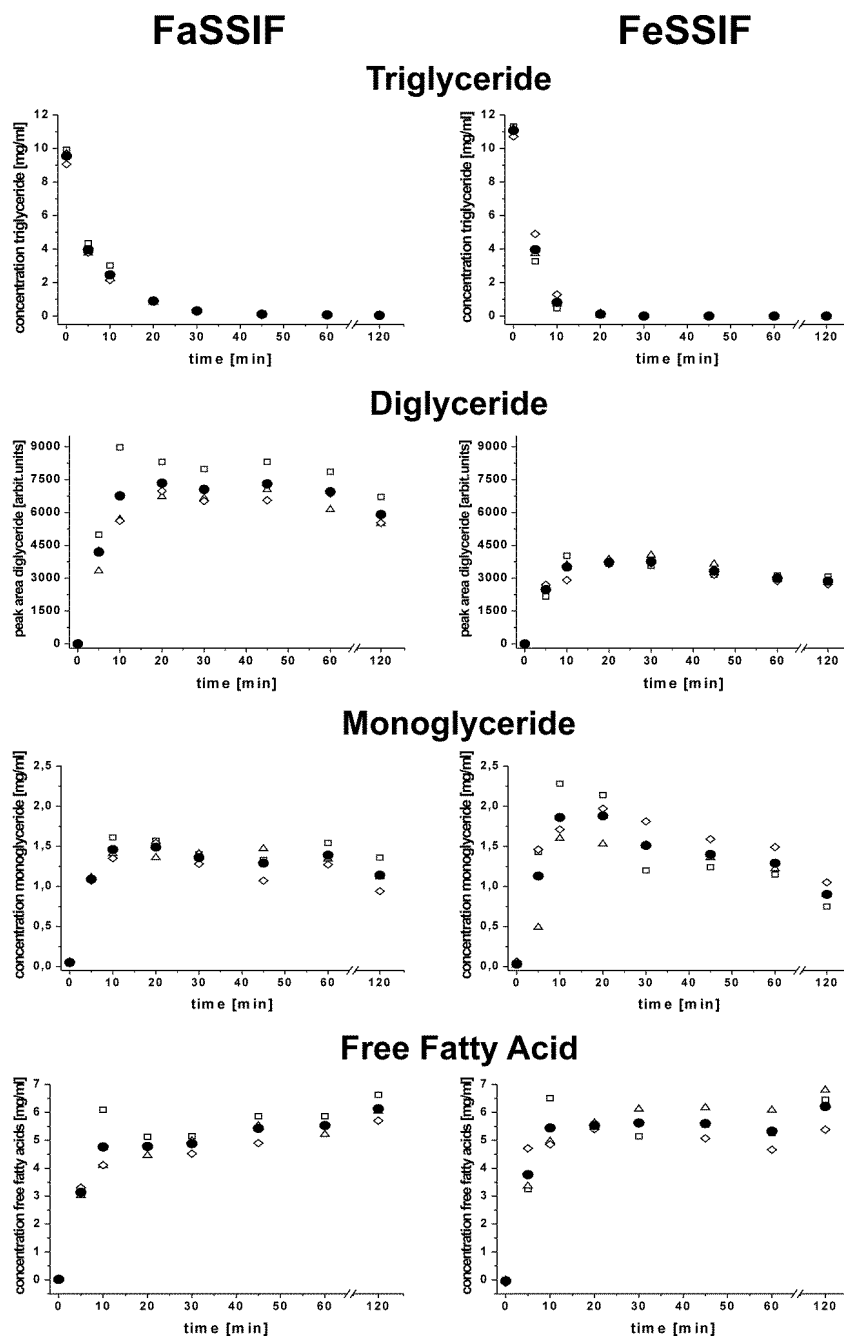


Figure 4.5-6 Concentration profiles of TM and its degradation products during the *in vitro* digestion of TMCurc-NS in simulated intestinal media. (●) mean of three digestion runs; (Δ), (○), (□) concentration profiles of the respective samples.

The curves of the lipid degradation products were of comparable shape the curves of the TMCurc-NE preparation (Fig. 4.5-6 and Fig. 4.5-5). The 1,2-diglyceride concentration was rapidly increasing and subsequently falling again, because of its degradation to 2-monoglyceride in the latter stages of the experiment. The digestion of the 1,2-diglyceride was more pronounced in FeSSIF than in FaSSIF. Though, in both media the diglyceride was not degraded completely in both media. With regard to the 2-monoglyceride curves, the

acyl group migration was also occurring when the TMCurc-NS samples were digested. In contrast to the TMCurc-NE samples, a higher maximum concentration of the 2-monoglyceride in FeSSIF compared to FaSSIF was verifiable for TMCurc-NS. The concentration curves of the free fatty acids did not reveal any significant differences in relation to the respective curves of the TMCurc-NE samples.

The *in vitro* digestion of the TMCurc-NE and TMCurc-NS, monitored by HPTLC/spectrodensitometry, revealed the fast and complete degradation of the triglyceride matrix. In contrast, the extent of digestion was not clearly provable by the pH-stat method. Though, the flat progression of the titration curves of TMCurc-NE and TMCurc-NS already pointed to a complete degradation of the triglyceride. As a consequence, the digestion of MCTCurc-NE and TSCurc-NS, determined by the pH-stat method, was thought to be complete as well, because their consumption curves were almost similar to the TM samples.

There are differing reports about the extent and velocity of the digestion of lipid nanoparticles in literature. A complete degradation of trimyristin nanoparticles, for example, was reported by Olbrich *et al.* (131,174). In contrast, Bonnaire and co-workers were reporting an incomplete digestion of lipid nanoparticles containing tripalmitin (175). The different outcomes of the *in vitro* lipid digestion might have various reasons. Naturally, the applied lipid is a key parameter. Triglycerides with medium chain fatty acids are digested faster and to a higher extent than triglycerides with long-chain fatty acids. This is attributed to the faster migration of the degradation products of the medium chain lipids from the oil/water interface into the digestion medium (176). Thus, the lipase/co-lipase complex is not hindered in its function. Additionally, it is of importance whether the triglyceride is in a liquid or crystalline form during digestion. The hydrolysis of crystalline TMCurc-NS was slower compared to the supercooled droplets of TMCurc-NE. Bonnaire *et al.* were also reporting an influence of the physical state of the lipid on the speed and extent of the digestion (175). In the present study, the differences in degradation between crystalline nanoparticles and liquid nanoemulsions were also proved, but the discrepancies were smaller than in the literature reports (175). Certainly, the lipid phase does not always consist of triglycerides. The application of waxes, like cetyl palmitate, as lipid matrix has been reported before (177,178). The wax nanoparticles were degraded more slowly than the triglyceride particles, because the lipase was not able to hydrolyze the ester bond of the wax effectively (131,178).

The particle size has also a distinct impact on degradation process. Small particles are generally degraded faster than larger ones, because they present a larger surface to the attacking lipase. In addition, an increased curvature might also speed up the digestion. So, the fast and complete degradation of the lipid nanoparticles in the present study has to be mainly attributed to the small particle size of the preparations. The small

differences in the mean particle size between the investigated preparations were thought to be negligible for the actual digestion speed, because an effect of the particle size on the digestion velocity was reported to be not verifiable until the size difference between the investigated formulations was bigger than 100 nm (174,176). Besides the used lipid and the particle size, the applied emulsifier also influences the digestion (176,178,179). The emulsifier on the surface of the particle has to be displaced by the bile salts of the digestive fluid, before the lipase/co-lipase complex can attach to the surface (180). Therefore, emulsifiers “sticking” on the particle surface or such with voluminous chains can delay this displacement step and the following lipid degradation (131,179). With regard to poloxamer 188, contrary reports of its effect on the digestion process have been found in the literature (174,179). Olbrich et al. found no retarding effect for this emulsifier, whereas Wulff-Pérez and co-workers reported a delay of the lipid digestion, when poloxamer 188 was used. They attributed the retarded digestion to a steric hindrance of the lipase caused by the hydrophilic PEG-chains of the emulsifier. In this study, the used emulsifier poloxamer 188 did not show any retarding effect on the lipid digestion. The presence of high amounts of phospholipids and bile salts was thought to displace the poloxamer 188 on the surface of the particles during the digestion process, so that the attachment of the lipase was not impaired.

Finally, the composition of the *in vitro* test medium is of elemental importance for the experimental outcome. Actually, the milieu of the small intestine should be rebuilt in the simulated media by the presence of bile salts, phospholipids and buffer salts. Therefore, a differentiation between fasted and fed state is made, which is expressed by different concentrations of bile salts and phospholipids within the respective medium. And indeed, higher concentrations of bile salts and phospholipids in FeSSIF compared to FaSSIF also resulted in a faster and more extensive degradation of the acylglycerides in the fed state medium (128). Moreover, the presence of bile salts and phospholipids was described to be necessary for the removal of the lipid degradation products from the oil/water interface by solubilizing them in mixed micelles (181). If these substances are missing or their concentration is too low, the lipase can be inhibited by the monoglycerides and free fatty acids, which accumulate at the phase interface (180). On the contrary, if the concentration is too high, they might act as an alternative location for the lipase, resulting in a decreased activity of the enzyme. However, there are distinct differences in composition and pH between the particular digestion media described in literature and due to these differences it was difficult to compare the reported *in vitro* digestion studies of lipid nanoparticles with the results of the present study (174,179,182). The heterogeneous data of *in vitro* digestion experiments and as a consequence the missing comparability of the gained results emphasize the need for a standardized operation procedure on this research field.

#### 4.5.2.4 Drug solubilization

The aim of orally administered lipid formulations is the release of the incorporated, poorly water-soluble drug through degradation of the lipid solvent and the subsequent solubilization of the released drug in colloidal species, like mixed micelles. A good solubilization of the drug is an indispensable prerequisite for the absorption by the small intestine. Therefore, this fact must be considered for *in vitro* digestion experiments as well. Porter *et al.* suggested three possible distribution zones for the drug in the *in vitro* medium: (1) the oil phase, (2) the aqueous phase with vesicular and micellar structures and (3) the pellet (183). The lipophilic drug can only remain in the oil phase when the digestion process is incomplete. In this case the lipophilic drug will mainly stay in the apolar oil, because of its low affinity to the polar aqueous environment. The presence of the drug in the oil-phase might result in a reduced absorption of the drug *in vivo*. The pellet is obtained by centrifuging the digestion medium after the experiment is finished. Amongst others, it is comprised of excessive enzyme, surplus ions and insoluble calcium soaps. The drug residing in the pellet was adsorbed onto these components of the digestive fluid during the digestion experiment. It remains unclear whether this *in vitro* effect also occurs *in vivo*. Nevertheless, if drug is adsorbed onto insoluble compounds a reduced *in vivo* absorption is probable. The destined compartment for the drug is the aqueous phase, where the drug is solubilized in mixed micelles and in swollen micelles. Swollen micelles consist of phospholipids, bile salts and the degradation products of the digested lipid. They are formed when the mixed micelles incorporate the partial glycerides and free fatty acids which occur at the oil/water interface during lipid degradation. The solubilization capacity of the mentioned structures depends on their concentration in the digestive media. Generally, swollen micelles take up more drug compared to pure mixed micelles (183).

The content of the curcuminoids in the supernatant of the centrifuged digestion media are shown in Figure 4.5-7. The amount of solubilized curcuminoids was considerably lower for the powder compared to the lipid formulations. In FaSSIF only 10 % of the curcuminoid powder was solubilized, whereas the incorporation into lipid nanoparticles provided a better solubilization of the drug. The total amount of solubilized drug was higher for FeSSIF than for FaSSIF. In the fed state medium, 50-60 % of the drug was found in the supernatant, when the TM nanoparticles were digested. In FaSSIF only half of this concentration was reached. The increase of the solubilized curcuminoid fraction in FeSSIF was attributed to the higher concentration of bile salts and phospholipids. As a consequence more mixed micelles were built and more curcuminoids were incorporated within these structures.

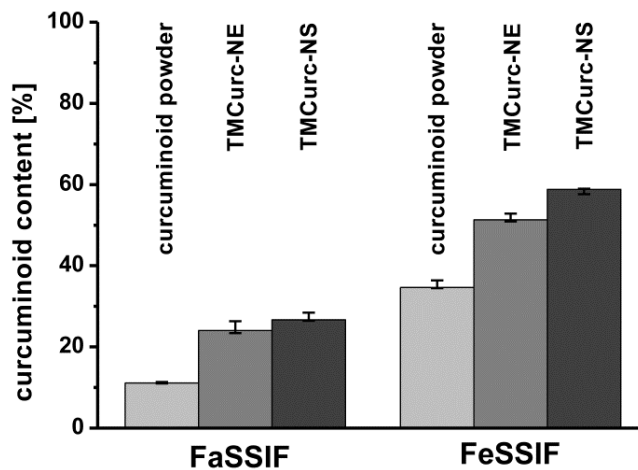


**Figure 4.5-7** Curcuminoid content in the supernatant of the simulated intestinal fluids after the digestion experiment. The respective column represents the median value (n=3). The error bars represent the span of the single values.

The higher solubilization efficiency of the drug-loaded nanoparticles was explained by the direct transfer of the drug from the particles into the mixed micelles during degradation of the triglyceride matrix. It is suggested, that the curcuminoids were transferred into the mixed micelles during the removal of the partial glycerides and the free fatty acids from the oil/water interface. Additionally, the presence of swollen micelles, caused by the degradation of the lipid, was also improving the solubilization capacity of the medium. In contrast, the big curcuminoid crystals and the low content of emulsifying compounds inhibited an effective solubilization of the drug in the powder samples. However, in all samples a substantial amount of the drug was not found in the supernatant. The missing fraction of the drug was supposed to be in the centrifugation pellet. After the digestion of the powder sample the pellet showed a white and an orange fraction. The white fraction was caused by the insoluble components of the medium and the orange fraction was the undissolved part of the used curcuminoids. The pellets of the TMCurc-NE or TMCurc-NS samples, respectively, were completely yellow. The released drug was therefore partially bound to the insoluble compounds of the medium. Additionally, the pellet exhibited a well-defined orange debris of crystalline drug. It is suggested that the colloidal structures of the media were oversaturated with drug during the rapid degradation of the triglyceride matrix at the beginning of the experiment. Consequently, the drug did recrystallize and precipitate in the latter stages of the experiment.



### 4.5.3 Cytotoxicity assessment

#### *In vitro* toxicity of free curcuminoids

The treatment of the Caco-2 cells with free curcuminoids considerably decreased the number of viable cells. If the curcuminoid concentration was above 20  $\mu\text{g}/\text{ml}$  (42  $\mu\text{mol}/\text{l}$ ), no fluorescence was detected after an incubation time of 24 h. Thus, no metabolically active cells were present in these samples. The cell viability was increasing when the curcuminoid concentration further decreased (Fig. 4.5-8). At a drug concentration of 5  $\mu\text{g}/\text{ml}$  (14  $\mu\text{mol}/\text{l}$ ) the fluorescence intensity was as high as in the control. The presence of 1 % (v/v) DMSO, which used as solvent for the curcuminoid stock solution, in the medium was non-toxic to the cells (data not shown).

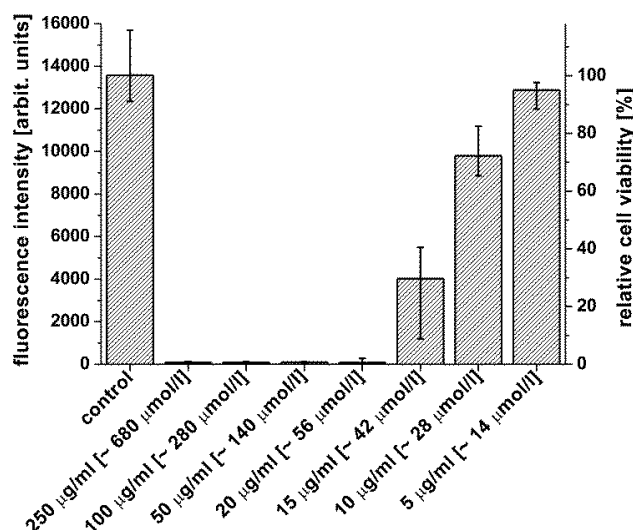


Figure 4.5-8 Fluorescence intensity of QBlue reagent and corresponding relative cell viability of Caco-2 cells after incubation with different concentrations of free curcuminoids (14 - 680  $\mu\text{mol}/\text{l}$ ) for 24 hours. The respective column represents the median of the fluorescence of three identical wells. The error bars represent the respective span of the single values.

The *in vitro* activity of curcumin against cancer cells has been widely reported in the literature (26,184). Curcumin influences various cellular signaling pathways and is able to inhibit cell proliferation and to induce apoptosis of cancer cells (33,72,184,185). However, the cytotoxic effect of free curcumin, found in the present study, was not attributed to apoptotic processes. The incubation time was thought to be too short to induce apoptosis in the cells. The acute toxic effect of the high curcumin doses (> 56  $\mu\text{mol}/\text{l}$ ) was

attributed to an interaction of the drug with the cell membrane, resulting in a breakdown of the membrane integrity and a subsequent lysis of the cell. The effects of free curcumin on Caco-2 cells have been investigated by other research groups recently (186,187). Wahlang et al. reported that no cytotoxic effects were detectable up to a curcumin concentration of 170  $\mu\text{mol/l}$  and 50 % of the cells survived a curcumin dose of 265  $\mu\text{mol/l}$  after an incubation time of 24 h (187). Additionally, Hou and co-workers showed that a curcumin concentration of 30  $\mu\text{mol/l}$  did not affect the cell viability of Caco-2 cells after an incubation time of 72 h (186). However, in the present work a curcuminoid concentration of 42  $\mu\text{mol/l}$  resulted in cell viability of approximately 30 %. Thus, the Caco-2 cells were more sensitive to the curcuminoids in our study. The differences in curcumin sensitivity of the Caco-2 cells between literature and present study might be attributed to the application of different viability assays. Wahlang et al. applied the MTT-assay for toxicity evaluation, whereas in the present study the QBlue assay was used to assess the cell viability (187). The comparability of the results of different cell viability assays has been discussed controversially in the literature (188-193). A resazurin-based assay (Alamar Blue) was described to be more sensitive than the MTT assay, but both viability tests gave approximately the same results (192,193). Mueller et al. reported a satisfying comparability of the results determined by MTT-, the ATP- and calcein assay (190). In contrast, other research groups found that the MTT-assay was not comparable to the ATP-assay (188,189). The MTT-assay was also shown to underestimate the growth inhibition of cytostatic drugs in some studies (188,191). The basic reason of the missing consistence between the particular viability assays is probably caused by the different measurement principles of the aforementioned assays. Resazurin, for example, is suggested to be reduced by cytosolic enzymes, the reduction MTT is done by mitochondrial dehydrogenases and the ATP assay determines the cell viability by assessing the ATP level. Thus, the endpoints for the viability determination are totally different. Furthermore, the QBlue-assay is executed with living cells, whereas MTT-assay and ATP-assay demands the killing of the tested cells. Therefore, MTT- and ATP-assay do not determine the actual viability of cells, but rather the amount of metabolically active residues and it is questionable, whether this viability determination might generate false negative or false positive results, respectively.

In addition, the outcomes of all *in vitro* viability assays, like MTT-assay or resazurin-based assays, are strongly dependent on the experimental conditions. The presence of protein and other colloids, for example, depressed the reduction of resazurin (194). And during the MTT assay, the extraction of the blue formazan crystals from the cell suspension is a very sensitive step, where errors can easily occur.

As a consequence, the detailed comparison of the data obtained by the present study with the literature data was seen as not advisable. Especially, the effective concentrations of

free curcumin were seen as a variable parameter, influenced by the experimental conditions as well as by the applied viability assay. After all, an activity of free curcumin against Caco-2 cells was confirmed by the data of the present study and by the respective report in literature (187). The cytotoxic effect, observed in the present work, was attributed to the interaction of curcumin with the cell membrane, resulting in a loss of membrane integrity. This acute toxic effect should be distinguished from a potential long term activity of curcumin against cancer cells. Long term activity of curcumin means the induction of apoptosis in cancer cells, which is a major requirement for the approval of curcumin as a cytostatic, curative drug. This desired and predicted effect of curcumin was not confirmed with the present investigations. To check whether curcumin induces apoptosis in Caco-2 cells, lower doses have to be applied, which show no acute toxic effects on the cells. Furthermore, the incubation time should be extended to allow an impact of curcumin on the cell signaling pathways, possibly followed by an induction of apoptosis.

### *In vitro* toxicity of curcuminoid loaded lipid nanoparticles

The curcuminoid-free lipid nanoparticles did not show a cytotoxic effect on Caco-2 cells (Fig. 4.5-9).

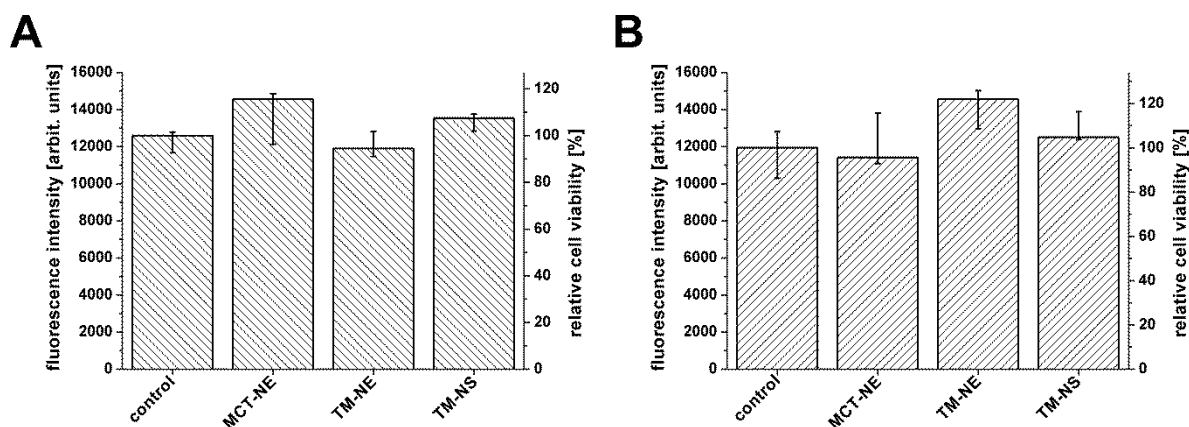


**Figure 4.5-9** Fluorescence intensity of QBlue reagent and the corresponding relative cell viability of Caco-2 cells after incubation with curcuminoid-free lipid nanoparticles for 24 h. (A) lipid concentration: 250 µg/ml; (B) lipid concentration: 25 mg/ml. The respective column represents the median of the fluorescence of three identical wells. The error bars represent the respective span of the single values.

The fluorescence intensity of the untreated control cells was as high as the fluorescence intensity of the cells incubated with lipid nanoparticles. Even the high lipid concentration

of 25 mg/ml did not have any effect on the cell viability. The viability of the Caco-2 cells was also not impaired by the presence of curcuminoid-loaded lipid nanoparticles (Fig. 4.5-10). The resulting fluorescence intensity was not different between untreated cells and cells, incubated with the drug-loaded nanoparticles.

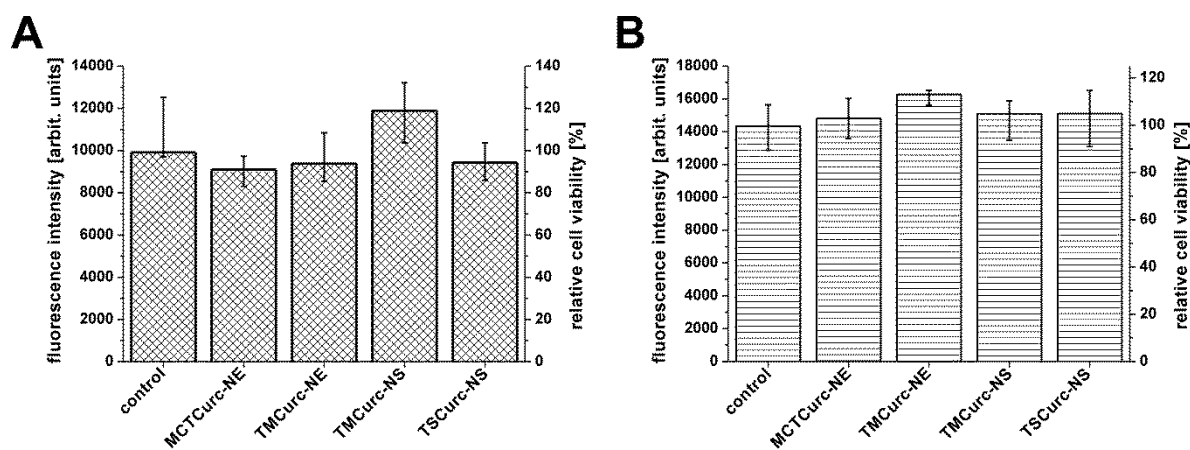


**Figure 4.5-10** Fluorescence intensity of QBlue reagent and corresponding relative cell viability of Caco-2 cells after incubation with curcuminoid-loaded lipid nanoparticles for 24 h. (A) curcuminoid concentration: 25 µg/ml (68 µmol/l), lipid concentration: 250 µg/ml; (B) curcuminoid concentration: 250 µg/ml (680 µmol/l), lipid concentration: 25 mg/ml. The respective column represents the median of the fluorescence of three identical wells. The error bars represent the respective span of the single values.

The lipid nanoparticles were composed of substances known to be non-toxic. The lipid matrix consisted of biodegradable fats like MCT, TM and TS. Although void TS nanoparticles were not tested in this study, a toxic effect of these particles was also improbable. The applied emulsifier, poloxamer 188, was reported to be also non-toxic (195). Thus, the good tolerance of the drug-free lipid nanoparticles by the Caco-2 cells was somewhat expected in advance. Indeed, the good biocompatibility of lipid nanoparticles even at high lipid concentrations, like the applied 25 mg/ml, was clearly demonstrated by the conducted experiments. Besides the use of biocompatible compounds, the missing toxic effect of the nanoparticles might also be attributed to an inhibited contact of the particles with the cells. The surrounding poloxamer layer was thought to hinder a direct interaction of the lipid nanoparticles with the cell surface. The PEG-chains of the emulsifier might build a hydrophilic shell around the lipid particle, which prevented the attachment of the particle onto the cell.

The cytotoxic activity of curcumin encapsulated in nanoparticles against various cancer cell lines has been reported by several research groups previously (163-165,196,197). In

the mentioned studies, the applied curcumin concentration ranged from 10  $\mu\text{mol/l}$  to 100  $\mu\text{mol/l}$  and the encapsulated curcumin revealed a similar activity as the free drug. A pronounced effect of comparable concentrations of free curcuminoids on Caco-2 cells was also confirmed by the present work. However, the drug-loaded nanoparticles did not show any cytotoxic effects on the Caco-2 cells. Even the administration of 680  $\mu\text{mol/l}$  of curcuminoids, encapsulated in the lipid nanoparticles, did not affect the viability of the Caco-2 cells. Free curcuminoids caused cell death at much lower doses, compared to the tolerated dose of encapsulated curcuminoids (see above). The missing immediate cytotoxic effect of the curcuminoids on the Caco-2 cells, was attributed to the association of the drug to the nanoparticles. As already mentioned, the lipid nanoparticles were assumed to be unable to interact with the cell surface, because of the surrounding hydrophilic poloxamer shell. Thus, an interaction of the curcuminoids with the Caco-2 cells was also inhibited, due to the incorporation of the drug in the particle. In addition, the missing effect of the curcuminoids on the cells indicated that the drug was not released during the incubation time. The marginal release of the curcuminoids from the nanoparticles under neutral conditions was already shown by the *in vitro* release studies (see chapter 4.5.1)

In summary, the curcuminoid-free as well as the curcuminoid loaded nanoparticles revealed no acute cytotoxic effect on the Caco-2 cells. The applied lipid and the emulsifier are known to be non-toxic, e.g. the lipids have been stated as GRAS-substances by the FDA. The curcuminoids, showing a severe effect on the cells in their free form, were thought to be effectively separated from the cells by incorporating them into the nanoparticles. Thus, the nanoparticles rather protected the cells, than supporting the drug in their action. The interaction of the nanoparticles with the cells has to be checked in further experiments with additional analytical methods, e.g. confocal microscopy and by using other cell lines. The long-term effects of the drug-loaded nanoparticles on growth and viability of various cell lines have to be further investigated as well. Especially the induction of apoptosis by the curcuminoid-loaded nanoparticles has to be in the focus of upcoming experiments. It is of distinct interest, whether the drug-loaded nanoparticles are capable of entering the cell and induce apoptotic cell death of cancer cells.

#### 4.5.4 Conclusion

The release of the curcuminoids from the lipid nanoparticles was an important point to consider in the present work. The investigation of the drug release from submicron-particles was reported to be a challenging and difficult task (157,159,161). Several models have been applied to determine the curcuminoid release from colloidal carriers so far

(70,73,163). However, these systems had serious drawbacks, such as the insufficient separation of drug and carrier, which have been discussed in detail chapter 4.5.1. Therefore, a new *in vitro* method for the determination of the curcuminoid release from the lipid nanoparticles was developed and tested to overcome these problems and to examine the drug-release in a sufficient way. The curcuminoid release was investigated in SGF, phosphate buffer pH 6.8, FaSSIF and FeSSIF. These media were chosen, because they simulate to some extent the path of the formulation after oral administration. The drug release was shown to be dependent on the release medium and the physical state of lipid matrix. The curcuminoids were hardly released in phosphate buffer pH 6.8. A distinct release was detected, when drug-loaded lipid nanoparticles were incubated in SGF and the fastest release was recorded in the simulated intestinal media FaSSIF and FeSSIF, with the release being more accelerated in FeSSIF. The determined release pattern was explained by the different solubility of the curcuminoids in the respective media. In addition, the present bile salts and phospholipids were thought to efficiently “wash-off” the curcuminoids from the lipid nanoparticles. The influence of the physical state of the lipid on the release properties was also verified by the conducted experiments. It was found that the curcuminoids were released faster from the crystalline TM nanoparticles compared to the supercooled TM nanoemulsions. This finding was explained by the localization of the drug on the surface of the crystalline particles, where the curcuminoids could diffuse easily into the surrounding medium. The fastest diffusion into the medium was found during the incubation of the preparations in FaSSIF or FeSSIF, respectively, because the drug was probably solubilized by the mixed micelles. In contrast, the drug diffusion out of the liquid droplets of the TM nanoemulsion was distinctly slower. The gained results supported the theory, drawn from the fluorescence and Raman measurements, that the curcuminoids are in contact with the surrounding environment and the lipid matrix, either solid or liquid, is not separating the drug. Therefore, a solid lipid matrix was considered to protect a drug only if it is incorporated within the lipid core. The highly crystalline order of the triglycerides prevented this incorporation for the curcuminoids in the developed formulations. It was summarized that the developed model was capable of estimating the release of the curcuminoids from the lipid nanoparticles, but the experimental setup provides options for further optimization and a final conclusion about the applicability, which is not possible yet.

The *in vitro* digestion of the lipid nanoparticles was monitored by two different methods, the pH-stat method and HPTLC/spectrodensitometry. The experiments were executed to gain more information about the potential fate of the lipid nanoparticles within the gastrointestinal tract. Additionally, it should be determined whether the driving force of the drug liberation is the lipid degradation or the drug release from the particle. The digestion of MCTCurc-NE, TMCurc-NE, TMCurc-NS and TSCurc-NS was conducted in

simulated fasted state and simulated fed state intestinal medium and the digestion velocity was recorded by the pH-stat method. It was shown that the major part of the lipid was digested in the first ten minutes of the experiment. The resulting progression of the titration curves and the cumulated consumption of sodium hydroxide were different for the particular formulations. These differences were mainly attributed to the different determinability of the released fatty acids. The release of longer fatty acids, e.g. stearic acids, was only ascertained to about 50 % by the pH-stat method, whereas 100 % of the released caprylic and capric acid were titrable. The underlying cause for this outcome was thought to be the different dissociation of the fatty acids at the given pH of 6.8. The pH-stat method was concluded to be a fast and easy method for the evaluation of the digestability of a lipid formulation, but the quantitative determination of the liberated fatty acids was shown to be not possible.

A comprehensive overview of the digestion process was gained by HPTLC/spectrodensitometry. TMCurc-NE and TMCurc-NS were investigated by this method, because the influence of the physical state of the lipid on the speed of digestion should be illustrated. In contrast to the pH-stat method, all involved compounds, except the diglycerides, were recorded and quantified. The liquid triglyceride matrix of TMCurc-NE was found to be degraded completely within the first ten minutes of the experiment. Moreover, no difference in digestion velocity was observed between fasted and fed state medium. In contrast, the complete digestion of the crystalline lipid matrix of TMCurc-NS took 30 minutes for FaSSIF and 20 minutes for FeSSIF, respectively. Hence, the examination of the digestion of TMCurc-NE and TMCurc-NS with HPTLC/spectrodensitometry revealed the slower digestion of a crystalline lipid matrix. Moreover, the accelerated lipid degradation in a simulated fed state was clearly demonstrated. The analysis with HPTLC/spectrodensitometry further allowed a better interpretation of the titration curves of the pH-stat method. It was verified that the steep initial slope of the titration curves was actually caused by the triglyceride degradation, whereas the digestion of the diglycerides and monoglycerides caused the little consumption of sodium hydroxide in the latter stages of the experiment. In summary, a detailed insight of the processes during the *in vitro* digestion of TM nanoparticles was gained by HPTLC/spectrodensitometry. Thus, the method was concluded to be superior compared to the pH-stat method, but the conduction of the experiments and the evaluation of the raw data is much more time-consuming and costly.

Subsequent to the digestion experiments, the solubilization of the curcuminoids within the simulated intestinal media was determined. The solubilized drug amount after digestion was higher for the curcuminoid-loaded TM nanoparticles compared to the curcuminoid bulk material and the solubilization capacity was higher for the fed state medium than for the fasted state medium.

When the aspects of the drug release experiments, the *in vitro* digestion and the drug solubilization studies are finally summarized, the following conclusions and suggestions for the *in vivo* fate can be made:

1. The lipid nanoparticles are degraded very fast and only a minor fraction of intact particles might be transferred to the lymphatic system.
2. The absorption of the curcuminoids is would involve the lipid digestion, the subsequent transfer into mixed micelles and the transport of the drug within micelles to the intestinal walls.
3. As a consequence, sole drug release from the nanoparticles plays only a minor role due to the rapid degradation of the particles and should not be used as a single parameter, when investigating the oral bioavailability of curcuminoids.
4. The presence of bile salts and phospholipids is an important prerequisite for the successful solubilization of the curcuminoids and therefore the fed state is to be favored over the fasted state.

The cell culture experiments showed the acute toxicity of curcuminoids on Caco-2 cells. The death of the cells was attributed to an interaction of the curcuminoids with the cell membranes, resulting in a breakdown of the membrane potential. In contrast, the curcuminoid-loaded lipid nanoparticles were non-toxic to the cells. It was concluded that the cells were not interacting with the nanoparticles, because of the shielding effect of the surrounding poloxamer layer of the nanoparticles. As a result, an uptake of the particles into the cells was not probable within the incubation time and an interaction of the curcuminoids with the cells was prevented. Therefore, the incorporation of the curcuminoids within the nanoparticles protected the cells from the acute toxicity of the drug. However, the performed experiments were designed to investigate the acute effects of free curcuminoids and curcuminoid-loaded nanoparticles on the Caco-2 cells. An assessment of the long-term effects, e.g. induction of apoptosis, is still to be addressed in future experiments. Furthermore, one has to keep in mind that cancer cells were used in the experiments and that such cells are more robust compared to normal cells. So the reaction of non-malignant cells to the curcuminoid-loaded lipid nanoparticles cannot be estimated from the conducted experiments. Though, the basic differences between free drug and drug-loaded nanoparticles were well demonstrated by the performed experiments.



## 5. Summary and Outlook

The aim of the present work was the production and comprehensive characterization of curcuminoid-loaded lipid nanoparticles, produced by high-pressure homogenization. Different triglycerides and emulsifiers were tested during formulation development. Nanoparticles consisting of MCT, TM or TS, respectively, and the emulsifier poloxamer 188 were chosen as the most suitable carrier systems for the curcuminoids. A maximum curcuminoid concentration of 1 % (w/w) related to the lipid phase was incorporated into the formulations. The achieved of incorporated drug was lower than expected, which was explained by the exclusion of the curcuminoids from the crystalline lipid matrix. Higher amounts of curcuminoids might be loaded onto nanoparticles consisting of other lipids, e.g. mono- or diglycerides, which tend to more imperfect crystalline lattices.

The particle size distribution of MCT-NE, TM-NE, TM-NS, TS-NS and their corresponding curcuminoid-loaded preparations was determined with PCS, LD and AF4/MALLS measurements. The mean particle size for the all prepared MCT and TM nanoemulsions, respectively, were between 125 nm and 150 nm. The different particle sizing techniques gave comparable results for the investigated nanoemulsions. In contrast, different mean particle sizes were determined by the PCS, LD and AF4/MALLS for the crystalline TM and TS nanoparticles. The discrepancies were caused by the anisometric shape of the solid lipid nanoparticles. It was clearly demonstrated, that the size characterization of a particle population by light scattering techniques is strongly dependent on the particle geometry and the underlying mathematical conversion of scattered light into a particle size distribution by the particular analytical method. Compared to the nanoemulsions, it was concluded to be unreasonable to declare a characteristic mean particle size of the crystalline nanoparticle preparations irrespective of the applied analytical method. LD was seen as the most convenient method for the particle size measurement, because it allowed a fast determination and the presence of unwanted large particles ( $> 1 \mu\text{m}$ ) could be detected sufficiently. If the values determined by LD are taken as a basis, the mean particle size of the different produced batches of TM and TS nanoparticles was between 135 nm and 180 nm.

The actual particle shape of the crystalline nanoparticles was investigated by TEM and AF4/MALLS. The TEM images revealed an anisometric, irregular and flat shape of the nanoparticles. The non-spherical particle shape of crystalline TM nanoparticles was further verified by AF4/MALLS experiments. The advantage of AF4/MALLS is the investigation of a higher amount of particles in comparison to TEM micrographs, which results in more representative information about the particle shape throughout the whole particle population. Though, the actual particle appearance can only be visualized by TEM

micrographs. In the end, the application of both methods was concluded to be needed for providing a comprehensive overview of the particle shape of the developed formulations. The investigation of the curcuminoid-loaded lipid nanoparticles with different physical methods provided information about the state of the lipid matrix and the curcuminoids. The crystallization behavior of the lipid nanoparticles was investigated by DSC and XRD. It was shown that the TM nanoparticles did crystallize at 11 °C and therefore supercooled melts were preserved when the TM-based formulations were stored above this temperature. The supercooled TM nanoemulsion stayed liquid during the whole observation period of 16 weeks at a storage temperature of 22 °C. However in some cases a partial recrystallization occurred. Hence, the supercooled state was concluded to be metastable and therefore inappropriate as a pharmaceutical formulation. The solid TM and TS nanoparticles were demonstrated by DSC and XRD to crystallize mainly in the stable  $\beta$ -modification. The TS nanoparticles exhibited also some traces of the  $\alpha$ -modification, which transformed to the  $\beta$ -modification within 16 weeks. The fast crystallization and the highly crystalline order strongly indicated the exclusion of the curcuminoids from the solid lipid matrix. This assumption was supported by the Raman and fluorescence measurements. The curcuminoids were shown to be in an amorphous state within the lipid nanoparticles by the Raman measurements. The fluorescence experiments demonstrated the influence of the physical state of the lipid on the fluorescence properties of the curcuminoids. In addition, the surrounding media also influenced the curcuminoids fluorescence, emphasizing the drug to be localized on the surface of the solid particles. Moreover, fluorescence anisotropy measurements revealed a considerable mobility of the drug associated to the TM nanoparticles, which further pointed to a localization of the curcuminoids apart from the rigid lipid matrix.

The curcuminoid content of the lipid nanoparticles was constant over a storage period of twelve months. In addition, the incubation of the curcuminoid-loaded nanoparticles in physiological media, e.g. SGF and phosphate buffer pH 6.8, revealed no degradation of the drug over an incubation period of eight hours. Thus, the stability of the curcuminoids *in vitro* makes a pronounced decomposition of the drug after the oral application and its subsequent contact with gastric and intestinal fluids rather improbable.

The curcuminoid release from the lipid nanoparticles was shown to be dependent on the respective release medium and on the physical state of the TM-based lipid matrix. The drug was not released from the nanoparticles during incubation in phosphate buffer pH 6.8. On the contrary, in SGF and in simulated intestinal fluids, a release between 30 % - 80 % was observed. Moreover, the curcuminoids were released faster from the crystalline TM nanoparticles in comparison to the TM nanoemulsion. In connection with the release experiments, the digestion of the lipid nanoparticles in simulated gastric and simulated intestinal fluid was assessed. No degradation of the lipid matrix was observed during the

incubation of the TM nanoparticles in SGF. In contrast, the *in vitro* digestion in simulated intestinal fluid revealed a rapid and complete degradation of the triglyceride particle matrix by the added lipase. The degradation of the lipid was faster in the fed state than in the fasted state. Furthermore, the crystalline TM nanoparticles were digested slower than the TM nanoemulsions. Nevertheless, the digestion was found to be much faster than the previously determined drug release from the nanoparticles. It was therefore concluded that liberation of the drug within the gastro-intestinal tract might be mainly caused by particle decomposition. The released curcuminoids were shown to be transferred to mixed micellar structures within the simulated intestinal fluids. Hence, it was seen as probable that the drug is also transferred to mixed micelles during *in vivo* digestion. Such a solubilisation of the curcuminoid meets the major prerequisite for the efficient uptake of the drug in the intestine.

The toxicity of the curcuminoid-loaded nanoparticles and the free curcuminoids was tested with Caco-2 cells. The cell culture experiments assessed the tolerance of the cells against the drug-loaded nanoparticles. In contrast, free curcuminoids reduced the viability of the cells in a considerable way. The conducted cell experiments were seen as basic evaluation of the biological activity of the curcuminoid-loaded formulations. The further investigation of the biological activity is considered to be the major challenge of future experiments. For this purpose further cell culture experiments have to be launched to investigate the long-term effects of the curcuminoid-loaded preparations on cells. Especially, the potential uptake of the particles by the cells and the activity of the incorporated curcuminoids are of certain interest. The next step should be the establishment of an efficient process for extracting the curcuminoids out of the blood and a convenient analytical method, allowing the detection of small amounts of drug and its metabolites. Though, the preparation and extraction of curcuminoids out of blood samples and the subsequent quantification have been already described in literature (198-201). Thereafter, curcuminoid-loaded preparations can be applied in a basic *in vivo* experiment to determine pharmacokinetic parameters of the drug and to assess potential adverse effects. The final step in the preclinical research would be application of the curcuminoid-loaded lipid nanoparticles in an animal cancer model and the evaluation of its curative or preventive potential.

## 6. Zusammenfassung und Ausblick

Das Ziel der Arbeit war die Herstellung und umfassende Charakterisierung von Curcuminoid beladenen Lipidnanopartikel, hergestellt durch Hochdruckhomogenisation. Verschiedene Triglyceride und Emulgatoren wurden untersucht, um geeignete Formulierungen zu finden. Nanopartikel, bestehend aus den Lipiden MCT, Trimyristin und Tristearin, sowie der Emulgator Poloxamer 188 wurden als am besten geeignete Arzneiträgersysteme für die Curcuminoide ausgewählt. Eine maximale Curcuminoidkonzentration von 1 % (w/w), bezogen auf die Lipidmenge, wurde in die betreffenden Formulierungen eingearbeitet. Der Beladungsgrad war daher niedriger als erwartet. Der Hauptgrund ist in der hohen kristallinen Ordnung der Lipidmatrix zu sehen, welche einen Einschluss des Wirkstoffes verhindert. Ein höherer Beladungsgrad kann wahrscheinlich erreicht werden, wenn andere Lipide, z.B. Mono- oder Diglyceride, verwendet werden, deren Kristallstruktur weniger geordnet ist.

Die Partikelgrößenverteilungen von MCT-NE, TM-NE, TM-NS, TS-NS und den jeweiligen Curcuminoid beladenen Formulierungen wurden mit PCS, LD und AF4/MALLS bestimmt. Die mittlere Partikelgröße der MCT- und TM-Nanoemulsionen lag zwischen 125 nm und 150 nm. Die verschiedenen Methoden, die zur Größenbestimmung eingesetzt wurden, ergaben hierbei vergleichbare Größenwerte für die jeweilige Nanoemulsion. Im Gegensatz dazu lieferten die oben genannten Methoden voneinander abweichende mittlere Partikelgrößen bei der Untersuchung der kristallinen TM- und TS-Nanopartikel. Die unterschiedlichen Ergebnisse der einzelnen Methoden wurden mit der anisometrischen Struktur der festen Lipidnanopartikel begründet. Mit den durchgeführten Experimenten wurde gezeigt, dass die Größencharakterisierung einer Partikelpopulation mit Lichtstreuungstechniken abhängig ist von der Partikelgeometrie und der zugrunde liegenden mathematischen Berechnung der Partikelgröße aus den aufgezeichneten Lichtstreuendaten der jeweiligen Methode. Daraus wurde geschlossen, dass eine charakteristische Partikelgröße für die hergestellten kristallinen, anisometrischen Nanopartikel unabhängig von der verwendeten Methode nur bedingt angegeben werden kann. Die statische Lichtstreuung wurde als geeignetste Methode angesehen, weil sie einen hohen Probendurchsatz erlaubt und auch größere Partikel ( $> 1 \mu\text{m}$ ) noch hinreichend genau detektiert. Werden die Werte der statischen Laserlichtstreuung deshalb als Grundlage genommen, dann ergibt sich eine mittlere Partikelgröße für die hergestellten Chargen von TM- und TS-Nanopartikeln zwischen 135 nm und 180 nm.

Die Partikelform der kristallinen Nanopartikel wurde mit TEM und AF4/MALLS untersucht. Die elektronenmikroskopischen Aufnahmen zeigten eine anisometrische, plättchenartige Geometrie der Nanopartikel. Die unregelmäßige Partikelform wurde auch durch die

AF4/MALLS-Messungen bestätigt. Der Vorteil von AF4/MALLS im Vergleich zu TEM ist die Untersuchung einer größeren Partikelmenge, was eine repräsentativere Aussage über die Partikelform der gesamten Partikelpopulation zulässt. Jedoch kann die tatsächliche Partikelbeschaffenheit nur durch TEM Aufnahmen veranschaulicht werden. Eine umfassende Charakterisierung der Partikelform der hergestellten Formulierungen war letztendlich nur durch die Anwendung beider Methoden möglich.

Die Untersuchung der Curcuminoid beladenen Lipidnanopartikel mittels verschiedener physikalischer Methoden lieferte wichtige Informationen über die Beschaffenheit der Lipidmatrix und des eingearbeiteten Arzneistoffes. Das Kristallisationsverhalten der Lipidnanopartikel wurde mit Kalorimetrie und Röntgenstreuung untersucht. Es wurde gezeigt, dass die TM-basierten Nanopartikel erst bei einer Temperatur von 11 °C kristallisierten und daher blieben die TM-basierten Formulierungen als unterkühlte Schmelzen erhalten, wenn diese bei einer Temperatur oberhalb von 11 °C gelagert wurden. Der unterkühlte Zustand der TM-Nanoemulsionen blieb bei einer Lagertemperatur von 22 °C über den Beobachtungszeitraum von 16 Wochen stabil. In einigen Fällen kam es aber zu einer teilweisen Rekristallisation der Lipidmatrix. Die unterkühlten Schmelzen sind daher als metastabiles System zu sehen und als pharmazeutische Formulierung ungeeignet. Die festen TM- und TS-Nanopartikel kristallisierten hauptsächlich in der stabilen  $\beta$ -Modifikation aus. Die TS-Nanopartikel zeigten auch einen kleinen Anteil an  $\alpha$ -Modifikation, welcher sich innerhalb von 16 Wochen in die  $\beta$ -Modifikation umwandelte. Die schnelle Kristallisation der Lipide in einer stabilen Modifikation deutete auf den Ausschluss der Curcuminoide aus der festen Partikelmatrix hin. Diese Annahme wurde durch die Untersuchung der verschiedenen Formulierungen mit Raman-Spektroskopie und Fluoreszenzspektroskopie bestätigt. Die Raman-Messungen zeigten, dass die Curcuminoide in einem amorphen Zustand in den Nanopartikeln vorlagen. Die Messung der Fluoreszenz der Curcuminoid beladenen Lipidnanopartikel veranschaulichte den Einfluss des Aggregatzustandes der Lipidmatrix auf die Fluoreszenzeigenschaften der Curcuminoide. Außerdem wurde gezeigt, dass das umgebende Medium ebenfalls einen Einfluss auf die Curcuminoidfluoreszenz hat. Dieses Ergebnis stützte die Annahme, dass sich die Curcuminoide auf der Oberfläche der Partikel befinden. Durch die Untersuchung der Lipidnanopartikel mit Fluoreszenzanisotropie konnte gezeigt werden, dass die Curcuminoide in den Nanopartikeln eine erhöhte Mobilität aufweisen, was ebenfalls daraufhin deutet, dass die Curcuminoide sich außerhalb der starren Lipidmatrix auf der Oberfläche der Partikel befinden.

Der Curcuminoidgehalt der Lipidnanopartikel war über einen Zeitraum von zwölf Monaten stabil. Des Weiteren zeigte sich kein Abbau des Arzneistoffes bei der Inkubation der Formulierungen in verschiedenen physiologischen Medien, z.B. SGF und Phosphatpuffer pH 6.8. Daraus wurde geschlossen, dass die orale Applikation der Arzneistoff beladenen

Nanopartikel und der anschließende Kontakt mit Magen- bzw. Darmsaft zu keinem nennenswerten Abbau der Curcuminoide führt.

Die Freisetzung der Curcuminoide aus den Nanopartikeln war abhängig von dem jeweils verwendeten Freisetzungsmedium sowie vom Aggregatzustand der TM-basierten Lipidmatrix. Bei der Inkubation der Partikel in Phosphatpuffer pH 6.8 konnte keine Freisetzung des Arzneistoffes festgestellt werden. Im künstlichen Magen- bzw. Darmsaft wurden hingegen 30 % - 80 % der Curcuminoide freigesetzt. Außerdem zeigte sich, dass die Freisetzung aus den kristallinen TM-Nanopartikeln schneller erfolgte als aus der TM-Nanoemulsion. Im Zusammenhang mit der Freisetzung wurde auch der Verdau der Lipidnanopartikel simuliert. In künstlichem Magensaft konnte kein Abbau der Partikel festgestellt werden. Ein sehr rascher und vollständiger Abbau der Triglyceride erfolgte hingegen in künstlichem Darmsaft durch das zugesetzte Enzym Lipase. Der Verdau der Partikel war im simulierten gesättigten Zustand schneller als im ungesättigten Zustand. Außerdem wurden die kristallinen Nanopartikel langsamer abgebaut, als die Nanoemulsionen. Der Abbau der Partikel war dennoch weit schneller als die vorher bestimmte Freisetzung der Curcuminoide aus den Partikeln. Daraus lässt sich schließen, dass die Freisetzung des Arzneistoffes im Gastrointestinaltrakt hauptsächlich durch den Abbau der Partikel gesteuert wird. Die Curcuminoide, die während des Abbaus der Nanopartikel im künstlichen Darmsaft freigesetzt wurden, wurden zu einem Teil in die vorhandenen Mischmizellen aufgenommen. Es ist daher wahrscheinlich, dass dieser Transfer des Arzneistoffes in die Mischmizellen auch während des *in vivo* Verdaus der Nanopartikel stattfindet. Durch eine derartige Solubilisation der Curcuminoide wäre eine wichtige Voraussetzung für eine effektive Absorption im Darm erfüllt.

Die Toxizität der beladenen Nanopartikel sowie der freien Curcuminoide wurde mit Caco-2 Zellen untersucht. Die Zellkulturexperimente bestätigten die gute Verträglichkeit der Curcuminoid-beladenen Nanopartikel. Im Gegensatz dazu verringerten die freien Curcuminoide die Vitalität der Zellen teilweise erheblich. Die durchgeführten Versuche sollten eine erste Einschätzung der biologischen Aktivität der Nanopartikel ermöglichen. Die weitere Untersuchung der biologischen Wirkungen der Curcuminoidformulierungen ist als ein Gebiet zu sehen auf dem das Hauptaugenmerk zukünftiger Forschung liegen sollte. Es müssen weitere Zellexperimente durchgeführt werden, um vor allem einen Einblick in die Effekte einer Langzeitanwendung der Nanopartikel zu erhalten. Besonders die potentielle Aufnahme der Partikel und die Wirkung der inkorporierten Curcuminoide sind von besonderem Interesse. Der nächste Schritt wäre die Entwicklung einer geeigneten analytischen Methode, die es erlaubt auch kleinste Mengen an Arzneistoff und seiner Metaboliten zuverlässig nachzuweisen. Die Extraktion von Curcuminoiden aus Blutproben und die anschließende Quantifizierung wurden aber bereits in der Literatur beschrieben (198-201). Danach können die Curcuminoid-beladenen Nanopartikel in einer ersten

Versuchsreihe *in vivo* appliziert werden, um entsprechende pharmakokinetische Parameter zu bestimmen und eventuelle Nebenwirkungen zu erfassen. Der letzte Schritt in der präklinischen Forschung wäre die Applikation der beladenen Nanopartikel in einen Krebsmodell am Tier und die Beurteilung des kurativen oder präventiven Potentials der Formulierungen.

## 7. References

1. Surh, Y. J.: Cancer chemoprevention with dietary phytochemicals, *Nature Reviews Cancer*, 2003, 3, 10, 768-780
2. Sporn, M. B. et al.: Chemoprevention of cancer with retinoids, *Federation proceedings*, 1979, 38, 11, 2528-2534
3. Wattenberg, L. W.: Chemoprevention of cancer, *Cancer research*, 1985, 45, 1, 1-8
4. Johnson, I. T. et al.: Anticarcinogenic factors in plant foods: a new class of nutrients?, *Nutrition Research Reviews*, 1994, 7, 01, 175-204
5. Johnson, I. T.: Phytochemicals and cancer, *Proceedings of the Nutrition Society*, 2007, 66, 02, 207-215
6. van Der Heijden, R. et al.: The Catharanthus alkaloids: pharmacognosy and biotechnology, *Current medicinal chemistry*, 2004, 11, 5, 607-628
7. Oberlies, N. H. et al.: Camptothecin and Taxol: Historic Achievements in Natural Products Research, *Journal of natural products*, 2004, 67, 2, 129-135
8. Susan, B. M. et al.: Green Tea Polyphenols and Cancer Chemoprevention: Multiple Mechanisms and Endpoints for Phase II Trials, *Nutrition Reviews*, 2004, 62, 5, 204-211
9. Lee, K. W. et al.: Molecular targets of phytochemicals for cancer prevention, *Nature Reviews Cancer*, 2011, 11, 3, 211-218
10. Athar, M. et al.: Multiple molecular targets of resveratrol: anti-carcinogenic mechanisms, *Archives of biochemistry and biophysics*, 2009, 486, 2, 95-102
11. Xu, C. et al.: Mechanism of action of isothiocyanates: the induction of ARE-regulated genes is associated with activation of ERK and JNK and the phosphorylation and nuclear translocation of Nrf2, *Molecular cancer therapeutics*, 2006, 5, 8, 1918-1926
12. Cheung, K. L. et al.: Synergistic effect of combination of phenethyl isothiocyanate and sulforaphane or curcumin and sulforaphane in the inhibition of inflammation, *Pharmaceutical research*, 2009, 26, 1, 224-231



13. Na, H. K. et al.: Modulation of Nrf2-mediated antioxidant and detoxifying enzyme induction by the green tea polyphenol EGCG, *Food and Chemical Toxicology*, 2008, 46, 4, 1271-1278
14. Singh, A. V. et al.: Soy phytochemicals prevent orthotopic growth and metastasis of bladder cancer in mice by alterations of cancer cell proliferation and apoptosis and tumor angiogenesis, *Cancer research*, 2006, 66, 3, 1851-1858
15. Takada, Y. et al.: Evodiamine abolishes constitutive and inducible NF-kappaB activation by inhibiting Ikappa kinase activation, thereby suppressing NF-kappaB-regulated antiapoptotic and metastatic gene expression, up-regulating apoptosis, and inhibiting invasion, *Journal of Biological Chemistry*, 2005, 280, 17, 17203-17212
16. Murakami, A. et al.: Targeting NOX, INOS and COX-2 in inflammatory cells: Chemoprevention using food phytochemicals, *International Journal of Cancer*, 2007, 121, 11, 2357-2363
17. Coussens, L. M. et al.: Inflammation and cancer, *NATURE-LONDON-*, 2002, 860-867
18. Mantovani, A.: Molecular pathways linking inflammation and cancer, *Current molecular medicine*, 2010, 10, 4, 369-373
19. Mantovani, A. et al.: Cancer-related inflammation, *Nature*, 2008, 454, 7203, 436-444
20. Subbaramaiah, K. et al.: Resveratrol inhibits cyclooxygenase-2 transcription and activity in phorbol ester-treated human mammary epithelial cells, *Journal of Biological Chemistry*, 1998, 273, 34, 21875-21882
21. Banerjee, S. et al.: Suppression of 7, 12-Dimethylbenz (a) anthracene-induced Mammary Carcinogenesis in Rats by Resveratrol, *Cancer research*, 2002, 62, 17, 4945-4954
22. Kimura, Y. et al.: Resveratrol isolated from *Polygonum cuspidatum* root prevents tumor growth and metastasis to lung and tumor-induced neovascularization in Lewis lung carcinoma-bearing mice, *The Journal of nutrition*, 2001, 131, 6, 1844-1849
23. Weng, Y. L. et al.: Oral administration of resveratrol in suppression of pulmonary metastasis of BALB/c mice challenged with CT26 colorectal adenocarcinoma cells, *Molecular nutrition & food research*, 2010, 54, 2, 259-267
24. Aggarwal, B. B. et al.: Potential therapeutic effects of curcumin, the anti-inflammatory agent, against neurodegenerative, cardiovascular, pulmonary, metabolic, autoimmune and neoplastic diseases, *The international journal of biochemistry & cell biology*, 2009, 41, 1, 40-59

25. Anand, P. et al.: Curcumin and cancer: An "old-age" disease with an "age-old" solution, *Cancer Letters*, 2008, 267, 1, 133-164
26. Lynne, M. H. et al.: Predicting the physiological relevance of in vitro cancer preventive activities of phytochemicals, *Acta Pharmacologica Sinica*, 2007, 28, 9, 1274-1304
27. Ammon, H. P. et al.: Pharmacology of *Curcuma longa*, *Planta Med*, 1991, 57, 1, 1-7
28. Hatcher, H. et al.: Curcumin: From ancient medicine to current clinical trials, *Cellular and Molecular Life Sciences*, 2008, 65, 11, 1631-1652
29. Thakur, R. S. et al.: Major medicinal plants of India, Lucknow: Central Institute of Medicinal and Aromatic Plants 585p. -illus., col.illus..En *Icones Geog*, 1989, 6
30. Payton, F. et al.: NMR Study of the Solution Structure of Curcumin, *Journal of Natural Products*, 2007, 70, 2, 143-146
31. Tønnesen, H. H. et al.: Studies on curcumin and curcuminoids VIII. Photochemical stability of curcumin, *Zeitschrift für Lebensmittel-Untersuchung und -Forschung*, 1986, 183, 2, 116-122
32. Tønnesen, H. H. et al.: Studies on curcumin and curcuminoids. VI. Kinetics of curcumin degradation in aqueous solution, *Zeitschrift für Lebensmittel-Untersuchung und -Forschung*, 1985, 180, 5, 402-404
33. Kunnumakkara, A. B. et al.: Curcumin inhibits proliferation, invasion, angiogenesis and metastasis of different cancers through interaction with multiple cell signaling proteins, *Cancer Letters*, 2008, 269, 2, 199-225
34. Ono, K. et al.: Curcumin has potent anti-amyloidogenic effects for Alzheimer's  $\beta$ -amyloid fibrils in vitro, *Journal of Neuroscience Research*, 2004, 75, 6, 742-750
35. Liacini, A. et al.: Induction of matrix metalloproteinase-13 gene expression by TNF- $\alpha$  is mediated by MAP kinases, AP-1, and NF- $\kappa$ B transcription factors in articular chondrocytes, *Experimental Cell Research*, 2003, 288, 1, 208-217
36. Venkatesan, N.: Curcumin attenuation of acute adriamycin myocardial toxicity in rats, *British Journal of Pharmacology*, 1998, 124, 3, 425-427
37. Zhang, L. et al.: Curcuminoids enhance amyloid- $\beta$ ; uptake by macrophages of Alzheimer's disease patients, *Journal of Alzheimer's Disease*, 2006, 10, 1, 1-7
38. Verma, S. P. et al.: Curcumin and Genistein, Plant Natural Products, Show Synergistic Inhibitory Effects on the Growth of Human Breast Cancer MCF-7 Cells Induced by Estrogenic Pesticides, *Biochemical and Biophysical Research Communications*, 1997, 233, 3, 692-696

39. Anto, R. J. et al.: Curcumin (diferuloylmethane) induces apoptosis through activation of caspase-8, BID cleavage and cytochrome c release: its suppression by ectopic expression of Bcl-2 and Bcl-xl, *Carcinogenesis*, 2002, 23, 1, 143-150
40. Han, S. S. et al.: Curcumin Causes the Growth Arrest and Apoptosis of B Cell Lymphoma by Downregulation of egr-1, C-myc, Bcl-XL, NF- $\hat{\imath}$ B, and p53, *Clinical Immunology*, 1999, 93, 2, 152-161
41. Jee, S. H. et al.: Curcumin induces a p53-dependent apoptosis in human basal cell carcinoma cells, *Journal of Investigative Dermatology*, 1998, 111, 4, 656-661
42. Chen, Y. R. et al.: Inhibition of the c-Jun N-terminal kinase (JNK) signaling pathway by curcumin, *Oncogene*, 1998, 17, 2, 173-178
43. Goel, A. et al.: Curcumin as "Curecumin": From kitchen to clinic, *Biochemical Pharmacology*, 2008, 75, 4, 787-809
44. Ichiki, K. et al.: Regulation of activator protein-1 activity in the mediastinal lymph node metastasis of lung cancer, *Clinical and Experimental Metastasis*, 2000, 18, 7, 539-545
45. Azuine, M. A. et al.: Chemopreventive effect of turmeric against stomach and skin tumors induced by chemical carcinogens in Swiss mice, *Nutrition and Cancer*, 1992, 17, 1, 77-83
46. Ikezaki, S. et al.: Chemopreventive effects of curcumin on glandular stomach carcinogenesis induced by N-methyl-N'-nitro-N-nitrosoguanidine and sodium chloride in rats, *Anticancer research*, 2001, 21, 5, 3407-3411
47. Inano, H. et al.: Potent preventive action of curcumin on radiation-induced initiation of mammary tumorigenesis in rats, *Carcinogenesis*, 2000, 21, 10, 1835-1841
48. Jobin, C. et al.: Curcumin blocks cytokine-mediated NF-kappaB activation and proinflammatory gene expression by inhibiting inhibitory factor I-kappaB kinase activity, *The Journal of Immunology*, 1999, 163, 6, 3474-3483
49. Singh, S. et al.: Activation of transcription factor NF-kappaB is suppressed by curcumin (diferuloylmethane), *Journal of Biological Chemistry*, 1995, 270, 42, 24995-25000
50. Goel, A. et al.: Specific inhibition of cyclooxygenase-2 (COX-2) expression by dietary curcumin in HT-29 human colon cancer cells, *Cancer Letters*, 2001, 172, 2, 111-118
51. Huang, M. T. et al.: Inhibitory effects of curcumin on in vitro lipoxygenase and cyclooxygenase activities in mouse epidermis, *Cancer Research*, 1991, 51, 3, 813-819

52. Salh, B. et al.: Curcumin attenuates DNB-induced murine colitis, *American Journal of Physiology - Gastrointestinal and Liver Physiology*, 2003, 285, 1, 235-243
53. Jian, Y. T. et al.: Preventive and therapeutic effects of NF-kappaB inhibitor curcumin in rats colitis induced by trinitrobenzene sulfonic acid, *World journal of gastroenterology : WJG*, 2005, 11, 12, 1747-1752
54. Balogun, E. et al.: Curcumin activates the haem oxygenase-1 gene via regulation of Nrf2 and the antioxidant-responsive element, *Biochemical Journal*, 2003, 371, Pt 3, 887-895
55. Jefremov, V. et al.: Antioxidative Effects of Plant Polyphenols, *Annals of the New York Academy of Sciences*, 2007, 1095, 1, 449-457
56. Susan, M. et al.: Induction of glutathione S-transferase activity by curcumin in mice, *Arzneimittel-Forschung*, 1992, 42, 7, 962-964
57. Ireson, C. et al.: Characterization of Metabolites of the Chemopreventive Agent Curcumin in Human and Rat Hepatocytes and in the Rat in Vivo, and Evaluation of Their Ability to Inhibit Phorbol Ester-induced Prostaglandin E2 Production, *Cancer Research*, 2001, 61, 3, 1058-1064
58. Pan, M. H. et al.: Biotransformation of curcumin through reduction and glucuronidation in mice, *Drug Metabolism and Disposition*, 1999, 27, 4, 486-494
59. Anand, P. et al.: Bioavailability of curcumin: Problems and promises, *Molecular Pharmaceutics*, 2007, 4, 6, 807-818
60. Ireson, C. R. et al.: Metabolism of the cancer chemopreventive agent curcumin in human and rat intestine, *Cancer Epidemiology Biomarkers & Prevention*, 2002, 11, 1, 105-111
61. Cheng, A. L. et al.: Phase I clinical trial of curcumin, a chemopreventive agent, in patients with high-risk or pre-malignant lesions, *Anticancer research*, 2001, 21, 4B
62. Shoba, G. et al.: Influence of piperine on the pharmacokinetics of curcumin in animals and human volunteers, *Planta Medica-Natural Products and Medicinal Plant Research*, 1998, 64, 4, 353-356
63. Lao, C. D. et al.: Dose escalation of a curcuminoid formulation, *BMC complementary and alternative medicine*, 2006, 6, 1
64. Dhillon, N. et al.: Phase II Trial of Curcumin in Patients with Advanced Pancreatic Cancer, *Clinical Cancer Research*, 2008, 14, 14, 4491-4499
65. Began, G. et al.: Inhibition of lipoxygenase 1 by phosphatidylcholine micelles-bound curcumin, *Lipids*, 1998, 33, 12, 1223-1228

66. Iwunze, M. O.: Binding and distribution characteristics of curcumin solubilized in CTAB micelle, *Journal of Molecular Liquids*, 2004, 111, 1-3, 161-165
67. Leung, M. H. M. et al.: Encapsulation of Curcumin in Cationic Micelles Suppresses Alkaline Hydrolysis, *Langmuir*, 2008, 24, 11, 5672-5675
68. Sahu, A. et al.: Synthesis of novel biodegradable and self-assembling methoxy poly(ethylene glycol)-palmitate nanocarrier for curcumin delivery to cancer cells, *Acta Biomaterialia*, 2008, 4, 6, 1752-1761
69. Takahashi, M. et al.: Evaluation of an Oral Carrier System in Rats: Bioavailability and Antioxidant Properties of Liposome-Encapsulated Curcumin, *Journal of Agricultural and Food Chemistry*, 2009, 57, 19, 9141-9146
70. Tiyaboonchai, W. et al.: Formulation and characterization of curcuminoids loaded solid lipid nanoparticles, *International Journal of Pharmaceutics*, 2007, 337, 1-2, 299-306
71. Wu, X. et al.: Self-microemulsifying drug delivery system improves curcumin dissolution and bioavailability, *Drug Development and Industrial Pharmacy*, 2011, 00, 1-10
72. Anand, P. et al.: Design of curcumin-loaded PLGA nanoparticles formulation with enhanced cellular uptake, and increased bioactivity in vitro and superior bioavailability in vivo, *Biochemical pharmacology*, 2010, 79, 3, 330-338
73. Kakkar, V. et al.: Exploring solid lipid nanoparticles to enhance the oral bioavailability of curcumin, *Molecular Nutrition & Food Research*, 2011, 55, 3, 495-503
74. Shaikh, J. et al.: Nanoparticle encapsulation improves oral bioavailability of curcumin by at least 9-fold when compared to curcumin administered with piperine as absorption enhancer, *European Journal of Pharmaceutical Sciences*, 2009, 37, 3-4, 223-230
75. Gupta, N. K. et al.: Bioavailability enhancement of curcumin by complexation with phosphatidyl choline, *Journal of Pharmaceutical Sciences*, 2011, 100, 5, 1987-1995
76. Gou, M. L. et al.: Curcumin-loaded biodegradable polymeric micelles for colon cancer therapy in vitro and in vivo, *Nanoscale*, 2011, 3, 1558-1567
77. Khoo, S. M. et al.: Intestinal lymphatic transport of halofantrine occurs after oral administration of a unit-dose lipid-based formulation to fasted dogs, *Pharmaceutical Research*, 2003, 20, 9, 1460-1465
78. Shackleford, D. M. et al.: Contribution of lymphatically transported testosterone undecanoate to the systemic exposure of testosterone after oral administration of two andriol formulations in conscious lymph duct-

cannulated dogs, *Journal of Pharmacology and Experimental Therapeutics*, 2003, 306, 3, 925-933

79. Fricker, G. et al.: Phospholipids and Lipid-Based Formulations in Oral Drug Delivery, *Pharmaceutical Research*, 2010, 27, 8, 1469-1486
80. Kuntsche, J. et al.: Solid Lipid Nanoparticles (SLN) for Drug Delivery, *Handbook of Materials for Nanomedicine*, 2010
81. Nguyen, T. H. et al.: Nanostructured liquid crystalline particles provide long duration sustained-release effect for a poorly water soluble drug after oral administration, *Journal of Controlled Release*, 2011, 153, 2, 180-186
82. Müller, R. H. et al.: Oral bioavailability of cyclosporine: Solid lipid nanoparticles (SLN®) versus drug nanocrystals, *International Journal of Pharmaceutics*, 2006, 317, 1, 82-89
83. Cai, S. et al.: Lymphatic drug delivery using engineered liposomes and solid lipid nanoparticles, *Advanced Drug Delivery Reviews*, 2011, 63, 10-11, 901-908
84. Kuntsche, J. et al.: Supercooled smectic nanoparticles: a potential novel carrier system for poorly water soluble drugs, *Pharmaceutical Research*, 2004, 21, 10, 1834-1843
85. Cervin, C. et al.: A combined in vitro and in vivo study on the interactions between somatostatin and lipid-based liquid crystalline drug carriers and bilayers, *European Journal of Pharmaceutical Sciences*, 2009, 36, 4-5, 377-385
86. Angelova, A. et al.: Self-Assembled Multicompartment Liquid Crystalline Lipid Carriers for Protein, Peptide, and Nucleic Acid Drug Delivery, *Accounts of Chemical Research*, 2011, 147-156
87. Bunjes, H. et al.: Lipid Nanoparticles Based on Liquid Crystalline Phases, *Handbook of Materials for Nanomedicine*, 2010, 1,
88. Mehnert, W. et al.: Solid lipid nanoparticles:: Production, characterization and applications, *Advanced Drug Delivery Reviews*, 2001, 47, 2-3, 165-196
89. Müller, R. H. et al.: Solid lipid nanoparticles (SLN) for controlled drug delivery-a review of the state of the art, *European Journal of Pharmaceutics and Biopharmaceutics*, 2000, 50, 1, 161-177
90. Müller, R. H. et al.: Solid lipid nanoparticles (SLN): An alternative colloidal carrier system for controlled drug delivery, *European Journal of Pharmaceutics and Biopharmaceutics*, 1995, 41, 1, 62-69
91. Jores, K. et al.: Solid Lipid Nanoparticles (SLN) and Oil-Loaded SLN Studied by Spectrofluorometry and Raman Spectroscopy, *Pharmaceutical Research*, 2005, 22, 11, 1887-1897

92. Priano, L. et al.: Solid lipid nanoparticles incorporating melatonin as new model for sustained oral and transdermal delivery systems, *Journal of Nanoscience and Nanotechnology*, 2007, 7, 10, 3596-3601
93. Westesen, K. et al.: Physicochemical characterization of lipid nanoparticles and evaluation of their drug loading capacity and sustained release potential, *Journal of Controlled Release*, 1997, 48, 2-3, 223-236
94. Jores, K., Mehnert, W., Bunjes, H., Drechsler, M., and Mäder, K.: From solid lipid nanoparticles (SLN) to nanospoons. Visions and reality of colloidal lipid dispersions, 2008
95. Schubert, M. A. et al.: Solvent injection as a new approach for manufacturing lipid nanoparticles-evaluation of the method and process parameters, *European Journal of Pharmaceutics and Biopharmaceutics*, 2003, 55, 1, 125-131
96. Müller, R. H. et al.: Solid lipid nanoparticles (SLN) as potential carrier for human use: interaction with human granulocytes, *Journal of Controlled Release*, 1997, 47, 3, 261-269
97. Schöler, N. et al.: Preserved solid lipid nanoparticles (SLN) at low concentrations do cause neither direct nor indirect cytotoxic effects in peritoneal macrophages, *International Journal of Pharmaceutics*, 2000, 196, 2, 235-239
98. Schöler, N. et al.: Surfactant, but not the size of solid lipid nanoparticles (SLN) influences viability and cytokine production of macrophages, *International Journal of Pharmaceutics*, 2001, 221, 1-2, 57-67
99. Bunjes, H. et al.: Crystallization tendency and polymorphic transitions in triglyceride nanoparticles, *International Journal of Pharmaceutics*, 1996, 129, 1-2, 159-173
100. Bunjes, H. et al.: Influence of emulsifiers on the crystallization of solid lipid nanoparticles, *Journal of Pharmaceutical Sciences*, 2003, 92, 7, 1509-1520
101. Unruh, T. et al.: Investigations on the melting behaviour of triglyceride nanoparticles, *Colloid & Polymer Science*, 2001, 279, 4, 398-403
102. Lee, M. K. et al.: Preparation, characterization and in vitro cytotoxicity of paclitaxel-loaded sterically stabilized solid lipid nanoparticles, *Biomaterials*, 2007, 28, 12, 2137-2146
103. de Jesus, M. B. et al.: Design of solid lipid nanoparticles for gene delivery into prostate cancer, *Journal of controlled release: official journal of the Controlled Release Society*, 2010, 148, 1, 89-90
104. Gasco, M. R.: Method for producing solid lipid microspheres having a narrow size distribution, 1993

105. Sjöström, B. et al.: Preparation of submicron drug particles in lecithin-stabilized emulsions: I. Model studies of the precipitation of cholesteryl acetate, *International Journal of Pharmaceutics*, 1992, 84, 2, 107-116
106. Sjöström, B. et al.: Preparation of submicron drug particles in lecithin-stabilized o/w emulsions: II. Characterization of cholesteryl acetate particles, *International Journal of Pharmaceutics*, 1993, 94, 1-3, 89-101
107. CHEN, D. B. et al.: In vitro and in vivo study of two types of long-circulating solid lipid nanoparticles containing paclitaxel, *Chemical & pharmaceutical bulletin*, 2001, 49, 11, 1444-1447
108. Yang, S. et al.: Body distribution of camptothecin solid lipid nanoparticles after oral administration, *Pharmaceutical Research*, 1999, 16, 5, 751-757
109. Luo, Y. F. et al.: Solid lipid nanoparticles for enhancing vinpocetine's oral bioavailability, *Journal of Controlled Release*, 2006, 114, 1, 53-59
110. Zhang, N. et al.: Lectin-modified solid lipid nanoparticles as carriers for oral administration of insulin, *International Journal of Pharmaceutics*, 2006, 327, 1-2, 153-159
111. Hu, L. D. et al.: Solid lipid nanoparticles (SLNs) to improve oral bioavailability of poorly soluble drugs, *Journal of pharmacy and pharmacology*, 2004, 56, 12, 1527-1535
112. Muchow, M. et al.: Lipid nanoparticles with a solid matrix (SLN®, NLC®, LDC®) for oral drug delivery, *Drug Development and Industrial Pharmacy*, 2008, 34, 12, 1394-1405
113. Blümer, C. et al.: Isostatic Ultra-High-Pressure Effects on Supercooled Melts in Colloidal Triglyceride Dispersions, *Pharmaceutical Research*, 2005, 22, 10, 1708-1715
114. Jores, K. et al.: Physicochemical Investigations on Solid Lipid Nanoparticles and on Oil-Loaded Solid Lipid Nanoparticles: A Nuclear Magnetic Resonance and Electron Spin Resonance Study, *Pharmaceutical Research*, 2003, 20, 8, 1274-1283
115. Bunjes, H. et al.: Effect of particle size on colloidal solid triglycerides, *Langmuir*, 2000, 16, 12, 5234-5241
116. Bunjes, H. et al.: Characterization of lipid nanoparticles by differential scanning calorimetry, X-ray and neutron scattering, *Advanced Drug Delivery Reviews*, 2007, 59, 6, 379-402
117. Rosenblatt, K. M. et al.: Poly(vinyl alcohol) as Emulsifier Stabilizes Solid Triglyceride Drug Carrier Nanoparticles in the alpha-Modification, *Molecular Pharmaceutics*, 2008, 6, 1, 105-120
118. Mulik, R. S. et al.: Transferrin mediated solid lipid nanoparticles containing curcumin: Enhanced in vitro anticancer activity by induction of



apoptosis, *International Journal of Pharmaceutics*, 2010, 398, 1-2, 190-203

119. Van, d. S. et al.: The size and shape of macromolecular structures: determination of the radius, the length and the persistence length of rod-like micelles of dodecyldimethylammonium chloride and bromide, *The Journal of Physical Chemistry*, 1985, 89, 3, 404-406
120. Wyatt, P. J.: Submicrometer Particle Sizing by Multiangle Light Scattering following Fractionation, *Journal of Colloid and Interface Science*, 1998, 197, 1, 9-20
121. Bunjes, H. et al.: Visualizing the Structure of Triglyceride Nanoparticles in Different Crystal Modifications, *Langmuir*, 2007, 23, 7, 4005-4011
122. Augsten, C. et al.: A detailed analysis of biodegradable nanospheres by different techniques - A combined approach to detect particle sizes and size distributions, *Journal of pharmaceutical and biomedical analysis*, 2008, 47, 1, 95-102
123. Delgado, A. V. et al.: Measurement and interpretation of electrokinetic phenomena, *Journal of Colloid and Interface Science*, 2007, 309, 2, 194-224
124. Förster, G. et al.: Influence of poly(l-lysine) on the structure of dipalmitoylphosphatidylglycerol/water dispersions studied by X-ray scattering, *European Biophysics Journal*, 2007, 36, 4, 425-435
125. Lakowicz, J. R. et al.: Principles of fluorescence spectroscopy, *Journal of Biomedical Optics*, 2008, 13, 029901
126. Schädlich, A. et al.: How Stealthy are PEG-PLA Nanoparticles? An NIR In Vivo Study Combined with Detailed Size Measurements, *Pharmaceutical Research*, 2011, 28, 8, 1-13
127. Abdalla, A. et al.: A new self-emulsifying drug delivery system (SEDDS) for poorly soluble drugs: Characterization, dissolution, in vitro digestion and incorporation into solid pellets, *European Journal of Pharmaceutical Sciences*, 2008, 35, 5, 457-464
128. Zangenberg, N. H. et al.: A dynamic in vitro lipolysis model:: I. Controlling the rate of lipolysis by continuous addition of calcium, *European Journal of Pharmaceutical Sciences*, 2001, 14, 2, 115-122
129. Rube, A. et al.: Monitoring of In Vitro Fat Digestion by Electron Paramagnetic Resonance Spectroscopy, *Pharmaceutical Research*, 2006, 23, 9, 2024-2029
130. Niepel, M. S. et al.: pH-dependent modulation of fibroblast adhesion on multilayers composed of poly(ethylene imine) and heparin, *Biomaterials*, 2009, 30, 28, 4939-4947

131. Olbrich, C. et al.: Lipase degradation of Dynasan 114 and 116 solid lipid nanoparticles (SLN)--effect of surfactants, storage time and crystallinity, *International Journal of Pharmaceutics*, 2002, 237, 1-2, 119-128
132. Unruh, T. et al.: Observation of size-dependent melting in lipid nanoparticles, *J.Phys.Chem.B*, 1999, 103, 47, 10373-10377
133. Kuntsche, J. et al.: Size Determinations of Colloidal Fat Emulsions: A Comparative Study, *Journal of Biomedical Nanotechnology*, 2009, 5, 4, 384-395
134. Nobbmann, U. et al.: Light scattering and nanoparticles, *Materials Today*, 2009, 12, 5, 52-54
135. Müller, R. H. et al.: Particle and surface characterisation methods, 1997, Medpharm Scientific Publishers Stuttgart, 3887630572
136. Weiss, V. M. et al.: Poly (glycerol adipate)-fatty acid esters as versatile nanocarriers: From nanocubes over ellipsoids to nanospheres, *Journal of Controlled Release*, 2011, 158, 1, 156-164
137. Müller, R. H. et al.: Zetapotential und Partikelladung in der Laborpraxis, PAPERBACK APV, 1996, 37
138. Moghimi, S. M. et al.: Poloxamers and poloxamines in nanoparticle engineering and experimental medicine, *Trends in biotechnology*, 2000, 18, 10, 412-420
139. Lutton, E. S.: The polymorphism of tristearin and some of its homologs, *Journal of the American Chemical Society*, 1945, 67, 4, 524-527
140. Westesen, K. et al.: Do nanoparticles prepared from lipids solid at room temperature always possess a solid lipid matrix?, *International Journal of Pharmaceutics*, 1995, 115, 1, 129-131
141. Small, D. M. et al. Small, D. M. et al.: The physical chemistry of lipids: from alkanes to phospholipids, 1986, Plenum press New York,
142. Holzgrabe, U. et al.: NMR spectroscopy in pharmacy, *Journal of pharmaceutical and biomedical analysis*, 1998, 17, 4-5, 557-616
143. Jennings, V. et al.: Solid lipid nanoparticles (SLN(TM)) based on binary mixtures of liquid and solid lipids: a <sup>1</sup>H-NMR study, *International Journal of Pharmaceutics*, 2000, 205, 1-2, 15-21
144. Al-Saden, A. A. et al.: Poloxamer association in aqueous solution, *Journal of Colloid and Interface Science*, 1982, 90, 2, 303-309
145. Schrader, B. et al. Schrader, B. et al.: Infrared and Raman spectroscopy: methods and applications, 1995, VCH Weinheim, 3527264469

146. Lippert, J. L. et al.: Raman active vibrations in long-chain fatty acids and phospholipid sonicates, *Biochimica et Biophysica Acta (BBA)- Biomembranes*, 1972, 282, 8-17
147. Litman, B. J. et al.: Packing characteristics of highly unsaturated bilayer lipids: Raman spectroscopic studies of multilamellar phosphatidylcholine dispersions, *Biochemistry*, 1991, 30, 2, 313-319
148. Baranska, M. et al.: Identification of secondary metabolites in medicinal and spice plants by NIR-FT-Raman microspectroscopic mapping, *Analyst*, 2004, 129, 10, 926-930
149. Khopde, S. M. et al.: Effect of Solvent on the Excited-state Photophysical Properties of Curcumin, *Photochemistry and Photobiology*, 2009, 72, 5, 625-631
150. Nardo, L. et al.: Role of H-bond formation in the photoreactivity of curcumin, *Spectroscopy*, 2008, 22, 2, 187-198
151. Jasim, F. et al.: A novel and rapid method for the spectrofluorometric determination of curcumin in curcumin spices and flavors, *Microchemical journal*, 1992, 46, 2, 209-214
152. Began, G. et al.: Interaction of Curcumin with Phosphatidylcholine: A Spectrofluorometric Study, *Journal of Agricultural and Food Chemistry*, 1999, 47, 12, 4992-4997
153. Kapoor, S. et al.: Protection of radiation-induced protein damage by curcumin, *Biophysical Chemistry*, 2001, 92, 1-2, 119-126
154. Wang, Y. J. et al.: Stability of curcumin in buffer solutions and characterization of its degradation products, *Journal of Pharmaceutical and Biomedical Analysis*, 1997, 15, 12, 1867-1876
155. Tønnesen, H. H.: Solubility, chemical and photochemical stability of curcumin in surfactant solutions, *Pharmazie*, 2002, 57, 12, 820-824
156. Chirio, D. et al.: Influence of alpha- and gamma- cyclodextrin lipophilic derivatives on curcumin-loaded SLN, *Journal of Inclusion Phenomena and Macrocyclic Chemistry*, 2009, 65, 3, 391-402
157. Washington, C.: Drug release from microdisperse systems: a critical review, *International Journal of Pharmaceutics*, 1990, 58, 1, 1-12
158. Rosenblatt, K. M. et al.: Drug release from differently structured monoolein/poloxamer nanodispersions studied with differential pulse polarography and ultrafiltration at low pressure, *Journal of Pharmaceutical Sciences*, 2007, 96, 6, 1564-1575
159. Levy, M. Y. et al.: Drug release from submicronized o/w emulsion: a new in vitro kinetic evaluation model, *International Journal of Pharmaceutics*, 1990, 66, 1-3, 29-37

160. Washington, C. et al.: Release rate measurements of model hydrophobic solutes from submicron triglyceride emulsions, *Journal of controlled release*, 1995, 33, 3, 383-390
161. Boyd, B. J.: Characterisation of drug release from cubosomes using the pressure ultrafiltration method\* 1, *International Journal of Pharmaceutics*, 2003, 260, 2, 239-247
162. Lukyanov, A. N. et al.: Micelles from lipid derivatives of water-soluble polymers as delivery systems for poorly soluble drugs, *Advanced Drug Delivery Reviews*, 2004, 56, 9, 1273-1289
163. Bisht, S. et al.: Polymeric nanoparticle-encapsulated curcumin ("nanocurcumin"): A novel strategy for human cancer therapy, *Journal of Nanobiotechnology*, 2007, 5
164. Gupta, V. et al.: Fabrication and characterization of silk fibroin-derived curcumin nanoparticles for cancer therapy, *International Journal of Nanomedicine*, 2009, 4, 115-122
165. Mukerjee, A. et al.: Formulation, characterization and evaluation of curcumin-loaded PLGA nanospheres for cancer therapy, *Anticancer research*, 2009, 29, 10, 3867-3875
166. Avgoustakis, K. et al.: PLGA-mPEG nanoparticles of cisplatin: in vitro nanoparticle degradation, in vitro drug release and in vivo drug residence in blood properties, *Journal of Controlled Release*, 2002, 79, 1â€“3, 123-135
167. Ptak, M. et al.: A NMR study of the ionization of fatty acids, fatty amines and N-acylamino acids incorporated in phosphatidylcholine vesicles, *Biochimica et Biophysica Acta (BBA)-Biomembranes*, 1980, 600, 2, 387-397
168. Small, D. M. et al.: The ionization behavior of fatty acids and bile acids in micelles and membranes, *Hepatology*, 1984, 4, S2, 77S-79S
169. Patton, J. S. et al.: Inhibition of human pancreatic lipase-colipase activity by mixed bile salt-phospholipid micelles, *American Journal of Physiology-Gastrointestinal and Liver Physiology*, 1981, 241, 4, 328-336
170. Fernandez, S. et al.: Comparative study on digestive lipase activities on the self emulsifying excipient Labrasol®, medium chain glycerides and PEG esters, *Biochimica et Biophysica Acta (BBA)-Molecular and Cell Biology of Lipids*, 2007, 1771, 5, 633-640
171. Fernandez, S. et al.: Lipolysis of the semi-solid self-emulsifying excipient Gelucire® 44/14 by digestive lipases, *Biochimica et Biophysica Acta (BBA)-Molecular and Cell Biology of Lipids*, 2008, 1781, 8, 367-375
172. Fureby, A. M. et al.: Acyl group migrations in 2-monoolein, *Biocatalysis and Biotransformation*, 1996, 14, 2, 89-111

173. Compton, D. L. et al.: Acyl migration kinetics of 2-monoacylglycerols from soybean oil via <sup>1</sup>H NMR, *Journal of the American Oil Chemists' Society*, 2007, 84, 4, 343-348
174. Olbrich, C. et al.: Enzymatic Degradation of Dynasan 114 SLN - Effect of Surfactants and Particle Size, *Journal of Nanoparticle Research*, 2002, 4, 1, 121-129
175. Bonnaire, L. et al.: Influence of lipid physical state on the in vitro digestibility of emulsified lipids, *Journal of agricultural and food chemistry*, 2008, 56, 10, 3791-3797
176. McClements, D. J. et al.: Structured emulsion-based delivery systems: Controlling the digestion and release of lipophilic food components, *Advances in colloid and interface science*, 2010, 159, 2, 213-228
177. Müller, R. H. et al.: Biodegradation of solid lipid nanoparticles as a function of lipase incubation time, *International Journal of Pharmaceutics*, 1996, 144, 1, 115-121
178. Olbrich, C. et al.: Enzymatic degradation of SLN--effect of surfactant and surfactant mixtures, *International Journal of Pharmaceutics*, 1999, 180, 1, 31-39
179. Wulff-Pérez, M. et al.: Delaying lipid digestion through steric surfactant Pluronic F68: a novel in vitro approach, *Food Research International*, 2010, 43, 6, 1629-1633
180. Golding, M. et al.: The influence of emulsion structure and stability on lipid digestion, *Current Opinion in Colloid & Interface Science*, 2010, 15, 1-2, 90-101
181. Bauer, E. et al.: Principles of physiology of lipid digestion, *Asian-australasian journal of animal sciences*, 2005, 18, 2, 282-295
182. Mun, S. et al.: Influence of emulsifier type on in vitro digestibility of lipid droplets by pancreatic lipase, *Food Research International*, 2007, 40, 6, 770-781
183. Porter, C. J. H. et al.: Use of in vitro lipid digestion data to explain the in vivo performance of triglyceride based oral lipid formulations of poorly water soluble drugs: Studies with halofantrine, *Journal of Pharmaceutical Sciences*, 2004, 93, 5, 1110-1121
184. Ravindran, J. et al.: Curcumin and cancer cells: how many ways can curry kill tumor cells selectively?, *The AAPS journal*, 2009, 11, 3, 495-510
185. Aggarwal, B. B. et al. Aggarwal, B. B. et al.: The molecular targets and therapeutic uses of curcumin in health and disease, 2007, Springer Verlag, 038746400X

186. Hou, X. L. et al.: Curcuma drugs and curcumin regulate the expression and function of P-gp in Caco-2 cells in completely opposite ways, *International Journal of Pharmaceutics*, 2008, 358, 1-2, 224-229
187. Wahlang, B. et al.: Identification of permeability-related hurdles in oral delivery of curcumin using the Caco-2 cell model, *European Journal of Pharmaceutics and Biopharmaceutics*, 2010, 77, 2, 275-282
188. Ulukaya, E. et al.: The MTT assay yields a relatively lower result of growth inhibition than the ATP assay depending on the chemotherapeutic drugs tested, *Toxicology in vitro*, 2008, 22, 1, 232-239
189. Petty, R. D. et al.: Comparison of MTT and ATP-based assays for the measurement of viable cell number, *Journal of bioluminescence and chemiluminescence*, 1995, 10, 1, 29-34
190. Mueller, H. et al.: Comparison of the usefulness of the MTT, ATP, and calcein assays to predict the potency of cytotoxic agents in various human cancer cell lines, *Journal of biomolecular screening*, 2004, 9, 6, 506-515
191. Jabbar, S. A. et al.: The MTT assay underestimates the growth inhibitory effects of interferons, *British journal of cancer*, 1989, 60, 4, 523-528
192. Hamid, R. et al.: Comparison of alamar blue and MTT assays for high throughput screening, *Toxicology in vitro*, 2004, 18, 5, 703-710
193. Back, S. A. et al.: A new Alamar Blue viability assay to rapidly quantify oligodendrocyte death, *Journal of neuroscience methods*, 1999, 91, 1-2, 47-54
194. Goegan, P. et al.: Effects of serum protein and colloid on the alamarBlue assay in cell cultures, *Toxicology in vitro*, 1995, 9, 3, 257-266
195. Schmolka, I. R.: A review of block polymer surfactants, *Journal of the American Oil Chemists' Society*, 1977, 54, 3, 110-116
196. Li, L. et al.: Liposome-encapsulated curcumin: In vitro and in vivo effects on proliferation, apoptosis, signaling, and angiogenesis, *Cancer*, 2005, 104, 6, 1322-1331
197. Thangapazham, R. L. et al.: Evaluation of a nanotechnology-based carrier for delivery of curcumin in prostate cancer cells, *International Journal of Oncology*, 2008, 32, 5, 1119-1123
198. Liu, A. et al.: Validated LC/MS/MS assay for curcumin and tetrahydrocurcumin in rat plasma and application to pharmacokinetic study of phospholipid complex of curcumin, *Journal of Pharmaceutical and Biomedical Analysis*, 2006, 40, 3, 720-727
199. Mandeville, J. S. et al.: Study of curcumin and genistein interactions with human serum albumin, *Journal of Pharmaceutical and Biomedical Analysis*, 2009, 49, 2, 468-474

200. Kakkar, V. et al.: Pharmacokinetic applicability of a validated liquid chromatography tandem mass spectroscopy method for orally administered curcumin loaded solid lipid nanoparticles to rats, *Journal of Chromatography B*, 2010, 878, 32, 3427-3431
201. Sharma, R. A. et al.: Phase I Clinical Trial of Oral Curcumin: Biomarkers of Systemic Activity and Compliance, *Clinical Cancer Research*, 2004, 10, 20, 6847-6854
202. Fraunhofer, W. et al.: The use of asymmetrical flow field-flow fractionation in pharmaceuticals and biopharmaceuticals, *European Journal of Pharmaceutics and Biopharmaceutics*, 2004, 58, 2, 369-383
203. Yohannes, G. et al.: Asymmetrical flow field-flow fractionation technique for separation and characterization of biopolymers and bioparticles, *Journal of Chromatography A*, 2011, 1218, 27, 4104-4116
204. Augsten, C. et al.: Characterizing molar mass distributions and molecule structures of different chitosans using asymmetrical flow field-flow fractionation combined with multi-angle light scattering, *International Journal of Pharmaceutics*, 2008, 351, 1-2, 23-30
205. Lohrke, J. et al.: Characterization of superparamagnetic iron oxide nanoparticles by asymmetrical flow-field-flow-fractionation, *Nanomedicine*, 2008, 3, 4, 437-452
206. Hagendorfer, H. et al.: Application of an asymmetric flow field flow fractionation (AF4) multi-detector approach for metallic engineered nanoparticle characterization-prospects and limitations demonstrated on Au nanoparticles, *Analytica chimica acta*, 2011
207. Fraunhofer, W. et al.: Asymmetrical flow field-flow fractionation and multiangle light scattering for analysis of gelatin nanoparticle drug carrier systems, *Analytical Chemistry*, 2004, 76, 7, 1909-1920
208. Bhajendra, N.: *Miscellaneous Submicrometer-Sized Particles*, Field flow fractionation handbook, 2000,
209. Litzén, A. et al.: Effects of temperature, carrier composition and sample load in asymmetrical flow field-flow fractionation, *Journal of Chromatography A*, 1991, 548, 393-406
210. Andreev, V. P. et al.: Theory of field-flow fractionation with the reversible adsorption on channel walls, *Chromatographia*, 1993, 37, 5, 325-328
211. Andersson, M. et al.: Accuracy in Multiangle Light Scattering Measurements for Molar Mass and Radius Estimations. Model Calculations and Experiments, *Analytical Chemistry*, 2003, 75, 16, 4279-4291
212. Jores, K. et al.: Investigations on the structure of solid lipid nanoparticles (SLN) and oil-loaded solid lipid nanoparticles by photon correlation

spectroscopy, field-flow fractionation and transmission electron microscopy, *Journal of Controlled Release*, 2004, 95, 2, 217-227

213. Fogh, J. et al.: One hundred and twenty-seven cultured human tumor cell lines producing tumors in nude mice, *Journal of the National Cancer Institute*, 1977, 59, 1
214. Pinto, M. et al.: Enterocyte-like differentiation and polarization of the human colon carcinoma cell line Caco-2 in culture, *Biol.Cell*, 1983, 47, 3, 323-330
215. Sambuy, Y. et al.: The Caco-2 cell line as a model of the intestinal barrier: influence of cell and culture-related factors on Caco-2 cell functional characteristics, *Cell biology and toxicology*, 2005, 21, 1, 1-26
216. Erb, R. E. et al.: Resazurin Reducing Time as an Indicator of Bovine Semen Fertilizing Capacity<sup>1</sup>, *Journal of Dairy Science*, 1950, 33, 12, 853-864
217. Anoopkumar-Dukie, S. et al.: Resazurin assay of radiation response in cultured cells, *British journal of radiology*, 2005, 78, 934
218. O'Brien, J. et al.: Investigation of the Alamar Blue (resazurin) fluorescent dye for the assessment of mammalian cell cytotoxicity, *European Journal of Biochemistry*, 2000, 267, 17, 5421-5426
219. Gonzalez, R. J. et al.: Evaluation of hepatic subcellular fractions for Alamar blue and MTT reductase activity, *Toxicology in vitro*, 2001, 15, 3, 257-259
220. Twigg, R. S.: Oxidation-reduction aspects of resazurin, *Nature*, 1945, 155, 3935, 401-402



## 8. Appendix

### Asymmetrical flow field-flow fractionation (AF4)

Asymmetric flow field-flow fractionation (AF4) has attracted attention for the characterization of macromolecules and colloidal carriers recently (202,203). AF4 was applied for the fractionation and molar mass determination of macromolecules (204). Furthermore, the determination of the particle size distribution of various colloidal particles by AF4 in combination with multi-angle laser light scattering (MALLS) has been reported (205-207).

The separation principle of the AF4 is outlined in Fig. A1. The separation is conducted in a flat and narrow channel. A constant laminar flow is applied, resulting in a parabolic flow profile in the channel (channel flow). Perpendicular to the laminar flow, a cross flow is applied. The cross flow solvent leaves the channel through a membrane at the bottom of the channel. If particles are injected into the channel, they are transported by the channel flow. If the cross flow is high enough, it presses the particles down to the membrane and arrests them within the channel. It is important that the particles cannot leave the channel via the membrane. So, the molecular cutoff should be chosen appropriately. The Brownian motion of the particles is acting the opposite way than the cross flow and drives the particles back into the middle of the channel. Therefore, particles with a high diffusion coefficient can diffuse faster into the middle of the channel again. Due to the parabolic flow profile, the velocity of the channel flow is higher in the middle of the channel compared to the channel wall. Thus, the particles located more in the channel middle elute faster out of the channel, than particles located closer to the membrane. The diffusion coefficient of a particle and its transition time (retention time) through the channel are therefore interdependent. Generally, small particles have a higher diffusion coefficient and a shorter retention time than large particles. At given flow conditions, the hydrodynamic radius (diameter) of the particle can be calculated by the retention time of the particles, via the Stokes-Einstein equation (202,208). However, this basic elution theory is only applicable for spherical particles and amongst others, dependent on the temperature, electrostatic interactions and the actual channel thickness (209,210).

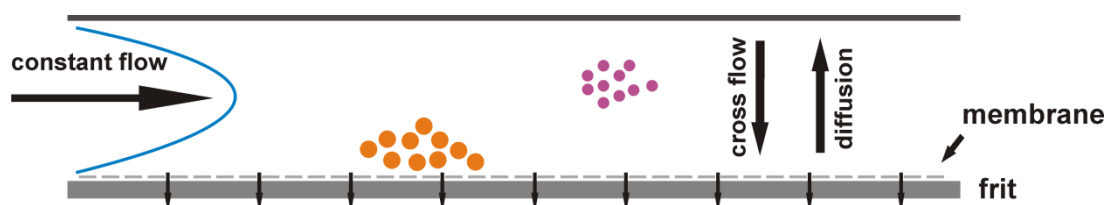


## Figure A1 Scheme of the AF4 separation principle

The fractionated samples can be detected by means of various techniques, like UV, refractive index (RI) or dynamic light scattering (DLS), which analyze the sample after it left the channel. The method of choice for the detection of particulate samples is multiangle laser light scattering [MALLS, (120)]. This method records the light scattered by the particles at different angles at each elution time. The particle size calculation from the scattering light intensity is based on the Rayleigh-Gans-Debye (RGD) approximation (120,211):

$$\frac{Kc}{R_{\theta}} \approx \frac{1}{M_w P(\theta)} \quad (\text{A1})$$

In this equation,  $K$  is an optical constant,  $c$  is the concentration,  $R_{\theta}$  is the Rayleigh ratio,  $M_w$  is the average molar mass,  $P(\theta)$  is the form factor, describing the dependence of light intensity on the angle and  $\theta$  is the respective detector angle. Based on the RGD approximation, the root mean square radius ( $r_{\text{RMS}}$ ) is calculated from the curve slope of the scattered light intensity in relation to the detector angle. The  $r_{\text{RMS}}$  is the root mean square of the distance of all parts of the object to its center of mass. Thus, information about the particle shape is implied in this value.

The particle sizes of spherical particles, determined with AF4/MALLS, were shown to be comparable to the “classical” particle measurement techniques, PCS and LD (122,133). One major advantage of AF4/MALLS compared to PCS and LD is the fractionation of the particle population and the independent analysis of every single fraction. Thus, the detailed investigation of complex samples can be conducted and more information about the characteristics of a particle population can be gained by AF4/MALLS compared to PCS and LD (207). In addition, AF4/MALLS can also give valuable information about the particle shape of the investigated samples. For example, anisometric, platelet-like SLN were shown to elute slower from the channel compared to round emulsion droplets (212). The differing shapes of the liquid and solid particles are also verifiable by the different light scattering profiles, recorded with the MALLS detector. Therefore, AF4/MALLS was seen as an important tool for the investigation of the particle size distribution and the particle shape of the produced lipid nanoparticles.

### ***Caco-2 cells***

Various cell lines have been developed for the *in vitro* evaluation of pharmacological and toxicological problems. Among the known cell lines, the Caco-2 cell line is of utmost importance for today's research. Caco-2 cells are human epithelial colorectal adenocarcinoma cells. The cell line was established in the 1970's for studying cancer mechanisms and testing cytostatic therapy (213). Caco-2 cells were found to differentiate in long-term culture and to express morphological and biochemical characteristics of small intestine enterocytes (214). Typical characteristics of Caco-2 cell cultures are the growth in monolayer, the polarized, cylindrical cell form, the presence of microvilli on the surface of the apical side, the existence of tight junctions and the expression of small intestine enzymes (215). Because of these characteristics, Caco-2 cells are widely used in research as well as in the pharmaceutical industry for the *in vitro* simulation of intestinal absorption of small molecules, like drugs.

In this work, Caco-2 cells were applied for a cell viability assay, because the curcuminoid loaded lipid nanoparticles should be administered orally. Therefore, the toxicity of the formulation and of the free drug, respectively, should be examined with a cell line mimicking the intestinal tissue. Nevertheless, it has to be kept mind that Caco-2 cells are malignant cancer cells. Thus, the reaction of these cells to the curcuminoid-loaded nanoparticles is not necessarily comparable to the reaction of non-malignant cells to the formulation. The gained results of the toxicity and biocompatibility evaluation of the tested formulations must therefore be interpreted with care.

### ***QBlue cell viability assay***

The QBlue assay, as well as the more common Alamar Blue<sup>®</sup> assay, is based on the reduction of the blue and nonfluorescent resazurin to the pink and fluorescent dye resorufin (Fig. A2). Resazurin-based assays have been utilized in the milk industry since the 1950's to assess the bacterial contamination of milk products (216). Resazurin is only reduced in the presence of metabolically active cells. Nonviable cells with no metabolic capacity do not cause such a conversion. Thus, the concentration of the reduced form, resorufin, is a true measure of the cell viability. The concentration of resorufin is either determined by colourimetry or fluorimetry (217). However, the actual mechanism of action of the resazurin reduction within a cell culture has not been verified yet (218,219). Furthermore, the outcome of resazurin-based assays was shown to be influenced by a variety of parameters, like medium composition and incubation time (194).

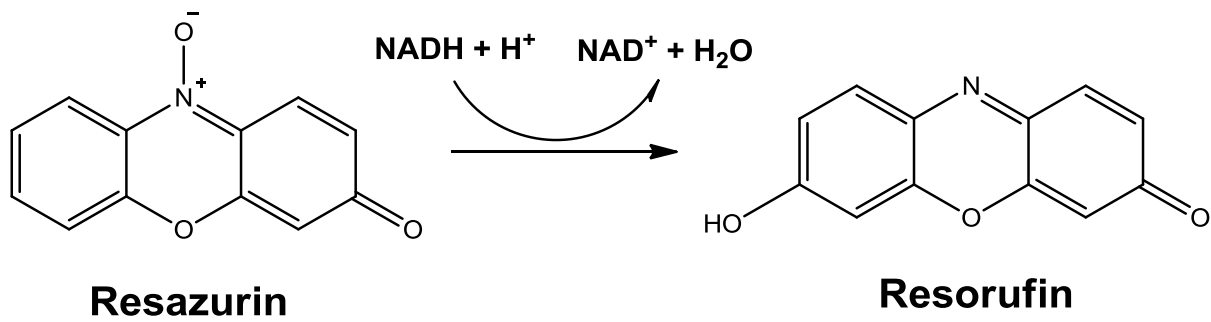


Figure A2 Scheme of the reduction of the blue and non-fluorescent resazurin to the pink and fluorescent resorufin [according to (220)].

Resazurin was reported to be non-toxic to cells and reacted very sensitive, so that already 80 metabolically active cells were detectable (218). One further advantage is the survival of the cells during the execution of the QBlue assay. This allows the reuse of the grown cells, after the viability determination. In contrast the frequently applied MTT-assay necessitates killing the cells, which is especially unfavorable for expensive cell lines.

# Certificates of Analysis

## Analysenzertifikat



Carl Roth GmbH + Co. KG • 76185 Karlsruhe  
Schoemperlenstraße 3-5  
Telefon: 0721 + 56 06-0  
Telefax: 0721 + 56 06-149  
E-Mail: info@carlroth.de  
http://www.carl-roth.de



Datum - Zeichen: 07.07.11 LAU/GR

Artikelnummer: 9469  
Produkt: Curcumin

Charge: 08974233  
Dichte:  
Formel:  $C_{21}H_{20}O_6$   
Schmelzpunkt: 173 - 180°C  
Flammpunkt:

Reinheit:  $\geq 99\%$ , nat., pulv., 811.  
CAS-Nummer: 458-37-7  
Molekulargewicht: 368,39  
Lagertemperatur:  
Siedepunkt:  
MHD: 05.05.2006

Aussehen:	orangefarbenes Pulver
Farbstoffgehalt:	93,4%
Wasser (ZF):	$\leq 1,0\%$
Arson (As):	$< 0,0003\%$
Blei (Pb):	$< 0,001\%$
Schwermetalle:	$\leq 0,004\%$
Schmelzbereich:	173°C
Farbintensität B/16/433 (CH <sub>2</sub> Cl <sub>2</sub> /BLON):	150

Unsere Produkte sind für Laborkoncke geprüft.

Carl Roth GmbH + Co.

  
i.A. TIMO GROSS

PRODUKT	3274	MIGLYOL® 812
SYNONYM		MITTELKETTIGE TRIGLYCERIDE
CHARGE		081028
PRUEFVORSCHRIFT		PH.EUR. 5.0
VERFALLDATUM		02.2011

PRÜFUNG	SPEZIFIKATION	ERGEBNIS
Eigenschaften	Gemäss Prüfvorschrift	Entspricht
-Aussehen	Gemäss Prüfvorschrift	Entspricht
-Löslichkeit	Gemäss Prüfvorschrift	Entspricht
Identität	Gemäss Prüfvorschrift	Entspricht
-Prüfung B, C	Gemäss Prüfvorschrift	Entspricht
Reinheit	Gemäss Prüfvorschrift	Entspricht
-Aussehen der Substanz	Gemäss Prüfvorschrift	Entspricht
-Alkalisch reag. Subst.	Gemäss Prüfvorschrift	Entspricht
-Relative Dichte	0,93 bis 0,96	0,9472
-Brechungsindex	1,440 bis 1,452	1,4491
-Viskosität mPa s	25 bis 33	29,7
-Säurezahl	max 0,2	0,03
-Hydroxylzahl	max 10	2,4
-Iodzahl	max 1,0	< 0,1
-Peroxidzahl	max 1,0	0,0
-Verseifungszahl	310 bis 360	335
-Unverseifb. Anteile m/m	max 0,5 %	< 0,3 %
-Schwermetalle	max 10 ppm	< 10 ppm
-Wasser	max 0,2 %	0,02 %
-Asche	max 0,1 %	< 0,01 %
Fettsäurezusammensetzung	Gemäss Prüfvorschrift	Entspricht
-Capronsäure	max 2,0 %	0,1 %
-Caprylsäure	50,0 bis 80,0 %	55,4 %
-Caprinsäure	20,0 bis 50,0 %	43,9 %
-Laurinsäure	max 3,0 %	0,3 %
-Myristinsäure	max 1,0 %	< 0,05 %



**Sasol Germany GmbH**

Standort Witten  
Arthur-Imhausen-Str. 92  
D-58453 Witten

Telephone +49(0)2302 925-390 Extension  
+49(0)2302/925-0 Switchboard  
Fax +49(0)2302 925-358

WITTEN, 10.03.2010

Fax:

## Inspection certificate 3.1 (DIN EN 10 204-3.1)

Product: **Dynasan 114**

Purchase order:  
Delivery number: 0002110202000100  
Order number: E-Mail  
Article no.: 6262 Quantity: 1.000 KG  
Batch: 905167  
Manufacturing date: 05/2009 Retestdate: 05/2011

Property	Value	Unit	Method
Acid value	0.2	mg KOH/g	Ph. Eur. 2.5.1
Saponificat. value	234	mg KOH/g	Ph. Eur. 2.5.6
Hydroxyl value	3	mg KOH/g	Ph. Eur. 2.5.3
Iodine colour no.	0.6	mg I/100ml	DGF C-IV 4a
Melting point (DSC)	58.0	°C	AN-SAA 0540
Water content	<=0.1	%	Ph. Eur. 2.5.12
Peroxide value	0.2	meq O/kg	Ph. Eur. 2.5.5
Unsaponifiable	<=0.5	%	Ph. Eur. 2.5.7

The a.m. methods lead to the same results as the respective methods of the European Pharmacopeia (Ph.Eur.).

**With these results of our inspections we certify that the material described above complies with the product specification.**

**Sasol Germany GmbH  
Dr. Oeser**

This document is automatically generated and no signature is needed.

*Die Übersendung dieses Analysenzertifikats erfolgt lediglich zur Information und stellt keine Zusicherung von Eigenschaften dar. Die Übersendung entbindet den Empfänger nicht von der Durchführung einer ordnungsgemäßen Wareneingangsprüfung. Dieses Analysenzertifikat begründet keine Ansprüche Dritter, an die es weitergeleitet wird. Im übrigen gelten unsere Allgemeinen Geschäftsbedingungen in der jeweils aktuellen Fassung.*

*This certificate of analysis is for information only and does not guarantee any particular product properties. It does not free the recipient of the obligation to carry out a product receiving inspection. This certificate of analysis does not create claims of third parties to which it is passed on. All transactions are subject to our General Business Conditions as amended up to the time concerned.*

**Sasol Germany GmbH**



**Sasol Germany GmbH**

Standort Witten  
Arthur-Imhausen-Str. 92  
D-58453 Witten

Telephone +49(0)2302 925-390 Extension  
+49(0)2302/925-0 Switchboard  
Fax +49(0)2302 925-358

**WITTEN, 10.03.2010**

Fax:

---

**Inspection certificate 3.1 (DIN EN 10 204-3.1)**

Product: **Dynasan 118**

Purchase order:  
Delivery number: 0002110202000200  
Order number: E-Mail  
Article no.: 6264 Quantity: 1.000 KG  
Batch: 902838  
Manufacturing date: 02/2009 Retestdate: 02/2011

---

Property	Value	Unit	Method
Acid value	0.3	mg KOH/g	Ph. Eur. 2.5.1
Saponificat. value	188	mg KOH/g	Ph. Eur. 2.5.6
Hydroxyl value	2.6	mg KOH/g	Ph. Eur. 2.5.3
Iodine colour no.	2.5	mg I/100ml	DGF C-IV 4a
Melting point (DSC)	73	°C	AN-SAA 0540
Water content	<=0.1	%	Ph. Eur. 2.5.12
Peroxide value	0.2	meq O/kg	Ph. Eur. 2.5.5
Unsaponifiable	<=0.5	%	Ph. Eur. 2.5.7

**With these results of our inspections we certify that the material described above complies with the product specification.**

**Sasol Germany GmbH  
Dr. Oeser**

This document is automatically generated and no signature is needed.

*Die Übersendung dieses Analysenzertifikats erfolgt lediglich zur Information und stellt keine Zusicherung von Eigenschaften dar. Die Übersendung entbindet den Empfänger nicht von der Durchführung einer ordnungsgemäßen Wareneingangsprüfung. Dieses Analysenzertifikat begründet keine Ansprüche Dritter, an die es weitergeleitet wird. Im übrigen gelten unsere Allgemeinen Geschäftsbedingungen in der jeweils aktuellen Fassung.*

*This certificate of analysis is for information only and does not guarantee any particular product properties. It does not free the recipient of the obligation to carry out a product receiving inspection. This certificate of analysis does not create claims of third parties to which it is passed on. All transactions are subject to our General Business Conditions as amended up to the time concerned.*

**Sasol Germany GmbH**



# Publications

## Poster presentations

A. Noack, K. Mäder: Lipid nanoparticles as a way to enhance the bioavailability of curcumin

7<sup>th</sup> APV World Meeting, Valetta, Malta, 2010

A. Noack, K. Mäder: Lipid nanoparticles as a way to enhance the bioavailability of curcumin

Annual Meeting of the German Pharmaceutic Society, Braunschweig, Germany, 2011

## Peer reviewed articles

A. Noack, G. Hause, K. Mäder: Physicochemical characterization of curcuminoid-loaded solid lipid nanoparticles

International Journal of Pharmaceutics, 2011, Volume 423, Issue 2

A. Noack, J. Oidtmann, J. Kutza, K. Mäder: *In vitro* digestion of curcuminoid-loaded lipid nanoparticles

Journal of Nanoparticle Research, 2012, accepted

# Curriculum vitae

Name: Andreas Noack  
Geburtsdatum: 05.01.1985  
Geburtsort: Dresden, Deutschland

## *Hochschulausbildung*

12/2008 - 12/2011 Doktorand am Institut für Pharmazie, Institutsbereich Pharmazeutische Technologie, Betreuer: Professor Dr. Karsten Mäder  
12/2008 Erteilung der Approbation als Apotheker  
11/2008 3. Staatsexamen  
11/2007 - 03/2008 Diplomarbeit im Rahmen des Praktischen Jahres im Institutsbereich Pharmazeutische Technologie, Betreuer: Professor Dr. Karsten Mäder, Titel: „Anwendung der ESR-Spektroskopie zur Optimierung künstlichen Gewebersatzes“  
10/2007 2. Staatsexamen  
09/2005 1. Staatsexamen  
10/2003 - 10/2007 Studium der Pharmazie an der Martin-Luther Universität Halle-Wittenberg

## *Praktische Erfahrungen*

02/2010 - heute Teilzeittätigkeit als Apotheker, Stern-Apotheke, Halle/Saale  
04/2009 - 11/2011 Lehrtätigkeit am Institut für Pharmazie im Fach Pharmazeutische Technologie  
12/2008 - 11/2010 Stipendiat der Landesgraduiertenförderung Sachsen-Anhalt  
12/2008 - 02/2009 Forschungsaufenthalt im Rahmen der Doktorarbeit an der Staatlichen Universität Seoul, Fakultät für Pharmazie, Betreuer: Professor Dr. Young-Joon Surh, Seoul, Republik Korea  
04/2008 - 10/2008 Pharmazeut im Praktikum, Kröllwitz-Apotheke, Halle/Saale  
02/2007 Praktikum im Rahmen des Wahlpflichtfaches bei Merck KGaA, Darmstadt, Bereich Pharmaceutical Global Development

08/2006 - 09/2006      Praktikum an der Jomo-Kenyatta Universität für Landwirtschaft  
und Technik, Fakultät für Chemie, Nairobi, Kenia

08/2004                Famulatur in der Krankenhausapotheke des  
Universitätsklinikums Dresden

03/2004                Famulatur in der Lilien-Apotheke, Dresden

***Schulbildung***

1996 - 2003            Marie-Curie-Gymnasium, Dresden

---

Andreas Noack

“My centre is giving way,  
my right is in retreat;  
situation excellent.  
I am attacking.”

-

Marshal Ferdinand Foch

# Acknowledgments

First of all, I want to thank my supervisor Professor Dr. Karsten Mäder for the opportunity to work in his research group, the suggestion of the research subject and the support during my scientific work.

I am also very grateful to Dr. Judith Kuntsche for the help with AF4 measurements, the fruitful discussions about particle size measurements and the critical revision of the respective chapters of this work.

I want to acknowledge Dr. Gerd Hause for the support and conservation regarding the TEM investigation.

Professor Groth and his working group helped me by conducting the cell culture experiments and I am very thankful for their support and helpful comments to my experiments.

Kerstin Schwarz and Ute Mentzel were of great help to me during the daily scientific life and I want to thank them cordially for their kindness and their helpfulness.

A special thanks goes to Professor Dr. Hans-Herrmann Rüttinger and his assistants for their contribution to my fluorescence measurements and the informative dialogues in their laboratory.

Furthermore, I want to thank Dr. Dieter Ströhl and Dr. Günter Förster for performing the NMR and XRD measurements, respectively, and for their kind help in evaluating the gained data.

I also want to thank all my colleagues for the great time we had. I will miss the kind and hearty atmosphere and the interesting discussions most notably at lunchtime. Johannes Kutza has to be thanked particularly for the support with the fluorescence imaging and for the patience with me and my computer. I am also very thankful to Johannes Oidtmann for his guidance to get a real scientist and to create a proper digestion. I thank Verena Weiss (formerly known as Verena Gläßer) for her cooperation during practical course and her support by fitting the homogenizer once in a while. And a very special thanks goes to my former room-mate Dr. Alexander Lochmann for the revision of this work and his critical view on nanotechnology.

I want to express my deep gratitude to my family for their support and appreciation during the good and the bad periods of the past years. I am especially indebted to my parents who supported all my plans and who gave me the opportunity of studying pharmacy and travelling the world.

Finally, I thank Julia for being on my side, her love and her belief in me.

At the very end I thank all the people who I may have forgotten.

# Selbstständigkeitserklärung

Hiermit erkläre ich, dass ich die Ergebnisse der vorliegenden Dissertationsarbeit an der Martin-Luther-Universität Halle-Wittenberg unter Anleitung von Herrn Professor Dr. rer. nat. habil. Karsten Mäder selbstständig erarbeitet bzw. im Rahmen der angegebenen Kooperation erhalten und die Dissertation ohne fremde Hilfe angefertigt habe.

Dazu habe ich keine anderen als die angegebenen Quellen oder Hilfsmittel benutzt und die den verwendeten Werken wörtlich oder inhaltlich entnommenen Stelle als solche kenntlich gemacht.

Weiterhin erkläre ich, dass ich mich mit der vorliegenden Dissertationsarbeit erstmals um die Erlangung eines Doktorgrades bewerbe.

Halle/Saale, den

---

Andreas Noack